

Linear Parameter Varying Control of Uncertain Time-Delay Systems  
with Application to Automated Blood Pressure Regulation

by  
Shahin Tasoujian

A dissertation submitted to the Department of Mechanical Engineering,  
Cullen College of Engineering  
in partial fulfillment of the requirements for the degree of

Doctor of Philosophy  
in Mechanical Engineering

Chair of Committee: Karolos M. Grigoriadis, Professor  
Co-Chair of Committee: Matthew A. Franchek, Professor  
Committee Member: Rose T. Faghieh, Assistant Professor  
Committee Member: Gangbing Song, Professor  
Committee Member: Zheng Chen, Assistant Professor

University of Houston  
December 2020

Copyright 2020, Shahin Tasoujian

## ACKNOWLEDGMENTS

This dissertation and Ph.D. degree become a reality with many individuals' support, without whom I would not have been able to complete this research. I would like to take this opportunity to extend my sincere thanks to all of them.

First and foremost, I would like to thank my advisors, Professor Karolos Grigoriadis and Professor Matthew Francheck, for their consistent encouragement, helpful advice, immense knowledge, and supporting me during my studies at the University of Houston. Both Dr. Grigoriadis and Dr. Francheck are certainly among the smartest and most knowledgeable people I know. I feel extremely lucky and grateful to have this amazing opportunity to perform research and complete several projects under the supervision of such distinguished scholars.

I want to gratefully acknowledge the financial support provided by the National Science Foundation (NSF) during the project and also the collaboration of the Resuscitation Research Laboratory (Dr. G. Kramer) at the University of Texas Medical Branch, Galveston, Texas, in providing experiment data. Many thanks to the committee members, Dr. Gangbing Song, Dr. Rose Faghil, and Dr. Zheng Chen, for providing valuable comments that helped to improve the contents of the dissertation.

I also would like to mention my friend and colleague, Dr. Saeed Salavati, and all my friends, who have been my second family here in the United States, and this journey would not have been possible without them.

Finally, I express my deepest and warmest gratitude to my greatest treasure, my mother, father, and brother, for their continuous and unconditional love. I am forever indebted to them for their unparalleled support and sacrifices. I dedicate this milestone and all my achievements to my lovely family for all they have done for me throughout my life.

## ABSTRACT

This dissertation examines the problem of real-time estimation and automated control of mean arterial blood pressure (MAP) response of a critical patient subject to the vasoactive drug infusion in emergency resuscitation scenarios. The proposed methodologies rely on the wealth of the system identification and feedback control theory and can provide reliable and efficient patient resuscitation tools via computerized drug administration. Therefore, such advanced resuscitation methods can reduce emergency care costs and significantly increase the survival chances by improving the patient's MAP regulation in an intensive care unit. In order to derive an appropriate mathematical description, a dynamic first-order linear time-varying model structure with varying parameters and time delay is employed to characterize the patient's complex physiological MAP response dynamics. In the first part of the dissertation, real-time estimation of the varying model parameters and delay is performed via a Bayesian-based multiple-model square-root cubature Kalman filtering (MMSR-CKF) approach. The estimation results substantiate the effectiveness of the utilized identification method using experimental data. Next, two classical frequency-domain control design methods, namely, IMC-PID and parameter-varying loop-shaping approaches, are proposed and implemented to achieve desired MAP regulation in various simulation scenarios.

The second part of the dissertation is devoted to the analysis and control synthesis of time-delayed linear parameter-varying (LPV) systems with norm-bounded parametric and/or time-delay uncertainties. LPV time-delay systems are linear dynamical systems whose dynamic characteristics rely on a measurable scheduling parameter vector, where the scheduling parameter vector is used systematically to capture the dynamics of time-varying and nonlinear systems. In order to reduce the design conservatism and handle the varying delay uncertainties, a Lyapunov-Krasovskii based approach is exercised, and by utilizing an improved parameter-dependent Lyapunov Krasovskii functional (LKF) candidate and applying an efficient cross-term bounding technique, the affine Jensen's inequality, sufficient stability and performance conditions are derived and formulated in terms of convex linear matrix inequality (LMI) framework. The final relaxed synthesis conditions are obtained to design a robust delay-dependent gain-scheduled controller which guarantees closed-loop stability and minimizes disturbance amplification in terms of the induced  $\mathcal{L}_2$ -norm performance specification. The effectiveness of the proposed control design algorithms is assessed through the automated MAP

regulation task, and the results are compared with the conventional control approaches in the literature. The final closed-loop simulation results confirm the potential and superiority of the adopted LPV methodologies.

# TABLE OF CONTENTS

<b>ACKNOWLEDGMENTS</b>		<b>iii</b>
<b>ABSTRACT</b>		<b>iv</b>
<b>LIST OF TABLES</b>		<b>viii</b>
<b>LIST OF FIGURES</b>		<b>x</b>
<b>1 INTRODUCTION</b>		<b>1</b>
1.1 Automated Blood Pressure Regulation in Critical Patient Resuscitation . . . . .		1
1.1.1 MAP Response Dynamics . . . . .		2
1.2 LPV Time-Delay Systems . . . . .		5
1.3 Outline of the Dissertation . . . . .		7
1.4 Notation . . . . .		9
<b>2 REAL-TIME BAYESIAN PARAMETER ESTIMATION OF BLOOD PRESSURE RESPONSE CHARACTERISTICS</b>		<b>11</b>
2.1 Introduction and Literature Review . . . . .		11
2.2 Estimation Preliminaries and Methodology . . . . .		14
2.2.1 SRCKF Algorithm . . . . .		14
2.2.2 Multiple-Model SRCKF for Input Delay Estimation . . . . .		21
2.3 MAP Response Estimation Results and Validations . . . . .		23
2.4 Chapter Conclusion . . . . .		32
<b>3 LOOP-SHAPING AND IMC-PID CONTROL FOR AUTOMATED BLOOD PRESSURE REGULATION</b>		<b>33</b>
3.1 Introduction . . . . .		33
3.2 Control System Design . . . . .		35
3.2.1 Loop-Shaping Control Design . . . . .		35
3.2.2 IMC-Based PID Control Design . . . . .		41
3.3 Simulations Results and Discussions . . . . .		44
3.3.1 PID Controller Tuning . . . . .		44
3.3.2 MAP Regulation Closed-Loop Simulation Results . . . . .		47
3.4 Chapter Conclusion . . . . .		52
<b>4 ROBUST CONTROL OF LPV TIME-DELAY SYSTEMS</b>		<b>53</b>
4.1 Introduction . . . . .		53
4.2 Delay-Dependent Gain-Scheduling Control Synthesis for LPV Time-Delay Systems . . . . .		55
4.2.1 Robust $\mathcal{H}_\infty$ Output-Feedback Control Design . . . . .		55
4.2.2 Improved Integral Inequality for Less Conservative Control Design . . . . .		65
4.3 Robust Control of LPV Systems with Uncertain Time-Delay . . . . .		75
4.3.1 State-Feedback Control of LPV Systems with Uncertain Time-Delay . . . . .		76
4.3.2 Dynamic Output-Feedback Control of LPV Systems with Varying Uncertain Time-Delay . . . . .		83
4.4 Sampled-Data LPV Control Design . . . . .		95

4.4.1	Digital Controller Derivation . . . . .	104
4.5	Closed-Loop MAP Regulation . . . . .	105
4.5.1	MAP Response Continuous-Time LPV Modeling . . . . .	105
4.5.2	Automated LPV MAP Control Simulation Results and Discussions . . . . .	107
4.6	Chapter Conclusion . . . . .	112
<b>5</b>	<b>CONCLUSION, CONTRIBUTIONS AND FUTURE WORK</b>	<b>114</b>
5.1	Summary of the Dissertation . . . . .	114
5.2	Future Research Direction . . . . .	116
	<b>Bibliography</b>	<b>118</b>

## LIST OF TABLES

1	Probabilistic distribution of patient model coefficients . . . . .	4
2	Estimation root mean square errors (RMSEs) . . . . .	28
3	Performance levels $\gamma$ of both methods for different maximum delay values $\bar{\tau}$ . . . . .	74
4	Performance levels $\gamma$ of both methods for different delay uncertainty values $\mu$ . . . . .	94
5	Design parameters and performance index . . . . .	109

## LIST OF FIGURES

1	Typical MAP response to a step vasopressor drug infusion . . . . .	3
2	Flowchart of SRCKF algorithm . . . . .	20
3	Bank of $N$ parallel SRCKFs for delay estimation . . . . .	21
4	Structure of nonlinear patient parameter generation . . . . .	24
5	Profile of piecewise constant PHP drug injection . . . . .	25
6	Nonlinear patient sensitivity estimation . . . . .	26
7	Nonlinear patient lag time estimation . . . . .	26
8	Nonlinear patient baseline MAP estimation . . . . .	27
9	Nonlinear patient input delay estimation . . . . .	27
10	Instantaneous blood pressure and MAP response to a piecewise constant PHP drug injection in an animal experiment . . . . .	29
11	MAP estimation results in an animal experiment . . . . .	30
12	Sensitivity estimation in an animal experiment . . . . .	30
13	Lag time estimation in an animal experiment . . . . .	31
14	Baseline MAP estimation in an animal experiment . . . . .	31
15	Time delay estimation in an animal experiment . . . . .	32
16	Closed-loop system structure . . . . .	35
17	Delay dependent time-varying controller gain, $K_c$ . . . . .	40
18	Bode plots for the closed-loop system for the time-delay interval $0.65\text{ sec} \leq \tau \leq 21.15\text{ sec}$ . . . . .	40
19	Schematic of the IMC strategy and equivalent closed-loop controller . . . . .	42
20	Robust stability criterion, Eq. (48) for different uncertainties on the delay and gain parameters with (a) lower bound of the time constant uncertainty, and (b) upper bound of the time constant uncertainty . . . . .	45
21	Logarithmic norm of the complementary sensitivity function vs. logarithmic dimensionless frequency, $\tilde{\omega}$ , for different values of delay uncertainty, $\epsilon$ , (a) not tuned, and (b) tuned controller . . . . .	46
22	Tracking performance and control effort for proposed controllers against a fixed PI controller with no disturbance and measurement noise . . . . .	48
23	Profile of disturbances in (a) input and (b) output channels . . . . .	49
24	Tracking performance and control effort for closed-loop system with disturbances and measurement noise . . . . .	50
25	Closed-loop performance of the parameter-varying loop-shaping and IMC-PID controllers in the presence of input and output disturbances and time delay estimation error (a) 30% overestimated time delay value, and (b) 30% underestimated time delay value . . . . .	51
26	Closed-loop response of system states $x_1$ , and $x_2$ subject to disturbance . . . . .	74
27	The overall interconnected system . . . . .	77
28	The overall interconnected system . . . . .	84
29	Varying uncertain time delay profile example . . . . .	93
30	Sampled-data closed-loop system configuration . . . . .	97
31	Closed-loop response and PHP injection rate of proposed LPV controller against fixed structure PI controller for disturbance and noise free case . . . . .	108
32	Closed-loop response and PHP injection rate of proposed LPV controller against fixed structure PI controller subject to disturbance and measurement noise . . . . .	109

33	Closed-loop MAP response and control effort (PHP injection rate) of robust LPV controller in the presence of model parameter uncertainty . . . . .	110
34	MAP response tacking performance and PHP injection rate of LPV controller against fixed structure PI controller under time delay uncertainty . . . . .	111
35	MAP response tacking performance and PHP injection rate of the proposed sample-data LPV controller under output disturbance . . . . .	112

# 1 Introduction

## 1.1 Automated Blood Pressure Regulation in Critical Patient Resuscitation

The human body has inherent feedback loops to maintain homeostasis, including the blood pressure regulation that may fail to perform properly under severe trauma, disease, or due to the administration of certain drugs. For this purpose, mean arterial blood pressure (MAP) regulation to the desired target value via administration of vasopressor drugs is essential in hypotensive critical emergency-care situations, such as resuscitation of patients with severe hemorrhage, septic shock, maternal cesarean hypotension treatment, and traumatic brain injury. The precise dosage of the administered vasopressor drug is essential to accomplish fast resuscitation and reliable manual MAP recovery, and therefore, sustain perfusions of vital organs without overdosing. Typically, in clinical care, MAP control and regulation procedures are carried out manually using a syringe or an infusion pump with a manual titration by the medical personnel. In these cases, drug delivery and adjustment may not be precisely managed, leading to undesirable or potentially fatal consequences, such as increased cardiac workload and cardiac arrest. Moreover, such drug administration methods are time-consuming and labor-intensive. Furthermore, inaccurate operator monitoring can lead to under- or over-resuscitation with potentially dangerous outcomes [39, 53]. Accordingly, the automation of the vasoactive drug infusion via feedback control has been proposed as a potential remedy to tackle the mentioned challenges of the manual drug administration [8]. To address the automated MAP regulation problem, several control design approaches including fractional-order proportional-integral (PI) and proportional-integral-derivative (PID) controls [86, 95], nonlinear PID digital control [83], adaptive predictive control [31, 38], robust multiple-model adaptive control [57], switching robust control [1], reinforcement learning [75], and more recently PID and loop-shaping control methods [91] have been considered.

In the first part of the dissertation, we address the computational modeling and online parameter estimation of the blood pressure response characteristics under vasoactive drug administration.

The second part will focus on the controller design methods for regulating MAP in hypotensive emergency-care situations.

### 1.1.1 MAP Response Dynamics

Mainly, two types of vasoactive drugs are being used to attain a target MAP in emergency resuscitation: (1) vasodilator drugs which decrease the MAP to a target value, like sodium nitroprusside (SNP) that reduces the tension in the blood vessel walls [33], and (2) vasopressor drugs which increase the MAP to a target value, like phenylephrine (PHP) that stimulates the depressed cardiovascular system and causes vasoconstriction [63]. In this dissertation, in line with the previous work in the literature (see [17, 53, 75, 91, 92]), a first-order model with a time delay is considered to characterize the patient's MAP response to the infusion of a vasoactive drug, such as PHP:

$$T(t) \cdot \Delta \dot{MAP}(t) + \Delta MAP(t) = K(t) \cdot u(t - \tau(t)), \quad (1)$$

where  $\Delta MAP(t)$  stands for the MAP changes in *mmHg* from its baseline value, *i.e.*,  $\Delta MAP(t) = MAP(t) - MAP_b(t)$ ,  $u(t)$  is the drug injection rate in *ml/h*,  $K(t)$  denotes the patient's sensitivity to the administered drug,  $T(t)$  is the lag time describing the uptake, distribution and bio-transformation of the drug [35], and  $\tau(t)$  is the time delay for the drug to reach the circulatory system from the injection site. The selected model structure seems to adequately describe a patient's physiological response to the PHP drug injection. Figure 1 presents a typical MAP response due to a step PHP infusion versus a matched response of (1). This figure also illustrates the interpretation of the model parameters  $K(t)$ ,  $T(t)$ ,  $\tau(t)$ ,  $MAP_b(t)$  which have been obtained to fit the MAP response using a least-squares optimization method. Data is collected from experiments on swine performed at the Resuscitation Research Laboratory at the University of Texas Medical Branch (UTMB), Galveston, Texas [53].

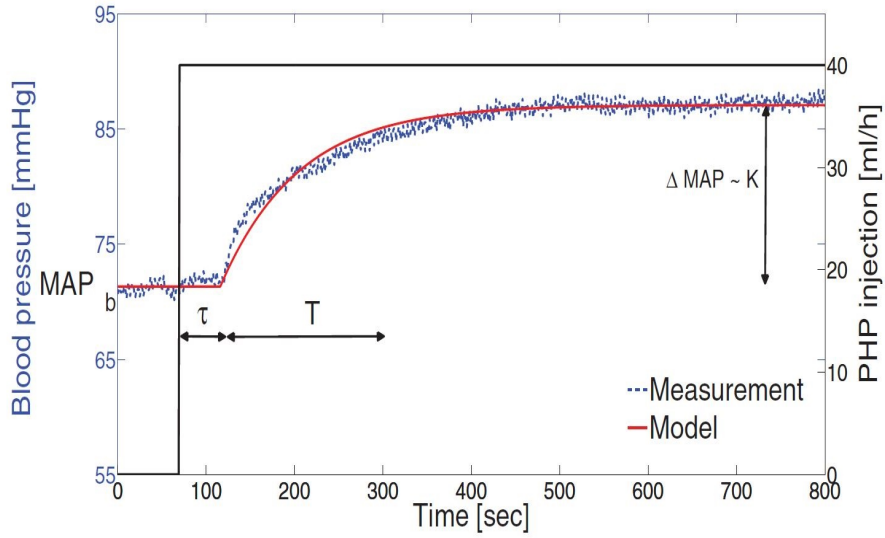


Figure 1: Typical MAP response to a step vasopressor drug infusion

Although the model (1) is qualitatively able to represent the characteristics of the MAP response, model parameters vary considerably over time due to the variability of patients' pharmacological state under the vasoactive drug infusion. That is, the model parameters and delay could vary significantly from patient-to-patient (inter-patient variability), as well as, for a patient over time (intra-patient variability) [35, 70].

For simulation purposes and in order to validate the proposed parameter estimation and control design algorithms in the dissertation, a patient simulation model is developed, where the instantaneous values of model parameters can be approximated as nonlinear functions of the drug injection rate. Model dynamics (1) with time-varying model parameters will address the patient's varying physiological response. Based on clinical observations, the model parameters are modeled as follows:

- Sensitivity,  $K(t)$ : In order to describe the time variation of the patient's sensitivity to the injected PHP drug, a simplified nonlinear model has been considered, which represent the dose response characteristic of PHP [21,26]. Moreover, experiments have confirmed a regressive nonlinear relationship between the vasoactive drug injection and the MAP response through

which the patient's sensitivity will decrease while having an ongoing vasoactive drug injection. Such a trend can be captured by the following nonlinear model

$$a_k \dot{K}(t) + K(t) = k_0 \exp\{-k_1 \mathcal{U}(t)\}, \quad (2)$$

where  $\mathcal{U}(t)$  denotes the injection rate in  $mm/h$  and  $a_k$ ,  $k_0$ , and  $k_1$  are uniformly distributed random coefficients based on Table 1 [21, 26]. For instance, a non-responsive patient to the injected vasoactive drug can be characterized by a low  $k_0$  and a high  $k_1$ .

Table 1: Probabilistic distribution of patient model coefficients

Parameter	Distribution
$a_k$	$\mathcal{U}(500, 600)$
$k_0$	$\mathcal{U}(0.1, 1)$
$k_1$	$\mathcal{U}(0.002, 0.007)$
$b_T$	$\mathcal{U}(10^{-4}, 3 \times 10^{-4})$
$a_{\tau,1}$	$\mathcal{U}(5, 15)$
$a_{\tau,2}$	$\mathcal{U}(5, 15)$
$b_{\tau,1}$	$\mathcal{U}(80, 120)$

- Lag time,  $T(t)$ : To characterize the variation of the drug distribution time, a saturation effect is assumed as follows:

$$T(t) = \text{sat}_{[T_{\min}, T_{\max}]} \{b_T \int_0^t \mathcal{U}(t) dt\}, \quad (3)$$

where  $b_T$  is a uniformly distributed random variable representing the inclination of the increase. Based on experiments, lag time parameter typically increases gradually proportional to the injected drug.

- Injection delay,  $\tau(t)$ : Based on the clinical observations, the delay value has a sharp peak shortly after the drug injection starts but decreases with further injections. The following

model is used to describe the time-varying behavior of delay parameter:

$$\begin{cases} a_{\tau,2}\ddot{\tau}(t) + a_{\tau,1}\dot{\tau}(t) + \tau(t) = b_{\tau,1}\dot{\mathcal{U}}(t) + \mathcal{U}(t), & t \geq t_0, \\ \tau(t) = 0, & \textit{otherwise}, \end{cases} \quad (4)$$

where the saturation should be imposed on the delay value, *i.e.*,  $\text{sat}_{[\tau_{\min}, \tau_{\max}]}$   $\tau$  and the uniformly distributed random variables  $a_{\tau,2}$ ,  $a_{\tau,1}$ , and  $b_{\tau,1}$  are listed in Table 1.

## 1.2 LPV Time-Delay Systems

Time-delay is ubiquitously encountered in numerous engineering systems due to measurement, transmission, computational delays, or unmodeled inertias of system components. In the context of feedback systems, time-delay or dead-time refers to the time that it takes for the closed-loop system to receive the required information, to make and execute control decisions, and to generate the control action [28]. Time delays can be constant or time-varying, point-wise or distributed, deterministic or stochastic [60]. In control systems, delay systems represent a class of infinite-dimensional systems, where the mathematical representation of such systems is given by infinite-dimensional functional differential equations (FDEs), as opposed to finite-dimensional systems with ordinary differential equations (ODEs). Moreover, time-delay is deemed as a source of instability and performance degradation, which complicate the controller design process. Time-delay induces a phase lag which generates oscillatory behavior, diminishes the stability margin of a control system, and limits the achievable bandwidth [2]. Some examples of extensively examined time-delay systems include automotive systems [89], communication systems [46], robotics [18], biomedical systems [91], network control systems [99], smart materials [55], and manufacturing and chemical processes [13].

Stability analysis and control design for time-delay systems have been broadly investigated using either frequency-domain or time-domain approaches. For instance, authors in [59, 66] used Smith predictor as a delay compensator for systems with a constant time delay that can be measured or estimated precisely. However, such predictors include additional unstable hidden modes, and also the utilized frequency-domain method is not applicable to the time-varying delay case. Another

indirect approach confronting systems with delay is to utilize methods, such as Padé approximation to approximate the infinite-dimensional time delay system by a rational finite-dimensional model to be able to take the advantages of the rich linear control design methodologies [24, 25].

Time delay systems cannot be treated properly and efficiently using conventional control design methods, such as Laplace domain-based methods since the corresponding transfer function of the time-delay system is not rational. In this regard, stability analysis and designing stabilizing controllers for time-delay systems have been divided into two main directions, namely, delay-independent and delay-dependent criteria [28]. The results obtained from delay-independent methods are very conservative since they must provide guarantees for all non-negative and finite time-delay values. Unlike the former direction, delay-dependent techniques take the size of delay into consideration and result in less conservative results. Indeed, approaches based on delay-dependent criteria result in less conservative conditions, ensuring the stability and the prescribed performance level of a delayed system with delay values smaller than a considered bound. Generally, in delay-dependent methods, Lyapunov theory is extended to either the Krasovskii method of Lyapunov functionals [40] or Razumnikhin theory of Lyapunov functions [36]. The former direction relies on using Lyapunov-Krasovskii functionals (LKFs) for accounting for the infinite-dimensionality of the system state in the time-delay systems and usually leads to less conservative results.

Linear parameter-varying (LPV) systems are linear dynamical systems whose dynamic characteristics depend on a time-varying measurable scheduling parameter vector. In this context of the LPV systems framework, the scheduling parameter vector captures the dynamics of nonlinear or time-varying systems in a systematic fashion [15] and has found applications in flight control [52], automotive systems [73, 89], energy [11], electromechanical [45], and biomedical systems [20, 91]. Traditional gain-scheduling controllers are designed by interpolation of separately designed controllers for the system's operation points. Such design methods suffer from implementation difficulties and lack of closed-loop stability and performance guarantees [10, 78]. In order to tackle these challenges, the LPV gain-scheduling control approach was introduced to provide a direct, efficient, simple-to-implement, and systematic design process to meet closed-loop stability and performance of nonlinear

and time-varying systems [77].

Motivated by LPV methodology, the mentioned delay-independent and delay-dependent approaches have also been developed for the stability analysis and control synthesis of time-delay LPV systems [15, 60, 73, 90, 92]. The mean-square stability of stochastic LPV systems with delayed measurements has been studied in [103]. The authors in [97], derived delay-dependent sufficient conditions for the closed-loop stabilization of LPV systems with an input delay. In another work, a robust static gain-scheduled controller design for discrete-time polytopic LPV systems with a state delay has been formulated in a delay-independent matrix inequality framework [72]. Dilated delay-dependent linear matrix inequalities (LMIs) for the control of state-delay polytopic LPV systems have been addressed in [62]. In this work, the coupling between controller matrices and Lyapunov matrix functions has been avoided, and a gain-scheduled dynamic output-feedback controller with memory has been designed to reject disturbances.

### 1.3 Outline of the Dissertation

The results presented in this dissertation either have been published or are under review for publication [89–93]. In this dissertation, we study the analysis and controller synthesis of time-delay systems. Furthermore, a robust control design for a class of LPV systems with parametric and delay uncertainties will be addressed. As a practical, real-life application, we assess the potential of the proposed estimation and control design strategies in the automated MAP regulation problem. Chapter 1 gives the background, main motivations, and design objectives behind the considered patient resuscitation task. Mathematical modeling is discussed, and the patient’s MAP response dynamics subject to vasoactive drug administration are characterized by a dynamic first-order linear time-varying model with adjustable, varying parameters and input delay. Such a dynamic model can effectively address the complexity and the intra- and inter-patient variability of the physiological response to vasoactive drugs.

In chapter 2, real-time dynamics identification of a patient’s MAP response to vasoactive drug

infusion is studied. A Bayesian-based multiple-model square root cubature Kalman filtering (MM-SRCKF) approach is utilized for the real-time estimation of the model's time-varying parameters. Validation results are proved to confirm the effectiveness of the developed identification algorithm both in simulation scenarios and using experiment data.

Chapter 3 introduces robust IMC-PID and parameter-varying loop-shaping as simple-to-implement frequency-domain-based control design approaches for automatically regulating blood pressure in critical hypotensive patients via vasopressor drug administration. The considered MAP response dynamics model includes a time-varying delay in the control input, which restricts the implementation of conventional control techniques. The proposed methods are examined to address the variability and the time-varying delay of the physiological response to the drug. First, a Padé approximation is used to transform the infinite-dimensional delay problem into a finite-dimensional model represented in the form of a non-minimum phase (NMP) system. A systematic parameter-varying loop-shaping control is proposed to provide the closed-loop system with stability and tracking performance in the presence of measurement noise and disturbances. Second, an internal model control (IMC) strategy is examined to design a fixed PID controller cascaded with a lag compensator by considering the time-varying model to be an uncertain perturbed system. The small-gain theorem has been employed to investigate the robust stability and account for system uncertainty. The proposed control methods are applied to critical hypotensive patient resuscitation to regulate MAP while considering the limitations posed by the time-varying parameters of the physiological response model and the large time-varying delay.

Chapter 4 details the development of robust delay-dependent gain-scheduling feedback control laws with guaranteed closed-loop stability and induced  $\mathcal{L}_2$  norm performance for continuous-time LPV systems with arbitrary time-varying delay in the presence of parametric or time-delay uncertainties. An extension of Lyapunov stability utilizing Krasovskii functionals is considered to derive stability analysis and synthesis conditions for delay-dependent dynamic output feedback LPV control design. The main challenges associated with this approach are selecting appropriate LKFs and finding efficient integral inequalities to bound the derivative of the LKF. Accordingly, a novel modified

parameter-dependent LKF candidate along with an affine version of Jensen’s inequality bounding technique are employed leading to the derivation of less conservative sufficient conditions expressed in terms of convex LMI optimization problems to be solved using efficient interior-point solvers. The proposed methodology is compared with past work in the literature in terms of conservatism reduction and performance improvement through a numerical example. Moreover, the stability analysis and control of LPV systems with varying uncertain delay is examined in this chapter. To this end, the time-delay LPV system is described in an input-output representation, and the scaled small-gain theorem is employed to analyze the varying delay in a less conservative approach. The proposed results are then utilized in the automated MAP regulation in the clinical resuscitation of patients sustaining hypotension. In order to conduct simulations, nonlinear model parameter generators are cascaded with the estimators, and closed-loop experiments confirm the proposed LPV control design benefits and efficacy.

Finally, chapter 5 concludes the dissertation by summarizing the present work’s essential contributions and providing remarks about future research directions.

## 1.4 Notation

The notation used in the dissertation is standard and as follows. Throughout the dissertation  $\mathbb{R}^n$  stands for the  $n$ -dimensional Euclidean space,  $\mathbb{R}^{k \times m}$  is the set of real  $k \times m$  matrices, and  $\mathbb{R}_+$  denotes the set of non-negative real numbers.  $\mathbb{S}^n$  and  $\mathbb{S}_{++}^n$  represent the set of real symmetric and real symmetric positive definite  $n \times n$  matrices, respectively.  $\mathbf{M} \succ \mathbf{0}$  and  $\mathbf{M} \succeq \mathbf{0}$  ( $\mathbf{M} \prec \mathbf{0}$  and  $\mathbf{M} \preceq \mathbf{0}$ ) denote the positive (negative) definiteness and semi-definiteness of the matrix  $\mathbf{M}$ . The inverse and transpose of a real matrix  $\mathbf{M}$  are presented by  $\mathbf{M}^T$  and  $\mathbf{M}^{-1}$ , respectively.  $He[\mathbf{M}]$  is Hermitian operator defined as  $He[\mathbf{M}] \triangleq \mathbf{M} + \mathbf{M}^T$ . In a symmetric matrix, terms denoted by an asterisk,  $\star$ , will be induced by symmetry as shown below:

$$\begin{bmatrix} S + W + J + (\star) & \star \\ Q & R \end{bmatrix} := \begin{bmatrix} S + W + W^T + J + J^T & Q^T \\ Q & R \end{bmatrix}$$

where  $S$  is symmetric.  $\mathcal{C}(J, K)$  stands for the set of continuous functions mapping a set  $J$  to a set  $K$ . Notation  $\mathcal{L}_2$  stands for the space of square integrable functions  $f : [0, \infty] \rightarrow \mathbb{R}^n$  with the  $\mathcal{L}_2$ -norm  $\|f\|_{\mathcal{L}_2} = \{\int_0^\infty f^T(t)f(t)dt\}^{1/2}$ , where  $f(t)$  is a vector valued function.  $\|f(t)\|_{\mathcal{L}_2}$  is also considered as the energy of  $f(t)$ . Moreover,  $t$  denotes the continuous-time domain, and  $k$  stands for the discrete-time variable. For a stochastic variable,  $\mathbf{x}_k$ ,  $\mathcal{E}[\mathbf{x}_k]$  denotes its expected value, and  $\mathcal{N}\{\mathbf{x}_k; \hat{\mathbf{x}}_{k|k}, \mathbf{P}_{k|k}\}$  represents a normal Gaussian probability distribution with the mean of  $\hat{\mathbf{x}}_{k|k}$  and the covariance of  $\mathbf{P}_{k|k}$ .

## 2 Real-Time Bayesian Parameter Estimation of Blood Pressure Response Characteristics

The following chapter first appeared in the proceedings of American Control Conference (ACC), 2020, pp. 3355-3362.

Title: Real-Time Cubature Kalman Filter Parameter Estimation of Blood Pressure Response Characteristics Under Vasoactive Drugs Administration

Authors: Shahin Tasoujian, Saeed Salavati, Karolos Grigoriadis, Matthew Franchek.

Reproduced in part with permission from IEEE American Control Conference Copyright 2020.

### 2.1 Introduction and Literature Review

There are multiple approaches to address the estimation of dynamical system parameters. Extended Kalman filtering (EKF) is one of the widely used methods [53]. However, it is only applicable to systems with mild nonlinearities, and it requires the Jacobian matrix computation. Moreover, numerical errors due to truncation and convergence problems are likely in EKF, and other local approximation based estimators [5]. In an alternative approach, known as the sampling method, the nonlinear representation of a system is used to estimate the parameters via a filter such as the unscented Kalman filter (UKF), which leads to more accurate estimation. In UKF, a set of weighted sampling points propagates via the nonlinear function of the system. However, for higher-order systems, UKF is prone to numerical instability since the weights of the sigma points may become negative [104]. Another sampling method is particle filtering (PF), which is an iterative Monte Carlo based method to compute the posterior probability distribution of the state of a nonlinear system even with non-Gaussian noise. PF requires a broad set of randomly generated particles to approximate the posterior probability density function. Under an increase in the number of iterations, PF encounters particle degradation and depletion. In order to overcome such issues, the authors in [5] have proposed a Bayesian filtering framework known as cubature Kalman filtering (CKF). The sample points in the CKF algorithm propagate via equally valued cubature points, which are twice

the size of the system nonlinear function. It uses a spherical-radial cubature rule to generate the weighted sum of sampling points to approximate the integrals in Bayesian estimation. CKF demonstrates better nonlinear performance, stability, and accuracy compared to EKF, PF, and UKF [104]. Similar to the EKF, the computational complexity of the CKF algorithm grows as  $n^3$ , where  $n$  is the dimension of the system state vector.

Traditional parameter estimation methods, such as the recursive least-squares algorithm and instrumental-variable approach, have been examined for real-time parameter estimation problems in biomedical applications [6, 49, 70]. Specifically, variance models have been proposed to characterize the mean arterial blood pressure (MAP) response of patients to drug infusion [8, 21]. However, these methods fail to sufficiently address the pharmacological variability challenge and often suffer from a slow convergence rate. In [29], the authors have used a first-order model with delayed measurements to describe the MAP dynamics in response to hypotensive drugs. They have pre-identified the parameters using dose-response characteristics induced by a rectangular test signal while avoiding any adverse effect on the patient. If the identified parameters are not within the prescribed bounds, then the experiment will be repeated. Nonetheless, in the case of outlying identification results, the worst-case parameters are used. The output is filtered by a constant filter, which has been derived using trial and error. The delay is determined via the response settling characteristics. In another work, a generalized fuzzy neural network framework has been studied to estimate and control MAP dynamics in response to vasodilator drugs [30]. The parameters have been assumed to be nonlinear functions of the measured MAP. This method requires a training dataset and an effective learning algorithm for the artificial scheme. Moreover, overparameterization and the determination of the number of perceptrons remain as other obstacles.

Based on the time delay model introduced in [84], the authors in [106] have proposed discrete-time parameters update laws. However, the procedure of the parameters identification of the original model has not been addressed. A bank of Kalman filters (KFs) augmented with a posterior probability estimator to match a candidate model to that of the patient has been designed in [57]. Each KF is responsible for generating the state vector updates for the next step, and the Kalman gain

is assumed to be generated a priori. Then, by calculating the residual of the actual and generated output, the state vector is updated accordingly. In order to capture the varying time delay, which a conventional KF is not capable of, the multiple-model (MM) approach has been adopted through which five equally spaced delay blocks from 10s to 50s, each is considered to be cascaded with the same bank of KFs. The recursive posterior probability estimation is calculated for each residual to update the input with the most likely delay. In a similar approach, [23] has examined KF to estimate the MAP dynamics parameters in hypertension. In this work, authors have utilized the model introduced first in [84]. They have discretized and transformed the infinite-dimensional model into a linear one that accommodates an input with three backward steps. Then, the parameters are gathered in a vector that is updated through the KF approach. However, it should be noted that the conventional KF algorithm's convergence can only be guaranteed in an ideal linear-Gaussian environment. Reference [56] has addressed the marginalized PF design to estimate the model parameters in the case of hypertension under SNP administration. The method allows considering linear and nonlinear states to be estimated separately to reduce the computational burden.

In more recent work, [54] utilized EKF for the real-time estimation of the MAP response model parameters. Although this approach can provide real-time parameter identification of a patient's MAP response dynamics, the estimation can be inaccurate when the response is away from the equilibrium point since EKF relies on local linearization [81]. Moreover, the utilized parameter identification approach is not capable of providing a consistent estimate of the time-lag parameter of the LPV model. Thus, to overcome the previously utilized estimation methods' inherent limitations, we propose a multiple-model square-root cubature Kalman filter (MMSRCKF) as a real-time model parameter and time-delay estimation method of the MAP response dynamics. MMSRCKF is a Bayesian filtering approach that can precisely estimate the model parameters and addresses the stochasticity in the nonlinear model without a need for linearization. Contributions of this chapter are as follows: MMSRCKF is proposed to estimate the nonlinear MAP response model parameters effectively. In the case of hypotension, the patient's MAP response dynamic under a vasopressor drug injection is described by a time-varying model with a varying input delay. These varying

quantities are augmented in a vector whose instantaneous values are estimated via MMSRCKF. The multiple-model part addresses the hypothesis testing and the estimation of the input delay. The square root (SR) algorithm employs the Cholesky factorization of the error covariance matrix to guarantee its positive definiteness during numerical operations [22]. For the verification of the proposed method, data from animal experiments is collected at the University of Texas, Medical Branch (UTMB) at Galveston. The estimation results are compared to that of MMEKF reported in [53].

## 2.2 Estimation Preliminaries and Methodology

In this section, a derivative-free online sequential state estimator known as the square root CKF (SRCKF) algorithm is formulated for a general nonlinear discrete-time stochastic system. Subsequently, the multiple-model approach is formulated and coupled with the introduced SRCKF algorithm for the time-delay estimation of a system with an input delay.

### 2.2.1 SRCKF Algorithm

The Bayesian-based CKF scheme aims at estimating the states of a dynamical system using a probabilistic framework [5]. The original CKF state estimation process is susceptible to numerical problems such as indefinite error covariance matrix, divergence phenomenon, and filter instability. To tackle these obstacles, CKF is enhanced with the square root computation, *i.e.*, the covariance matrix is decomposed using a factorization method, such as the Cholesky factorization to guarantee positive definiteness within numerical operations [50]. The resulting square roots of the error covariance matrices propagate through the sequential state estimation process. Next, the third-degree spherical-radial rule is used to approximate the multidimensional integrals involved in the Bayesian filtering [37].

Consider a general nonlinear discrete-time stochastic system

$$\begin{cases} \mathbf{x}_{k+1} &= \mathbf{f}(\mathbf{x}_k, \mathbf{u}_k) + \mathbf{w}_k, \\ \mathbf{y}_k &= \mathbf{h}(\mathbf{x}_k, \mathbf{u}_k) + \mathbf{v}_k, \quad k = 0, 1, \dots, k_f, \end{cases} \quad (5)$$

where  $\mathbf{x}_k \in \mathbb{R}^n$  stands for the unmeasured state vector of the system,  $\mathbf{u}_k \in \mathbb{R}^{n_u}$  is the input vector, and  $\mathbf{y}_k \in \mathbb{R}^{n_y}$  is the measurement vector at the time  $k$ , and  $k_f$  is the final time.  $\mathbf{f}(\mathbf{x}_k, \mathbf{u}_k) : (\mathbb{R}^n, \mathbb{R}^{n_u}) \mapsto \mathbb{R}^n$  and  $\mathbf{h}(\mathbf{x}_k, \mathbf{u}_k) : (\mathbb{R}^n, \mathbb{R}^{n_u}) \mapsto \mathbb{R}^{n_y}$  are known general nonlinear vector mappings, and  $\mathbf{w}_k \in \mathbb{R}^n$  and  $\mathbf{v}_k \in \mathbb{R}^{n_y}$  are statistically independent zero-mean Gaussian process and measurement noise signals, respectively. The probability distribution functions (PDFs) of the noise vectors, namely  $p(\mathbf{w}_k)$  and  $p(\mathbf{v}_k)$  are known, as well as, the initial state vector PDF, *i.e.*,  $p(\mathbf{x}_0)$ .

SRCKF seeks to find the estimation of the state vector in the form of a conditional PDF,  $p(\mathbf{x}_k | \mathbf{y}^k)$ , that has the entire knowledge about the current state vector,  $\mathbf{x}_k$ , given the entire measurement vectors sequence, *i.e.*,  $\mathbf{y}^k = [\mathbf{y}_0 \ \mathbf{y}_1 \ \dots \ \mathbf{y}_k]$ . However, in some cases, a Gaussian approximation of the conditional PDF allows to only compute the first two conditional moments, *i.e.*, the mean  $\widehat{\mathbf{x}}_{k|k} = \mathcal{E}[\mathbf{x}_k | \mathbf{y}^k]$  and the error covariance matrix  $\mathbf{P}_{k|k} = \text{cov}[\mathbf{x}_k | \mathbf{y}^k]$  which results in  $p(\mathbf{x}_k | \mathbf{y}^k) \approx \mathcal{N}\{\mathbf{x}_k; \widehat{\mathbf{x}}_{k|k}, \mathbf{P}_{k|k}\}$ . By assuming Gaussian white noise vectors, the prediction step (state prediction) and correction step (measurement update) are carried out via integrating a nonlinear function concerning a normal distribution, *i.e.*,

$$\widehat{\mathbf{x}}_{k+1|k} = \mathcal{E}[\mathbf{x}_{k+1} | \mathbf{y}^k] = \int_{\mathbb{R}^n} \mathbf{f}(\mathbf{x}_k, \mathbf{u}_k) p(\mathbf{x}_k | \mathbf{y}^k) d\mathbf{x}_k \approx \int_{\mathbb{R}^n} \mathbf{f}(\mathbf{x}_k, \mathbf{u}_k) \mathcal{N}\{\mathbf{x}_k; \widehat{\mathbf{x}}_{k|k}, \mathbf{P}_{k|k}\} d\mathbf{x}_k, \quad (6)$$

and

$$\begin{aligned} \widehat{\mathbf{y}}_{k+1|k} &= \mathcal{E}[\mathbf{y}_{k+1} | \mathbf{x}_{k+1}] = \int_{\mathbb{R}^n} \mathbf{h}(\mathbf{x}_{k+1}, \mathbf{u}_{k+1}) p(\mathbf{y}_{k+1} | \mathbf{x}_{k+1}) d\mathbf{x}_{k+1} \\ &\approx \int_{\mathbb{R}^n} \mathbf{h}(\mathbf{x}_{k+1}, \mathbf{u}_{k+1}) \mathcal{N}\{\mathbf{x}_{k+1}; \widehat{\mathbf{x}}_{k+1|k}, \mathbf{P}_{k+1|k}\} d\mathbf{x}_{k+1}. \end{aligned} \quad (7)$$

The third-degree spherical-radial rule is utilized to compute the numerical approximation of the moment integrals (6) and (7). Next, for an arbitrary function  $g(\mathbf{x})$  with  $\Sigma$  as the covariance of  $\mathbf{x}$ ,

the integral

$$I(g) = \sqrt{2\pi} |\boldsymbol{\Sigma}|^{-\frac{1}{2}} \int_{\mathbb{R}^n} g(\mathbf{x}) \exp \left[ -\frac{1}{2} (\mathbf{x} - \boldsymbol{\mu})^T \boldsymbol{\Sigma}^{-1} (\mathbf{x} - \boldsymbol{\mu}) \right] d\mathbf{x}, \quad (8)$$

in the spherical coordinate system becomes

$$I(g) = (2\pi)^{-\frac{n}{2}} \int_{r=0}^{\infty} \int_{\mathbb{U}_n} g(\mathbf{C}r\mathbf{z} + \boldsymbol{\mu}) d\mathbf{z} r^{n-1} e^{-\frac{r^2}{2}} dr, \quad (9)$$

where  $\mathbf{x} = \mathbf{C}r\mathbf{z} + \boldsymbol{\mu}$  with  $\|\mathbf{z}\| = 1$ ,  $\boldsymbol{\mu}$  is the mean and  $\mathbf{C}$  is the Cholesky factor of the covariance,  $\boldsymbol{\Sigma}$ , and  $\mathbb{U}_n$  is the unit sphere. Then, we used the symmetric spherical cubature rule to further approximate the integral as

$$I(g) \approx \frac{1}{2n} \sum_{i=0}^{2n} g(\sqrt{n}(\mathbf{C}\xi_i + \boldsymbol{\mu})), \quad (10)$$

where  $\xi_i$  denotes the  $i$ th cubature point at the intersection of the unit sphere and its axes. The main benefit of this scheme is that the cubature points are obtained off-line using a third-degree cubature rule [48]. We follow the steps introduced next to compute the estimation of the state vector via the SRCKF algorithm:

1. **Initialization:** The state initial condition is given by  $\mathbf{x}_{0|0} \equiv \mathbf{x}_0$  with  $\widehat{\mathbf{x}}_0 = \mathcal{E}[\mathbf{x}_0]$  where the initial covariance matrix is  $\mathbf{P}_{0|0}$ . We decompose it as  $\mathbf{P}_{0|0} = \mathbf{S}_{0|0} \mathbf{S}_{0|0}^T$  through the Cholesky factorization, *i.e.*,

$$\mathbf{S}_{0|0} = \text{chol}\{[\mathbf{x}_0 - \widehat{\mathbf{x}}_0][\mathbf{x}_0 - \widehat{\mathbf{x}}_0]^T\}.$$

Then, generate the cubature points,  $\boldsymbol{\xi}_i$ , for the initial state vector and the fixed weights,  $w_i = w = \frac{1}{2n}$ , for  $i = 1, 2, \dots, 2n$ .

2. **Time update (Prediction)** ( $k = 1, 2, \dots, k_f$ ):

a) Evaluation of the cubature points

$$\mathbf{X}_{i,k-1|k-1} = \mathbf{S}_{k-1|k-1} \boldsymbol{\xi}_i + \widehat{\mathbf{x}}_{k-1|k-1}. \quad (11)$$

b) Evaluation of the propagated cubature points via the system dynamics

$$\mathbf{X}_{i,k|k-1}^* = \mathbf{f}_k(\mathbf{X}_{i,k-1|k-1}, \mathbf{u}_{k-1}). \quad (12)$$

c) Evaluation of the predicted states based on the generated weights and propagated points

$$\widehat{\mathbf{x}}_{k|k-1} = \sum_{i=1}^{2n} w_i \mathbf{X}_{i,k|k-1}^*. \quad (13)$$

d) Evaluation of the square root of the covariance matrix of the predicted state error covariance

$$\mathbf{S}_{k|k-1} = \mathit{triangle}\{\boldsymbol{\chi}_{k|k-1}^*, \mathbf{S}_{\mathbf{Q}_{k-1}}\}, \quad (14)$$

where  $\boldsymbol{\chi}_{k|k-1}^*$  is a centered weighted matrix, *i.e.*,

$$\boldsymbol{\chi}_{k|k-1}^* = \frac{1}{\sqrt{2n}} [\mathbf{X}_{1,k|k-1}^* - \widehat{\mathbf{x}}_{k|k-1} \quad \mathbf{X}_{2,k|k-1}^* - \widehat{\mathbf{x}}_{k|k-1} \quad \cdots \quad \mathbf{X}_{2n,k|k-1}^* - \widehat{\mathbf{x}}_{k|k-1}], \quad (15)$$

and  $\mathbf{S}_{\mathbf{Q}_{k-1}}$  is the square-root of the the process noise such that  $\mathbf{Q}_{k-1} = \mathbf{S}_{\mathbf{Q}_{k-1}} \mathbf{S}_{\mathbf{Q}_{k-1}}^T$ . Moreover,  $\mathbf{B} = \mathit{triangle}\{\mathbf{A}\}$  stands for a general triangularization algorithm, *e.g.* QR decomposition, where  $\mathbf{B}$  is a lower triangular matrix. If  $\mathbf{C}$  is an upper triangular matrix obtained through the QR decomposition of  $\mathbf{A}^T$ , then the lower triangular matrix is given by  $\mathbf{B} = \mathbf{C}^T$ .

### 3. Measurement update (Correction) ( $k = 1, 2, \dots, k_f$ ):

a) Evaluation of the cubature points using the predicted square root matrix,  $\mathbf{S}_{k|k-1}$ ,

$$\mathbf{X}_{i,k|k-1} = \mathbf{S}_{k|k-1} \boldsymbol{\xi}_i + \widehat{\mathbf{x}}_{k|k-1}. \quad (16)$$

b) Evaluation of the propagated cubature point via the output dynamics

$$\mathbf{Y}_{i,k|k-1} = \mathbf{h}(\mathbf{X}_{i,k|k-1}, \mathbf{u}_k). \quad (17)$$

c) Estimation of the predicted measurement vector

$$\widehat{\mathbf{y}}_{k|k-1} = \sum_{i=1}^{2n} w_i \mathbf{Y}_{i,k|k-1}. \quad (18)$$

d) Evaluation of the square root of the innovation covariance matrix

$$\mathbf{S}_{yy,k|k-1} = \text{triangle}\{[\mathbf{Y}_{k|k-1}, \mathbf{S}_{\mathbf{R}_k}]\}, \quad (19)$$

where  $\mathbf{Y}_{k|k-1}$  is a centered weighted matrix, *i.e.*,

$$\mathbf{Y}_{k|k-1} = \frac{1}{\sqrt{2n}} [\mathbf{Y}_{1,k|k-1} - \widehat{\mathbf{y}}_{k|k-1} \quad \mathbf{Y}_{2,k|k-1} - \widehat{\mathbf{y}}_{k|k-1} \quad \cdots \quad \mathbf{Y}_{2n,k|k-1} - \widehat{\mathbf{y}}_{k|k-1} ]. \quad (20)$$

$\mathbf{S}_{\mathbf{R}_k}$  is also the square-root of the the measurement noise such that  $\mathbf{R}_k = \mathbf{S}_{\mathbf{R}_k} \mathbf{S}_{\mathbf{R}_k}^T$ .

e) Evaluation of the cross-covariance matrix

$$\mathbf{P}_{xy,k|k-1} = \boldsymbol{\chi}_{k|k-1} \mathbf{Y}_{k|k-1}^T, \quad (21)$$

with the centered weighted matrix  $\boldsymbol{\chi}_{k|k-1}$  given by

$$\boldsymbol{\chi}_{k|k-1} = \frac{1}{\sqrt{2n}} [\mathbf{X}_{1,k|k-1} - \widehat{\mathbf{x}}_{k|k-1} \quad \mathbf{X}_{2,k|k-1} - \widehat{\mathbf{x}}_{k|k-1} \quad \cdots \quad \mathbf{X}_{2n,k|k-1} - \widehat{\mathbf{x}}_{k|k-1} ]. \quad (22)$$

f) Evaluation of the SRCKF filter gain

$$\mathbf{W}_k = \mathbf{P}_{xy,k|k-1} \mathbf{S}_{yy,k|k-1}^{-T} \mathbf{S}_{yy,k|k-1}^{-1}. \quad (23)$$

g) Evaluation of the corrected state update based on the measurement

$$\widehat{\mathbf{x}}_{k|k} = \widehat{\mathbf{x}}_{k|k-1} + \mathbf{W}_k (\mathbf{y}_k - \widehat{\mathbf{y}}_{k|k-1}). \quad (24)$$

h) Evaluation of the square-root of the corrected error covariance matrix

$$\mathbf{S}_{k|k} = \mathit{triangle}\{\boldsymbol{\chi}_{k|k-1} - \mathbf{W}_k \mathbf{Y}_{k|k-1}, \mathbf{W}_k \mathbf{S}_{\mathbf{R}_k}\}. \quad (25)$$

The state estimation process continues iteratively from the second step of the algorithm, *i.e.*, the time update (prediction) by setting  $k = k + 1$ . The flowchart depicting the SRCKF algorithm is shown in Fig. 2.

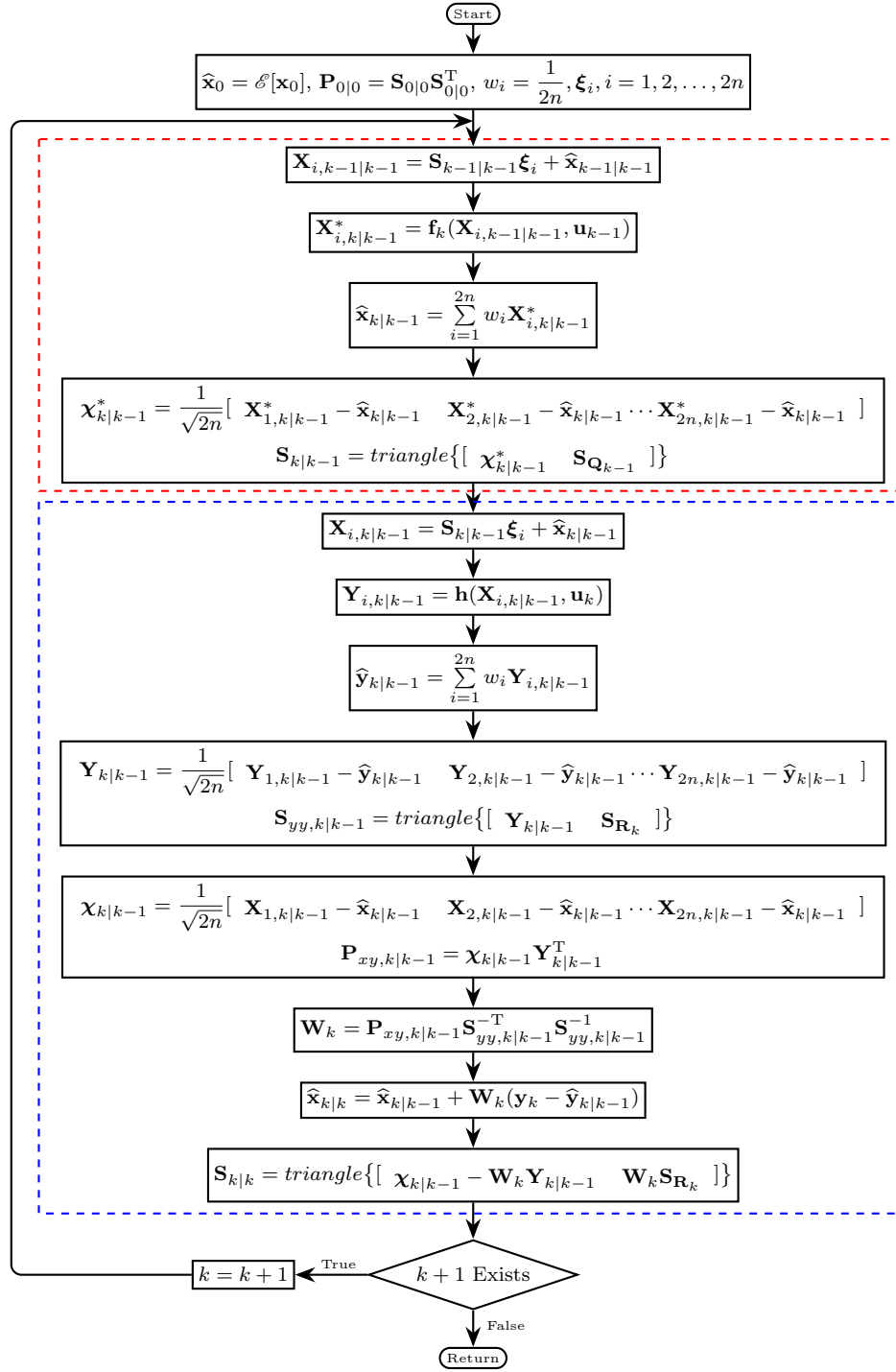


Figure 2: Flowchart of SRCKF algorithm

### 2.2.2 Multiple-Model SRCKF for Input Delay Estimation

Time delay estimation introduces a challenge in the parameter identification framework since the variable delay is not transformable to an equivalent random walk process. Rational approximations of the delay, such as Padé approximation, can be considered as alternative solutions; however, the introduced truncation error may be significant and problematic, especially for large and time-varying delays. Thus, to obtain a more accurate delay estimation, the aforementioned SRCKF algorithm is equipped with a multiple-model framework cascaded with a hypothesis testing module [32].

The underlying idea of the MMSRCKF method is to use a bank of  $N$  identical SRCKFs in a parallel setting, as shown in Fig. 3.

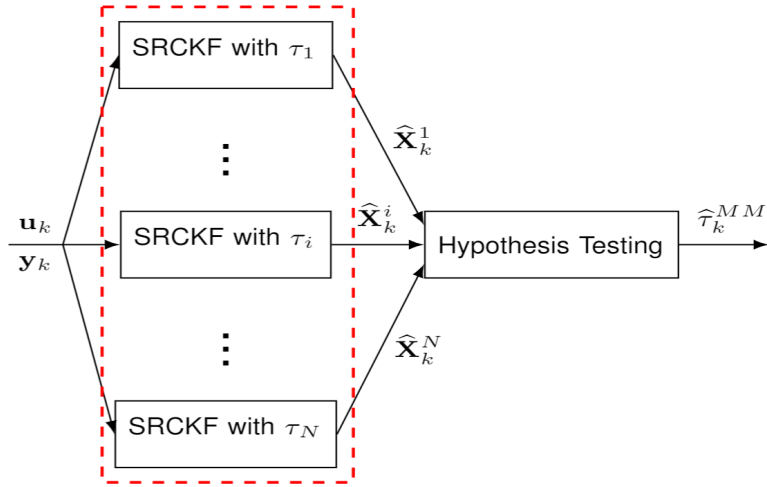


Figure 3: Bank of  $N$  parallel SRCKFs for delay estimation

Every SRCKF uses the same measurement and input data, but a different delay is assigned to each filter. The  $i$ th element in the bank provides us with a state vector estimation  $\mathbf{X}_k^i$  together with the residuals  $\mathbf{r}_k^i = \mathbf{y}_k - \hat{\mathbf{y}}_k^i$ . By having this information, a hypothesis testing block can then be used to estimate the value of the delay. Specifically, if the delay matches the one assigned to the  $i$ th SRCKF element, then the corresponding residual is essentially a zero-mean white noise process,

*i.e.*,  $\mathcal{E}[\mathbf{r}_k^i] = 0$ , and its covariance is given by

$$\mathcal{E}[\mathbf{r}_k^i(\mathbf{r}_k^i)^T] = \mathbf{H}\mathbf{P}_k^i\mathbf{H}^T + \mathbf{R} \triangleq \mathbf{R}_k^i, \quad (26)$$

with  $\mathbf{H} = [1 \ 0 \ 0 \ 1]$ ,  $\mathbf{P}_k^i$  denotes the estimation covariance at the  $k$ th step, and  $\mathbf{R}$  stands for the measurement noise covariance. The conditional probability density function of the  $i$ th SRCKF element measurement can be computed through

$$f(\hat{y}_k^i|y_k) = \frac{1}{(2\pi)^{\frac{m}{2}} |\mathbf{R}_k^i|^{\frac{1}{2}}} \exp\left\{-\frac{1}{2}(\mathbf{r}_k^i)^T(\mathbf{R}_k^i)^{-1}\mathbf{r}_k^i\right\}, \quad (27)$$

where  $m$  is the dimension of available measurements at each time step. Then, the conditional probability of each hypothesis is

$$p_k^i = \frac{f(\hat{y}_k^i|y_k)p_{k-1}^i}{\sum_{j=1}^N f(\hat{y}_k^j|y_k)p_{k-1}^j}, \quad (28)$$

where  $p_k^i$  can be interpreted as the normalized conditional probability of the case when the delay equals the assigned value to the  $i$ th filter, *i.e.*,  $\sum_{j=1}^N p_k^j = 1$ . Now, it is possible to estimate the delay according to the filter, which has the highest probability. However, for a more accurate delay estimation and to avoid large fluctuations, instead of choosing the block with the most probable delay estimation, we treat the hypotheses resulting as weights and blend them to improve the delay estimation. In other words, we can estimate the time delay as

$$\hat{\tau}_k^{MM} = \sum_{j=1}^N p_k^j \tau_k^j, \quad (29)$$

and  $\tau_k^j$  is the delay estimation of the  $i$ th filter. Next, a bank of  $N$  parallel SRCKF estimators of the MMSRCKF (see Fig. 3) will be implemented for the model parameter and time delay estimation of the MAP response dynamics.

### 2.3 MAP Response Estimation Results and Validations

Considering the continuous-time model (1), which characterizes the patient's MAP response to the infusion of a vasoactive drug, to implement recursive sequential estimation tools, we need to discretize the continuous-time model at the sampling rate of  $T_s$  as follows

$$\begin{cases} x_{k+1} &= \left(1 - \frac{T_s}{T_k}\right)x_k + \frac{K_k T_s}{T_k} u_{(k - \frac{\tau_k}{T_s})}, \\ y_k &= x_k + MAP_{b_k}, \end{cases} \quad (30)$$

where  $x_k = \Delta MAP_k = MAP_k - MAP_{b_k}$  at the  $k$ th time instant. In (30), we augment the state vector with the parameters to be estimated, namely  $K_k, T_k$ , and  $MAP_{b_k}$ , *i.e.*,

$$\mathbf{X}_k^T = [X_k^1 \quad X_k^2 \quad X_k^3 \quad X_k^4] = [\Delta MAP_k \quad K_k \quad T_k \quad MAP_{b_k}]. \quad (31)$$

Since model parameters are time-varying and assumed to be *a priori* unknown, (30) represents a nonlinear equation with regards to the state vector,  $\mathbf{X}_k$ , that can be expressed as the following nonlinear dynamics

$$\begin{cases} X_{k+1}^1 &= \mathbf{f}_k(\mathbf{X}_k, u_k) + w_k, \\ y_k &= h_k(\mathbf{X}_k) + v_k, \end{cases} \quad (32)$$

with

$$\begin{cases} f_k^1(\mathbf{X}_k, u_k) &= \left(1 - \frac{T_s}{X_k^3}\right)X_k^1 + \frac{T_s X_k^2}{X_k^3} u_{(k - \frac{\tau_k}{T_s})}, \\ h_k(\mathbf{X}_k) &= X_k^1 + X_k^4, \end{cases} \quad (33)$$

and  $f_k^i(\mathbf{X}_k, u_k) = X_k^i$ , for  $i = 2, 3, 4$ . The process noise,  $w_k$ , and the measurement noise,  $v_k$ , are both assumed to be additive and statistically independent zero-mean Gaussian processes with covariances given by  $\mathbf{Q}_k$  and  $R_k$ , respectively. Although such an augmentation facilitates the estimation procedure, the time-varying input delay neither can be included in the augmented state vector nor be captured by a random walk process. Thus, time-delay is estimated through a multiple-model

hypothesis testing process along with the SRCKF, discussed in Section 2.2.

Next, we test the proposed MMSRCKF estimation algorithm in simulation where the patient's model parameters are generated by nonlinear functions based on clinical observations (2)-(4). Then, the verified estimation framework is validated using the experimental data from animal experiments.

In order to build a realistic simulation model of an individual's MAP response to the drug infusion with some known model parameters, we use (2)-(4) to generate the patient's nonlinear time-varying model parameters, *i.e.*,  $K(t)$ ,  $T(t)$ ,  $\tau(t)$ , and  $MAP_b(t)$ , where model parameters are nonlinear functions of the drug infusion rate,  $\mathcal{U}(t)$ . Figure 4 demonstrates the general structure of the nonlinear patient parameter generation process.

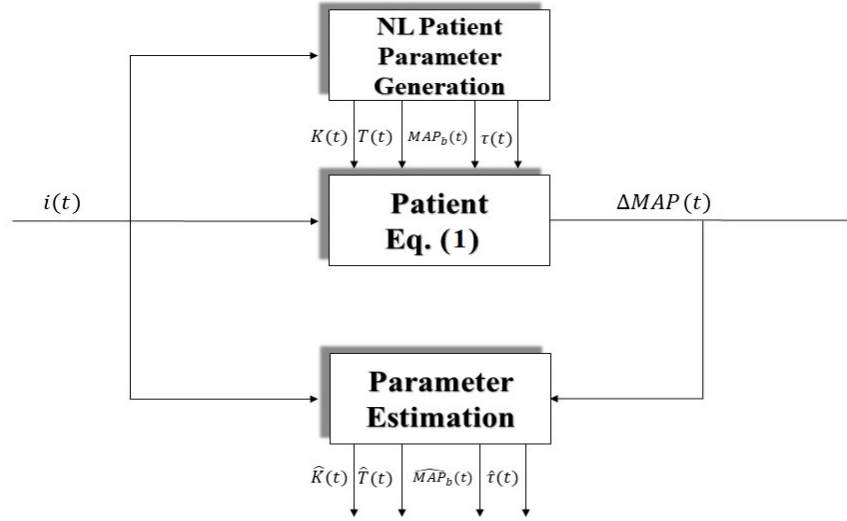


Figure 4: Structure of nonlinear patient parameter generation

As shown, the model parameters are generated based on the given infusion rate,  $\mathcal{U}(t)$ , while the parameter estimation tool estimates the model parameters sub-optimally, using the input drug infusion rate and measured output MAP. Figure 5 depicts the piecewise constant phenylephrine (PHP) drug infusion profile used to generate the nonlinear patient parameters.

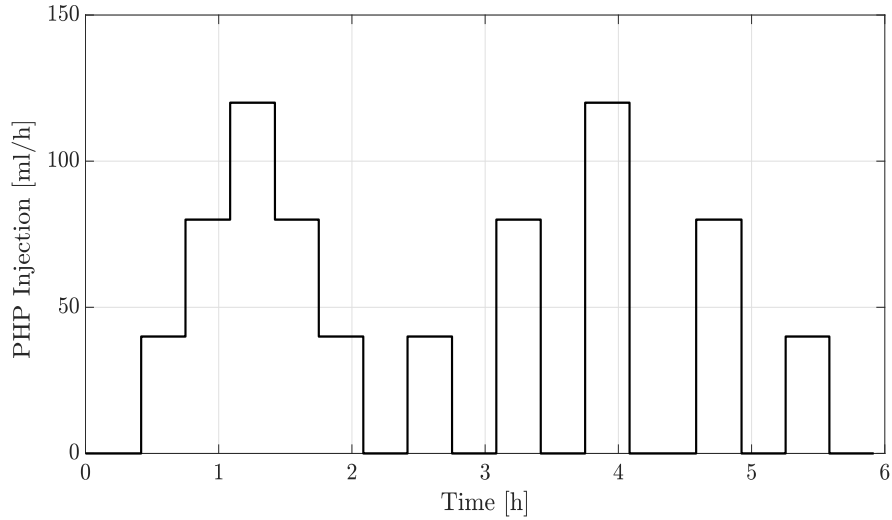


Figure 5: Profile of piecewise constant PHP drug injection

Using the generated nonlinear patient, we evaluate the proposed MMSRCKF in estimating model parameters, and the results are compared to the previously reported EKF algorithm [53]. Figures 6, 7, 8, and 9 present the estimation results for the varying model parameters, namely sensitivity  $K(t)$ , time constant  $T(t)$ , MAP baseline value  $MAP_b(t)$ , and time delay  $\tau(t)$ , respectively. As demonstrated, the implemented MMSRCKF method outperforms the EKF in terms of accuracy and convergence speed. Additionally, MMSRCKF online estimation shows more desirable matches with the generated nonlinear patient parameters based on pharmacodynamics [21]. It should be noted that although the computation complexity of both CKF and EKF algorithms equally grows as  $n^3$  with  $n$  denotes the system size, the former filter is more accurate and numerically more stable. Table 2 further compares the root mean square errors (RMSEs) of the model parameters and estimated MAP response in both algorithms by which the error reduction is obvious using MMSRCKF.

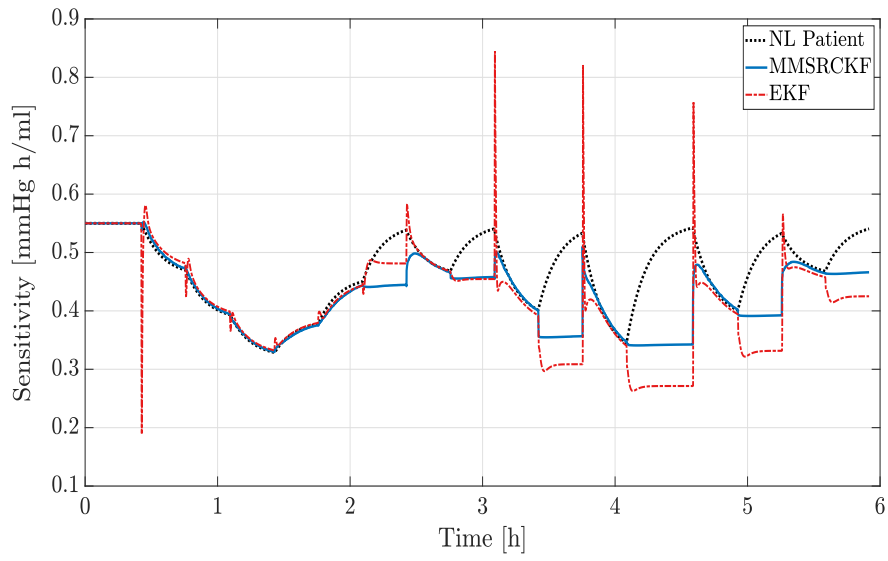


Figure 6: Nonlinear patient sensitivity estimation

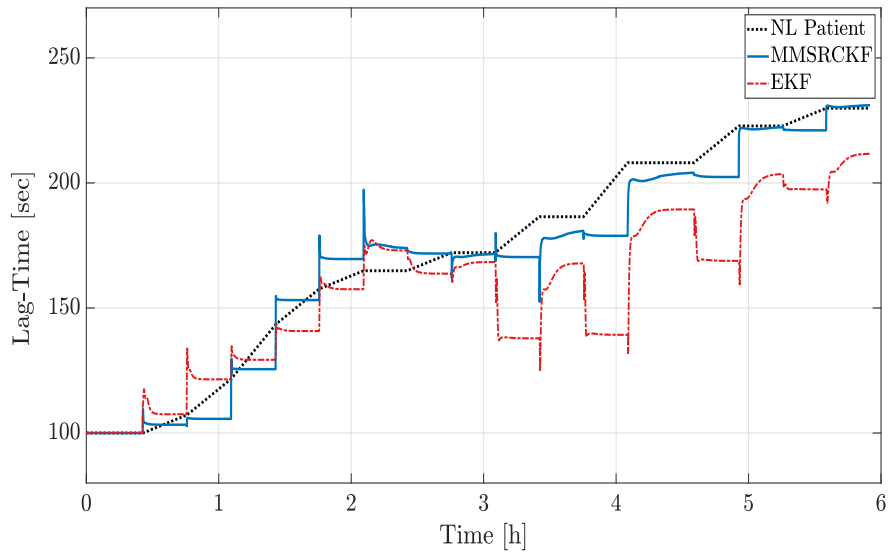


Figure 7: Nonlinear patient lag time estimation

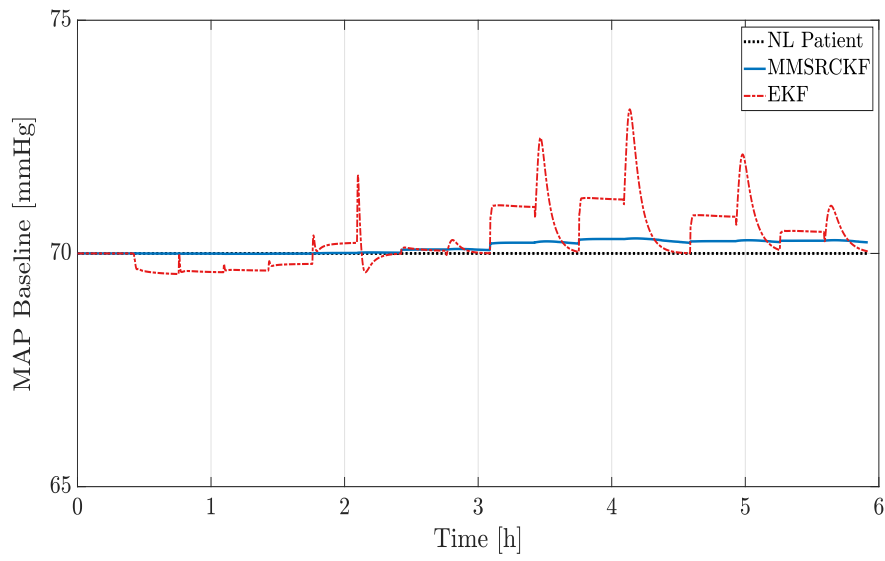


Figure 8: Nonlinear patient baseline MAP estimation

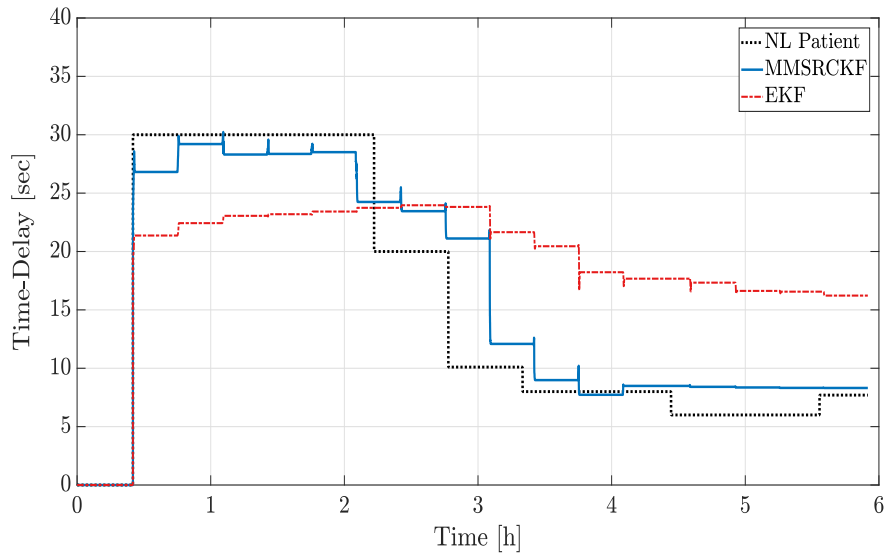


Figure 9: Nonlinear patient input delay estimation

Table 2: Estimation root mean square errors (RMSEs)

Parameter	RMSE	
	MMSRCKF	EKF
$K$	0.061	0.095
$T$	8.370	24.917
$MAP_b$	0.188	0.706
$\tau$	3.128	9.114
$MAP$	0.008	0.202

In the next step, we implement the MMSRCKF algorithm on the collected data from an actual animal experiment. The input PHP drug infusion rates and output MAP measurements for a 55 kg anesthetized swine were recorded at the Resuscitation Research Laboratory at the Department of Anesthesiology, UTMB at Galveston, Texas. An intramuscular injection of ketamine was used to sedate the swine, maintained under anesthetic conditions by the continuous infusion of propofol. A Philips MP2 transport device with a sampling frequency of 20 Hz was used to monitor the blood pressure response over a 6-hour experiment, while the PHP drug was being infused through a bodyguard infusion pump. Figure 10 shows the piecewise constant PHP drug infusion profile versus the corresponding measured raw blood pressure response and the MAP response over time. We then use this dataset to validate the estimation of the MAP dynamic model parameters using the proposed MMSRCKF methodology. The experimental dataset has been re-sampled at the sampling frequency of 0.2 Hz.

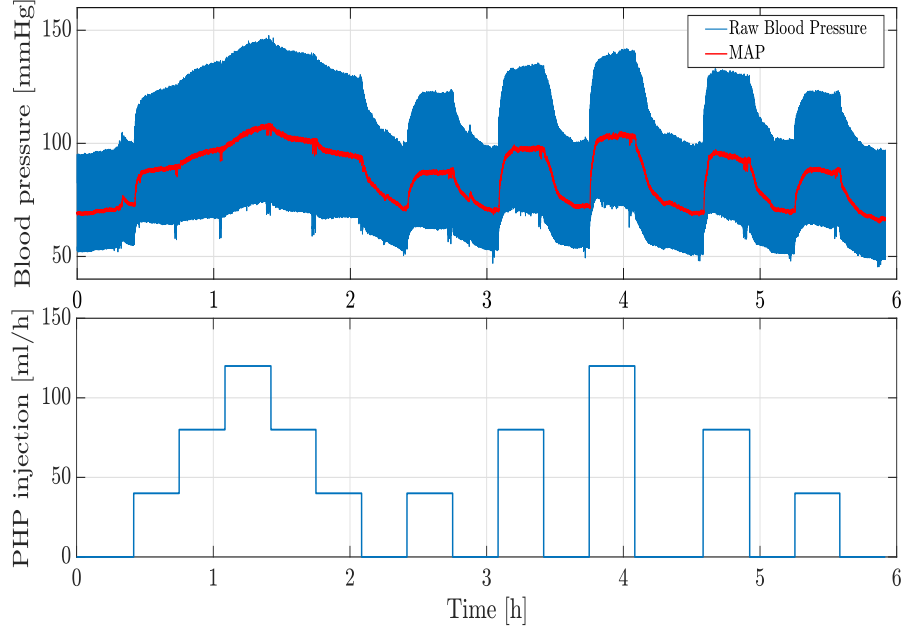


Figure 10: Instantaneous blood pressure and MAP response to a piecewise constant PHP drug injection in an animal experiment

Regarding the multiple-model step of the MMSRCKF algorithm adopted for the time-delay estimation, the estimation accuracy versus the algorithm speed of convergence triggered a trade-off which needed to be addressed with care; hence, it is essential to choose an appropriate number of the bank of SRCKFs constructing the MMSRCKF structure. In this work, we examined a bank of 11 SRCKFs with the delay interval of  $\tau \in [0 \ 100]s$ . Consequently, the time gridding for the evenly distributed filters was equal to  $10s$ . The MAP estimation of the proposed algorithm, as well as the clinically acquired MAP measurements, are illustrated in Fig. 11, which suggests that the proposed identification method is capable of accurately capturing the MAP response of the swine to the injection of the PHP drug. Additionally, the estimation of the model parameters, namely the sensitivity  $K(t)$ , time constant  $T(t)$ , MAP baseline value  $MAP_b(t)$ , and time delay  $\tau(t)$ , are depicted in Figs. 12, 13, 14, and 15, respectively. The estimated parameter values followed the expected trends, as discussed in detail in [92]. Furthermore, the delay estimation in Fig. 15

demonstrated a sharp initialization peak right after the initial injection of the drug and followed a slowly decaying trend during the rest of the experiment as anticipated [21] and obeys (4).

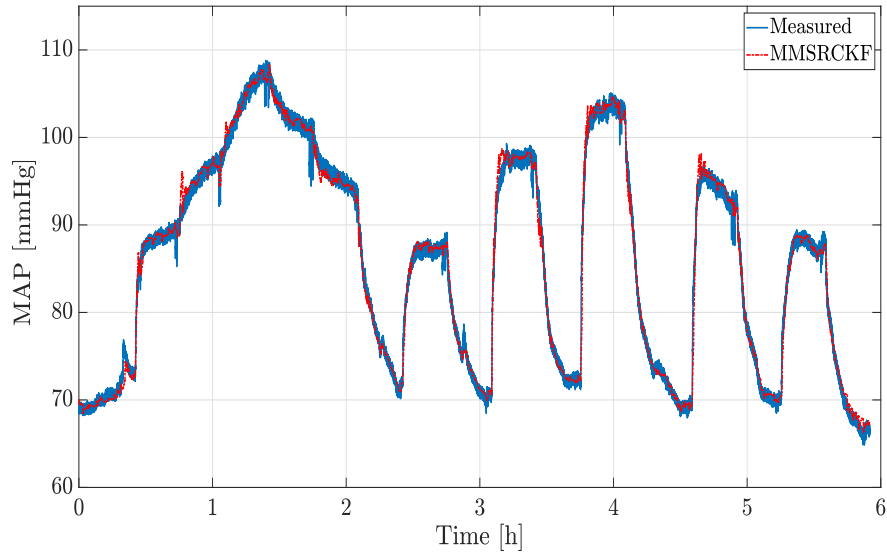


Figure 11: MAP estimation results in an animal experiment

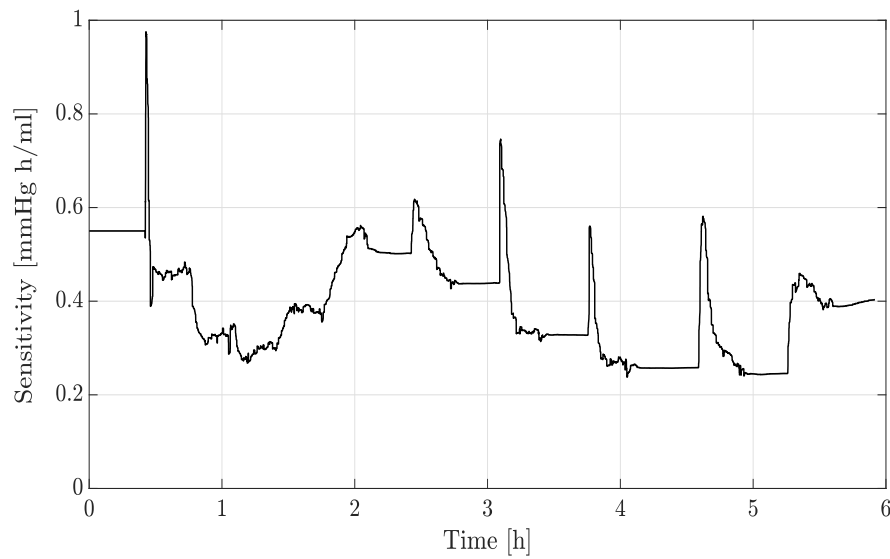


Figure 12: Sensitivity estimation in an animal experiment

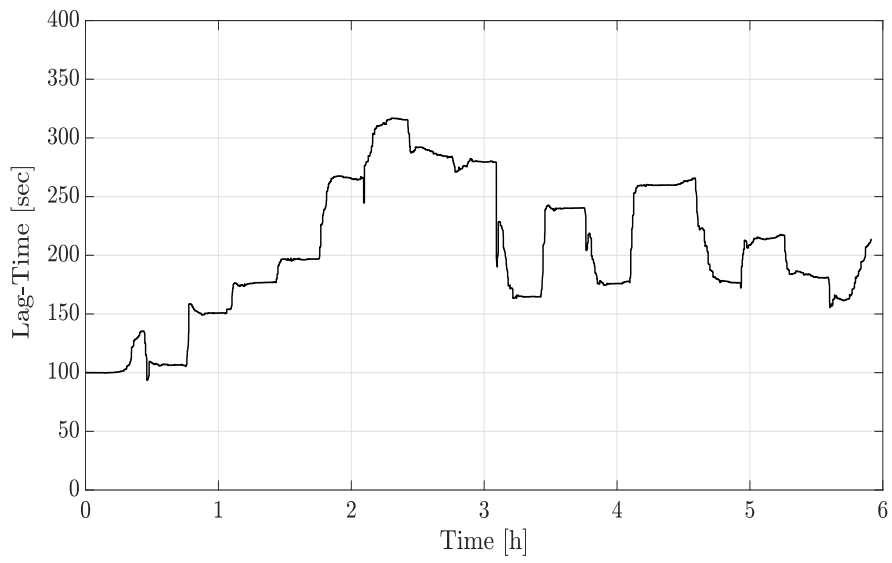


Figure 13: Lag time estimation in an animal experiment

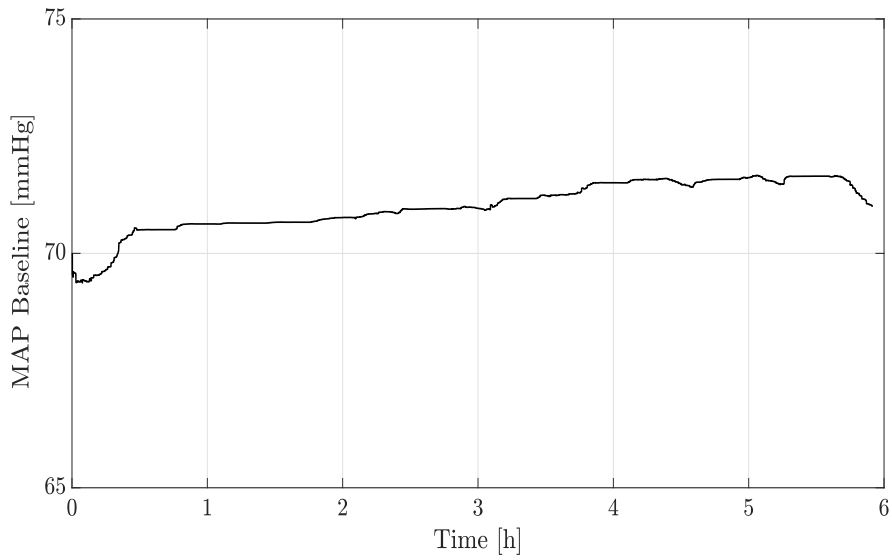


Figure 14: Baseline MAP estimation in an animal experiment

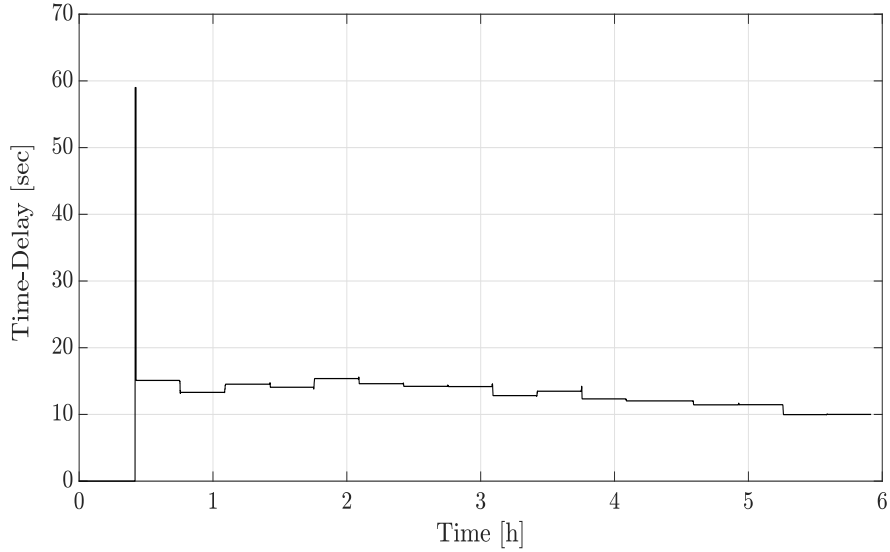


Figure 15: Time delay estimation in an animal experiment

## 2.4 Chapter Conclusion

In this chapter, precise real-time estimation of hemodynamics characteristics and mean arterial blood pressure in response to vasoactive drug administration are considered, which are pivotal to design an efficient controller to meet closed-loop physiological response requirements in various clinical scenarios. Real-time estimation of such dynamic models was examined in this chapter. Due to the inter-and intra-patient variabilities, an input-delay time-varying system was deemed to capture the model parameter variations. A Bayesian estimation scheme known as cubature Kalman filter was developed because of its convergence speed, nonlinear system handling, and numerical stability. The varying parameters of the nonlinear system corrupted by noise were estimated through the proposed framework. Since the input delay cannot be captured via a random-walk process, the filter was augmented with a multiple-model module. Time delay and parameter estimation results of the proposed Bayesian-based multiple-model square root cubature Kalman filtering (MMSRCKF) algorithm were compared to the extended Kalman filter (EKF), which verified the advantage of the utilized Bayesian-based approach.

## 3 Loop-Shaping and IMC-PID Control for Automated Blood Pressure Regulation

The following chapter first appeared in International Journal of Control, Automation and Systems (IJCAS), 2019, 17 (7), pp. 3355-3362.

Title: Robust IMC-PID and Parameter-Varying Control Strategies for Automated Blood Pressure Regulation

Authors: Shahin Tasoujian, Saeed Salavati, Matthew Franchek, Karolos Grigoriadis.

Reproduced in part with permission from International Journal of Control, Automation and Systems, Institute of Control, Robotics and Systems and The Korean Institute of Electrical Engineers, Copyright 2019.

### 3.1 Introduction

In general, analysis and control of time-delay systems using frequency-domain methods can provide necessary and sufficient conditions with less computational complexity. Among the frequency-domain methods, the internal model control (IMC) approach holds inherent robustness against parameter perturbations with a favorable disturbance rejection while providing a simple-to-implement structure [61]. Moreover, the IMC structure allows the designer to address the plant uncertainties and perform sensitivity analysis directly. The method has been widely used in time-delay systems control [76] and has been further developed to address the control of unstable time-delay systems [79], as well. Furthermore, the Smith predictor (SP), as the first systematic approach to deal with input delays, is a particular case of the IMC strategy [85].

For some plant models, the IMC structure can be approximated by a proportional-integral-derivative (PID) control structure [71] to account that the classic PID configuration is still the dominant controller in the vast majority of industrial systems [101]. In this chapter, an equivalent PID controller with a lag compensator is designed based on a robust IMC methodology that explicitly addresses the control of time-delay systems [74]. As another frequency-domain method, a

parameter-varying loop-shaping approach is investigated in which, by using the Padé approximation, the infinite-dimensional system with pure delay is transformed into a finite-dimensional but nonminimum phase (NMP) system. While carefully regarding the limitations posed by the internal dynamics of the NMP system, this framework imposes phase and gain margins constraints to meet performance and robustness requirements of the closed-loop system [89]. The loop-shaping method aims at designing the closed-loop controller to meet bandwidth requirements in a straightforward manner.

In this chapter, a first-order time-delay model is assumed to describe the MAP response to vasoactive drugs (see chapter 1). For the control design, first, the NMP system resulted by the rational approximation of the delay relinquishes the infinite-dimensional delay problem; however, it suffers from a lack of adequate phase margin inherited by the delay magnitude. Consequently, the loop-shaping algorithm is presented to introduce a parameter-varying controller to track the reference MAP. In the second method, the system is regarded as a nominal plant with the time-varying delay and the parameters treated as uncertainties. The small-gain theorem explicitly characterizes necessary and sufficient conditions for robust stability of the closed-loop system with the IMC controller. Then, an equivalent IMC-PID controller is derived, and the previous robust condition is used to design the PID coefficients. Furthermore, closed-loop performance degradation imposed by the time delay presence is investigated by examining the complementary sensitivity function. Due to their simplified underlying structure, the proposed controls are easily implementable for clinical applications while achieving the desired MAP regulation. For control validation purposes, a nonlinear simulation model with time-varying parameters is utilized to capture the varying physiological characteristics of patients' MAP response.

### 3.2 Control System Design

Considering the patient's MAP response continuous-time dynamics (1), a first-order single-input single-output (SISO) model with time-delay in the control input is presented in Laplace domain as

$$G_p(s) = \frac{\Delta MAP(s)}{I(s)} = \frac{K}{Ts + 1} e^{-\tau s}. \quad (34)$$

The major obstacle in the control design process is the large varying time-delay, which results in a reduced system bandwidth and poor closed-loop system performance. Subsequently, two feedback control design methods are examined in this chapter: (1) loop-shaping controller whose structure is varying with the variation of the system parameters, and (2) IMC-PID controller with a time-invariant structure whose parameters are derived by considering the time variations as uncertainties and employing the small-gain theorem.

#### 3.2.1 Loop-Shaping Control Design

The structure of a closed-loop system with a loop shaping controller is shown in Fig. 16.

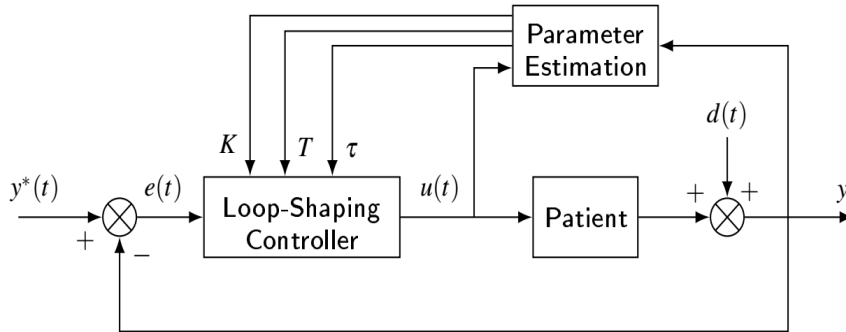


Figure 16: Closed-loop system structure

The first-order Padé approximation is used to transfer the infinite-dimensional time-delay model

(34) into a finite-dimensional one as

$$G_p(s) = \frac{\Delta MAP(s)}{I(s)} \approx \frac{K}{Ts + 1} \cdot \frac{2 - \tau s}{2 + \tau s}. \quad (35)$$

The model (35) is an NMP system with a right-hand plane (RHP) zero posing restrictions on the achievable bandwidth [82]. The loop transfer function is  $L(s) = G_p(s)G_c(s)$  where  $G_c(s)$  is the feedback controller to be designed and  $G_p(s)$  is the product of all other transfer functions around the loop including the plant, the actuator, and sensor. By splitting the plant transfer function into a minimum phase (MP) stable open-loop transfer function and a NMP part,  $G_p(s)$  can be rewritten as  $G_p(s) = G_{MP}(s)G_{NMP}(s)$ , where  $G_{MP}(s) = \frac{K}{Ts + 1}$  and  $G_{NMP}(s) = \frac{2 - \tau s}{2 + \tau s}$ , which is also known as a Blaschke product. The presence of an RHP zero in  $G_{NMP}$  contributes to additional phase lag and restricts the achievable bandwidth region, which is closely characterized by the gain crossover frequency,  $\omega_c$ , that is, the smallest frequency at which  $|L(j\omega_c)| = 1$ . To find the crossover frequency with the desired phase margin,  $\varphi_m$ , based on desired performance and stability conditions, we consider the phase of  $L(j\omega_c)$

$$\angle L(j\omega_c) = \angle G_c(j\omega_c) + \angle G_{MP}(j\omega_c) + \angle G_{NMP}(j\omega_c) \geq -\pi + \varphi_m. \quad (36)$$

By assuming Bode's ideal loop transfer function for the minimum phase and the control transfer functions ( $L_i(s) = (\frac{s}{\omega_c})^n$ ), we have

$$\angle G_c(s) + \angle G_{MP}(j\omega_c) = n\frac{\pi}{2}, \quad (37)$$

by which (36) can be expressed as [7]

$$\angle G_{NMP}(j\omega_c) \geq -\pi + \varphi_m - n\frac{\pi}{2}, \quad (38)$$

where  $n = \frac{d \log |L(j\omega)|}{d \log \omega}$  is defined as the logarithmic slope of the loop transfer function. By replacing

$\angle G_{NMP}(j\omega_c) = -2 \tan^{-1} \frac{\tau\omega_c}{2}$  in (38), we have

$$\omega_c \leq 2\tau^{-1} \tan\left(\frac{\pi}{2} - \frac{\varphi_m}{2} + n\frac{\pi}{4}\right). \quad (39)$$

Equation (39) gives the upper bound of the crossover frequency with respect to the inverse value of the delay for a given phase margin. For larger delays, the attainable crossover frequency decreases, thereby slowing down the system closed-loop response. This limitation plays a crucial role in determining the achievable bandwidth in designing the control system.

Loop-shaping is a classical method that aims to design a controller to explicitly shape the magnitude of the loop transfer function,  $|L(j\omega)|$ , as a function of frequency to achieve desired bandwidth and performance specifications. Considering the sensitivity transfer function  $\mathbb{S}(s) = [1 + L(s)]^{-1}$  and the complementary sensitivity function  $\mathbb{T}(s) = 1 - \mathbb{S}(s) = L(s)[1 + L(s)]^{-1}$ , the closed-loop system response in terms of the tracking error in the presence of disturbances and measurement noise can be written as

$$e = y - y^* = -\mathbb{S} \cdot y^* + \mathbb{S} \cdot G_d \cdot d - \mathbb{T} \cdot n, \quad (40)$$

where  $e$  is the error,  $y^*$  is the reference command,  $G_d$  is the disturbance model,  $d$  is the disturbance and  $n$  denotes measurement noise. To achieve a “perfect control” we should have  $e = 0$ ; that is  $e = 0 \cdot y^* + 0 \cdot G_d \cdot d - 0 \cdot n$ .

Regarding Eq. (40), in order to achieve perfect command tracking and disturbance rejection one may design  $G_c(s)$  such that it increases the magnitude of the loop transfer function,  $|L(j\omega)|$ , so that  $\mathbb{S} \approx 0$ , and  $\mathbb{T} \approx 1$ . On the other hand, in order to have zero noise transmission, the design procedure should be altered to decrease the magnitude of the loop transfer function,  $|L(j\omega)|$ , so that  $\mathbb{T} \approx 0$  and equivalently  $\mathbb{S} \approx 1$ . All these objectives cannot be achieved simultaneously, which is a fundamental nature of the feedback design, and a trade-off should be achieved between the sensitivity and the complementary sensitivity functions. However, since those mentioned conflicting objectives are generally in different frequency ranges, the reference tracking, and the disturbance rejection requirements can be achieved by a large loop gain ( $|L(j\omega)| \gg 1$ ) at low frequencies below

the gain crossover frequency,  $\omega_c$ , and a small gain ( $|L(j\omega)| \ll 1$ ) at high frequencies above  $\omega_c$  for noise attenuation. Hence, to take advantage of the feedback control and achieve the desired reference command tracking, we need large controller gains, *i.e.*, the loop gain  $|L(j\omega)|$  has to be made as large as possible within the bandwidth region. However, due to the time delay, which is translated into an RHP zero in the present formulation, and the unmodeled high-frequency dynamics, it is desired for  $|L(j\omega)|$  to drop sharply below one in the frequencies above the crossover region [82]. Typically, the desired slope at the crossover region and at low frequencies below the crossover depends on the nature of the reference command and disturbance signals. So, as a rule of thumb, to achieve zero offset and reference command tracking (*i.e.*,  $e \approx 0$  for  $t \rightarrow \infty$ ), the loop transfer function,  $L(s)$ , must contain at least one integrator for each integrator in the reference signal,  $y^*(s)$  [82]. Now, considering that we are designing a proper controller for the step changes in the reference command and disturbances, the logarithmic slope of the loop transfer function  $|L(s)|$ ,  $n = \frac{d \log |L(j\omega)|}{d \log \omega}$ , is desired to be at least  $n = -1$  at the crossover region and at low frequencies below the crossover and it is desired to have a larger roll-off, *e.g.*  $n \leq -2$  for the loop transfer function,  $|L(s)|$ , at high frequencies above  $\omega_c$  (at least one decade above  $\omega_c$ ) for noise attenuation.

By having the desired slopes and phase margin in mind and considering (39), the upper bound of crossover frequency is obtained as

$$\omega_c \leq 2\tau^{-1} \tan \frac{\pi}{4} - \frac{\varphi_m}{2}. \quad (41)$$

By assuming the desired phase margin to be  $\varphi_m = \frac{\pi}{3}$ , the upper bound on the crossover frequency (41) will be  $\omega_c \leq 2\tau^{-1} \tan \pi/12$  and the parameter-varying delay-dependent controller will be

$$G_c(s) = G_{MP}^{-1} \cdot \frac{K_c}{s(\frac{1}{10\omega_c}s + 1)} = \frac{K_c(T_c s + 1)}{s(\frac{1}{10\omega_c}s + 1)}, \quad (42)$$

where  $G_{MP}^{-1}$  is added as the inverse of the MP stable transfer function to cancel the effect of the lag term in  $G_p(s)$  and eliminate the undesired break frequencies before  $\omega_c$ . Assuming stepwise reference command, to achieve perfect reference command tracking performance, one integrator,  $1/s$ , is added

to provide  $|L(s)|$  with the slope  $n = -1$  at the crossover region and frequencies below that. The term  $(\frac{1}{10\omega_c}s + 1)$  is added to introduce a low-pass filter into the controller dynamics and to make  $|L(s)|$  have a large roll-off with a higher slope at high frequencies above  $\omega_c$  (one decade above  $\omega_c$ ). Consequently, the desired loop transfer function  $L(s)$  is shaped as

$$L(s) = \frac{KK_c(1 - \frac{\tau}{2}s)}{s(\frac{1}{10\omega_c}s + 1)(1 + \frac{\tau}{2}s)}. \quad (43)$$

Equation (43) can be used to determine the control gain,  $K_c$ , by setting  $|L(j\omega_c)| = 1$ , *i.e.*,

$$K_c = |1 + j0.1| \cdot \left| \frac{1 + j\omega_c \frac{\tau}{2}}{1 - j\omega_c \frac{\tau}{2}} \right| \cdot \frac{\omega_c}{K} = 1.005 \cdot \frac{\omega_c}{K}, \quad (44)$$

where Eq. (44) represents the control gain explicitly as a function of the model gain and the delay term incorporated indirectly through (41). Shown in Fig. 17 is the control gain,  $K_c$ , calculated through considering time-varying patient sensitivity,  $K$ , according to Eq. (2), and the crossover frequencies obtained from (41) for various time-varying delay values according to Eq. (4). It should also be clarified that  $K$ ,  $T$ , and  $\tau$  are considered to be slowly varying parameters such that the dynamic response is faster than the parameter variations. The relevance and accuracy of using the Padé approximation has been extensively addressed in [89]. Figure 18 shows the Bode plots for the closed-loop system for the time-delay interval  $0.65 \text{ sec} \leq \tau \leq 21.15 \text{ sec}$  with increments of  $1.025 \text{ sec}$ , where the stability condition and the desired phase margin is satisfied for all the delay values.

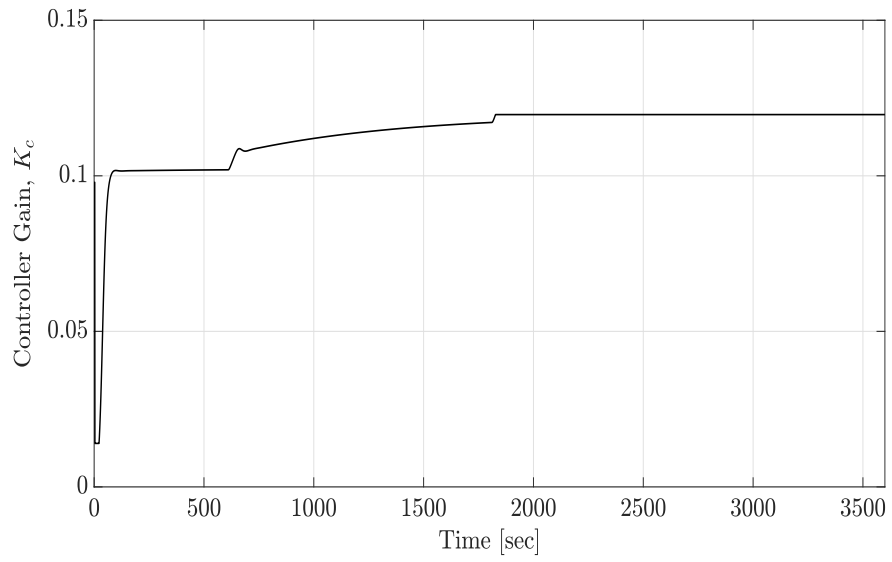


Figure 17: Delay dependent time-varying controller gain,  $K_c$

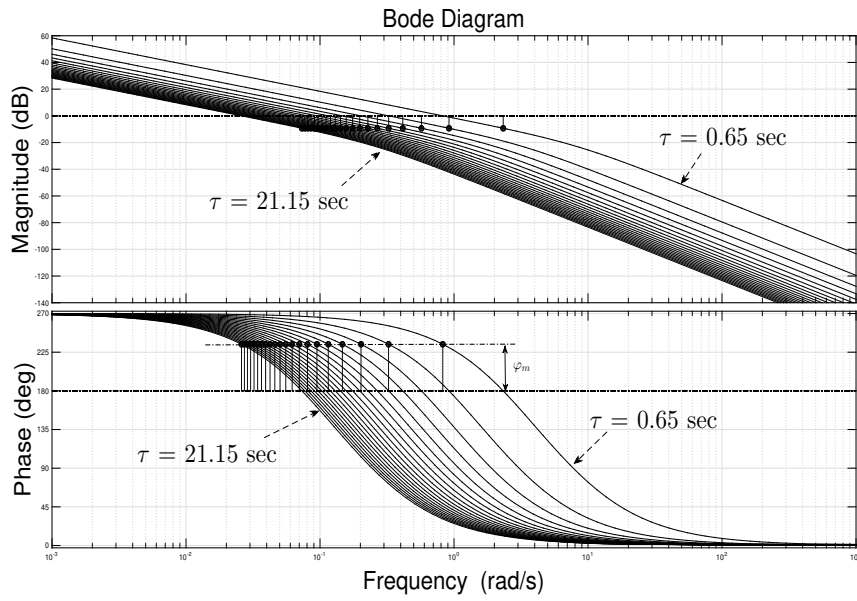


Figure 18: Bode plots for the closed-loop system for the time-delay interval  $0.65 \text{ sec} \leq \tau \leq 21.15 \text{ sec}$

As shown, gain crossover frequency,  $\omega_c$ , decreases as the time-delay increases. This implies that the limitation on a system with a large time-delay is much stricter and requires the system to have a lower  $\omega_c$  in order to compensate for the larger time-delays.

### 3.2.2 IMC-Based PID Control Design

A family of first-order time-delay systems subject to parametric uncertainties can be expressed by a set of plants with a multiplicative uncertainty defined by

$$\Omega = \{G_p(s) | G_p(s) = \bar{G}_p(s)(1 + \Delta), \|\Delta\|_\infty \leq 1\}, \quad (45a)$$

$$\bar{G}_p(s) = \frac{\bar{K}}{\bar{T}s + 1} e^{-\bar{\tau}s}, \quad (45b)$$

where  $\bar{G}_p$  denotes the known nominal system and  $G_p(s)$  is any perturbed plant of interest with a time-varying delay and parameters all varying within the prescribed bounds. Model uncertainties are embedded in a stable rational transfer function,  $\Delta$ , and the delay-free plants are all analytic functions and bounded in  $\mathbb{C}^+$  (or  $\frac{K}{Ts + 1} \in \mathcal{RH}_\infty$ ). The bounded parameters  $K$ ,  $\tau$ , and  $T$  and their nominal counterparts denoted by  $\bar{K}$ ,  $\bar{\tau}$ , and  $\bar{T}$  define the relative errors through

$$\delta \triangleq \frac{K - \bar{K}}{\bar{K}}, \quad (46a)$$

$$\epsilon \triangleq \frac{\tau - \bar{\tau}}{\bar{\tau}}, \quad (46b)$$

$$\gamma \triangleq \frac{T - \bar{T}}{\bar{T}}, \quad (46c)$$

which are bounded by known parameters as  $|\delta| \leq p$ ,  $|\epsilon| \leq q$ , and  $|\gamma| \leq r$ . The schematic of the proposed IMC method is shown in Fig. 19.

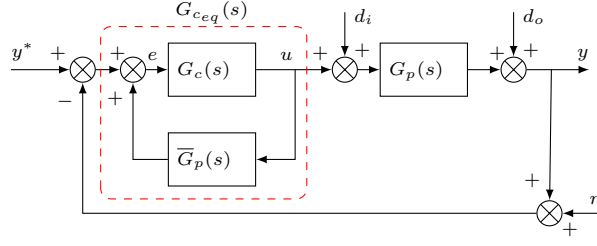


Figure 19: Schematic of the IMC strategy and equivalent closed-loop controller

A candidate for the controller that enables the closed-loop system to track a step reference signal with a satisfactory level of disturbance rejection and noise attenuation is given by [74],

$$G_c(s) = \frac{1}{K} \cdot \frac{\bar{T}s + 1}{\lambda s + 1}, \quad (47)$$

which is referred to a  $\lambda$ -tuned controller. Then, the following result as a consequence of the small-gain theorem gives the necessary and sufficient condition for robust stability of the closed-loop system.

**Theorem 1.** Consider  $\Omega$  as a set of perturbed time-delay plants satisfying the multiplicative uncertainty given by (45). The controller (47) then robustly stabilizes the family of the input-delay plants with the bounded relative uncertainties (46) if and only if the following inequality is met:

$$\left\{ \delta^2 + 4(\delta + 1) \left[ \left( 1 + (\gamma + 1) \tilde{\omega}^2 \tilde{T}^2 \right) \sin^2 \frac{\epsilon \tilde{\omega}}{2} + \frac{1}{2} \gamma \tilde{\omega} \tilde{T} \sin \epsilon \tilde{\omega} \right] + \tilde{\omega}^2 \left[ \tilde{T}(\delta - \gamma) \right]^2 \right\} \cdot \left\{ 1 + \left[ \tilde{\omega}(\gamma + 1) \tilde{T} \right]^2 \right\}^{-1} < \left( \frac{\lambda}{\bar{T}} \tilde{\omega} \right)^2 + 1, \quad (48)$$

with  $\tilde{\omega} = \omega \bar{\tau}$  and  $\tilde{T} = \frac{\bar{T}}{\bar{\tau}}$ .

*Proof.* As per the small-gain theorem, if a family of uncertain systems, fulfilling the multiplicative uncertainty condition given by (45), satisfies the  $\mathcal{H}_\infty$  norm inequality

$$\|\bar{\eta}(s)\Delta(s)\|_\infty < 1, \quad (49)$$

then internal stability for these systems is guaranteed. Since  $\|H(s)\|_\infty = \sup \bar{\sigma}(H(s)) < 1$  corresponds to  $|H(j\omega)| < 1$ , for all  $\omega$ , using the expressions for  $\bar{\eta}(j\omega)$  and  $\Delta(j\omega)$ , (49) yields

$$\left| G_c(j\omega) \cdot \bar{G}_P(j\omega) \cdot \frac{G_P(j\omega) - \bar{G}_P(j\omega)}{\bar{G}_P(j\omega)} \right| = |G_c(j\omega) \cdot [G_P(j\omega) - \bar{G}_P(j\omega)]| < 1. \quad (50)$$

By substituting the equations (45b) and (47) into (50), one can obtain

$$\begin{aligned} & \left| \frac{j\bar{T}\omega + 1}{\bar{K}} \cdot \frac{1}{j\lambda\omega + 1} \cdot \left( \frac{K e^{-j\tau\omega}}{1 + jT\omega} - \frac{\bar{K} e^{-j\bar{\tau}\omega}}{1 + j\bar{T}\omega} \right) \right| = \\ & \left| \frac{K(1 + j\bar{T}\omega)e^{-j\tau\omega} - \bar{K}(1 + jT\omega)e^{-j\bar{\tau}\omega}}{\bar{K}(1 + jT\omega)} \cdot \frac{1}{j\lambda\omega + 1} \right| < 1. \end{aligned} \quad (51)$$

After carrying out some mathematical manipulations, the above inequality becomes

$$\begin{aligned} & \left\{ \left( \frac{K - \bar{K}}{\bar{K}} \right)^2 + 4 \frac{K}{\bar{K}} \sin^2 \frac{\omega(\tau - \bar{\tau})}{2} + (\omega\bar{T})^2 \left[ \left( \frac{K}{\bar{K}} - \frac{T}{\bar{T}} \right)^2 + 4 \frac{K}{\bar{K}} \frac{T}{\bar{T}} \sin^2 \frac{\omega(\tau - \bar{\tau})}{2} \right] \right. \\ & \left. + 2\omega \frac{K}{\bar{K}} (T - \bar{T}) \sin \omega(\tau - \bar{\tau}) \right\}^{\frac{1}{2}} \times \left\{ [1 + (\omega T)^2] [1 + (\lambda\omega)^2] \right\}^{-\frac{1}{2}} < 1. \end{aligned} \quad (52)$$

Using the relative error definitions for the parameters in (52), the inequality (48) is obtained.  $\square$

After establishing robust stability conditions, the next section introduces a PID controller structure derived from the IMC framework.

### Derivation of Equivalent PID Structure

As per Fig. 19, a feedback loop with an equivalent controller transfer function,  $G_{ceq}(s)$  can be used to design a PID controller with a low-pass filter to enhance robustness, *i.e.*,

$$G_{ceq}(s) = \frac{G_c(s)}{1 - G_c(s)\bar{G}_p(s)} = \frac{1}{\bar{K}} \cdot \frac{\bar{T}s + 1}{\lambda s + 1 - e^{-\bar{\tau}s}} \quad (53a)$$

$$\equiv \mathcal{K}_p \left( 1 + \frac{1}{\mathcal{T}_i} \cdot \frac{1}{s} + \mathcal{T}_d s \right) \cdot \frac{1}{\mathcal{T}_F s + 1}, \quad (53b)$$

where (53) is a PID plus lag compensator with appropriate coefficients to be computed. Using the

first-order Padé approximation of the delay, the right-hand side (RHS) of (53a) is

$$\frac{\bar{T}s + 1}{\bar{K}(\lambda s + 1) - \bar{K}e^{-\bar{\tau}s}} \approx \frac{1}{\bar{K}} \cdot \frac{(\bar{T}s + 1)(1 + \frac{\bar{\tau}}{2}s)}{\frac{\lambda\bar{\tau}}{2}s^2 + (\lambda + \bar{\tau})s} = \underbrace{\frac{(\frac{1}{2} + \frac{\bar{T}}{\bar{\tau}})}{\bar{K}(1 + \frac{\lambda}{\bar{\tau}})}}_{\mathcal{K}_p}$$

$$\cdot \left[ 1 + \underbrace{\frac{1}{(\bar{T} + \frac{\bar{\tau}}{2})}}_{\mathcal{T}_i} \cdot \frac{1}{s} + \underbrace{\left( \frac{1}{\frac{2}{\bar{\tau}} + \frac{1}{\bar{T}}} \right)}_{\mathcal{T}_d} s \right] \frac{1}{\underbrace{\left( \frac{\frac{\lambda}{\bar{\tau}}}{\frac{\lambda}{\bar{\tau}} + 1} \cdot \frac{\bar{\tau}}{2} \right)}_{\mathcal{T}_F} s + 1}.$$

The next section examines the closed-loop performance of the proposed control structures for the blood pressure regulation problem.

### 3.3 Simulations Results and Discussions

#### 3.3.1 PID Controller Tuning

Nominal values for the blood pressure response to phenylephrine (PHP) are obtained experimentally [98]. The parameters of the plant are perturbed from the nominal values  $\bar{K} = 0.55$ ,  $\bar{T} = 700$ , and  $\bar{\tau} = 40$  by relative errors of  $|\delta| \leq 0.182$ ,  $|\gamma| \leq 0.143$ , and  $|\epsilon| \leq 0.75$ , respectively. For determining the robustly stabilizing range of the tuning parameter, the left-hand side (LHS) and RHS of (48) are considered as separate functions of the uncertainties and the nominal values. Provided that any assigned value of  $\lambda$  renders the RHS greater than LHS, the robust stability requirement is fulfilled. In general, these two functions are close to each other if the uncertainties are at their lower and upper bounds. Choosing  $\frac{\lambda}{\bar{\tau}} = 1.2$ , the RHS and LHS of (48) versus the dimensionless frequency  $\tilde{\omega}$  are shown in Fig. 20 as two shaded areas where the robust stability condition holds.

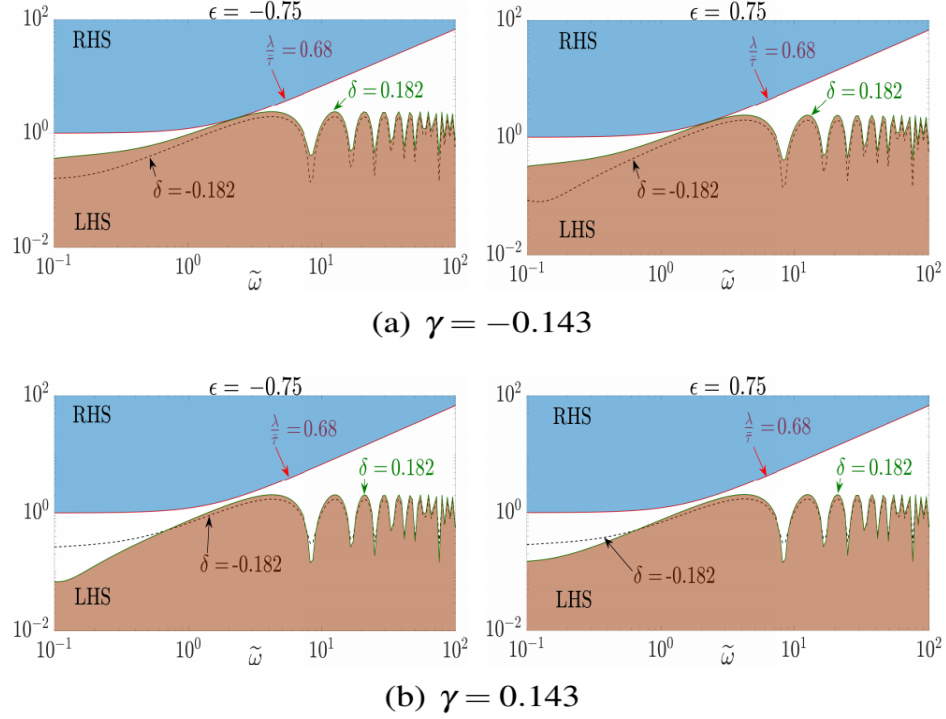


Figure 20: Robust stability criterion, Eq. (48) for different uncertainties on the delay and gain parameters with (a) lower bound of the time constant uncertainty, and (b) upper bound of the time constant uncertainty

**Remark 1.** For time constant values without uncertainty, i.e.,  $\gamma = 0$ , mathematical manipulations reveal that

$$\frac{\lambda}{\tau} \approx q, \quad (54)$$

satisfies the robust stability condition.

In order to improve the closed-loop system performance, let us define  $M_T = \|\mathbb{T}(s)\|_\infty$  as the maximum value of the magnitude of the complementary sensitivity function,  $\mathbb{T}(s)$ . Typically, a large value of  $M_T$  (about 0.5 dB) is indicating inadequate performance and this is the case as Fig. 21(a) illustrates. In classical feedback control design, usually an upper bound is placed on  $M_T$  as a prevalent design requirement. In particular, it is meaningful to set  $M_T$  less than 1.25 (2 dB) [82].

By retuning the controller parameter and increasing  $\frac{\lambda}{\tau}$  to 2.5, Fig. 21(b) indicates that  $\mathbb{T}(s)$

rolls off more smoothly and performance is enhanced with  $M_T \approx 1.5$ . Such a value for the tuning parameter is used to evaluate the closed-loop performance in the next section.

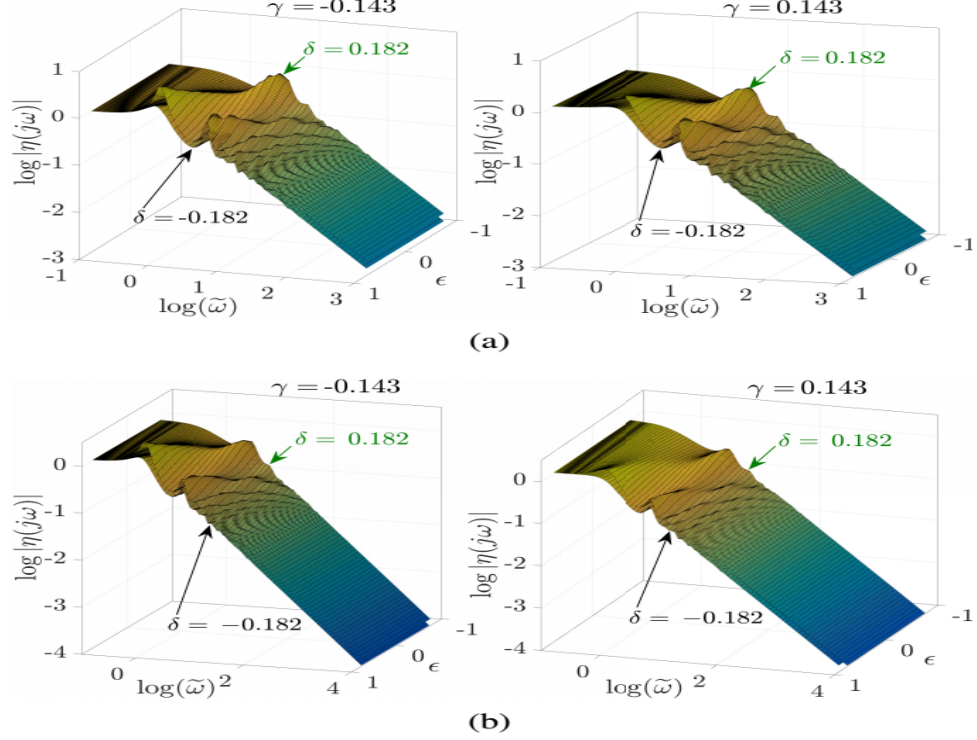


Figure 21: Logarithmic norm of the complementary sensitivity function vs. logarithmic dimensionless frequency,  $\tilde{\omega}$ , for different values of delay uncertainty,  $\epsilon$ , (a) not tuned, and (b) tuned controller

**Remark 2.** *In general, increasing the filter time-constant will decrease the overshoot and consequently yields an improved performance [16]. However, increasing  $\lambda$  leads to a more conservative controller because of the fact that the open-loop gain decreases [76] and the resulting closed-loop dynamics exhibits more sluggish behavior.*

**Remark 3.** *In general,  $M_T$  is a better measure of robustness than the gain margin (GM) or the phase margin ( $\varphi_m$ ). Robustness based on GM and  $\varphi_m$  tends to be overly optimistic and their*

associated lower bounds can be established through

$$GM \geq 1 + \frac{1}{M_T}, \quad (55a)$$

$$\varphi_m \geq 2 \sin^{-1} \left( \frac{1}{2M_T} \right) \approx \frac{1}{M_T}. \quad (55b)$$

However, to reduce conservatism, the structured singular value,  $\mu$  can be used by constraining the phase and gain variations to the diagonal elements of the transfer function matrix [71].

### 3.3.2 MAP Regulation Closed-Loop Simulation Results

In order to evaluate the performance of the proposed controllers, experimental data are used to build a realistic nonlinear patient's MAP response model based on (34) where instantaneous values of model parameters  $K$ ,  $T$ , and  $\tau$  are generated based on (2)-(4).

For comparison purposes, we implement the proposed loop-shaping and the IMC-PID controllers and evaluate their performance against a fixed structure PI controller (see [98]). Given nominal values of the model parameters as  $\bar{K} = 0.55$ ,  $\bar{T} = 700$ , and  $\bar{\tau} = 40$ , the tuned PI controller transfer function is as follows

$$G_C(s) = 10 + \frac{0.018}{s}, \quad (56)$$

which is obtained to meet the prescribed gain and phase margin constraints [105]. In the absence of disturbances and measurement noise, the tracking profile and the control effort are shown in Fig. 22, where the objective is to elevate the MAP to track the stepwise MAP reference.

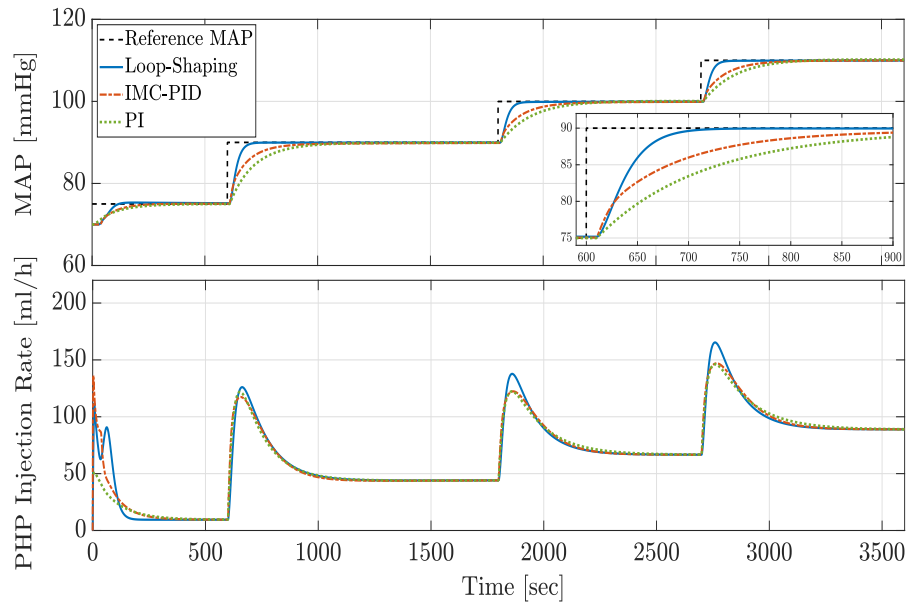
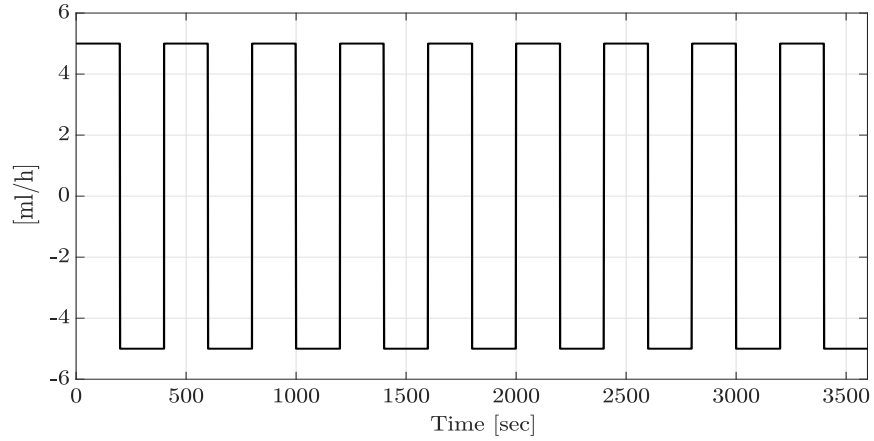
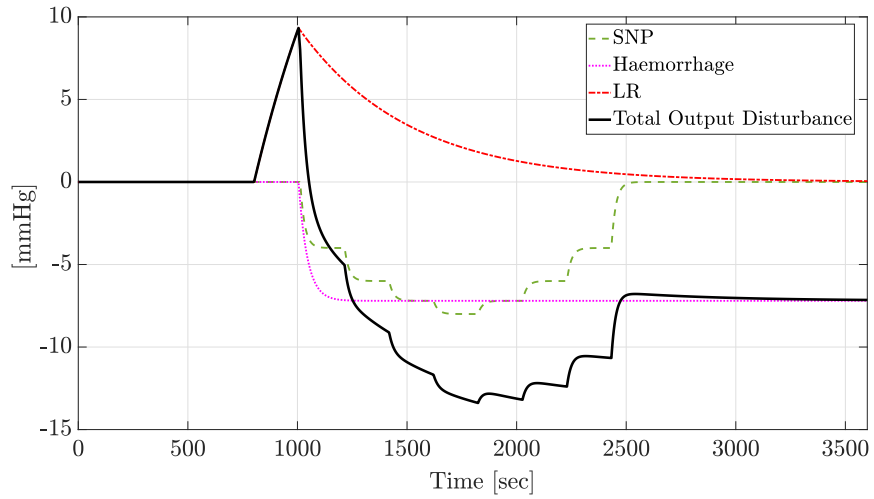


Figure 22: Tracking performance and control effort for proposed controllers against a fixed PI controller with no disturbance and measurement noise

According to Fig. 22, the overshoot of the closed-loop response remains within the acceptable range, and the parameter varying controller provides the fastest response with the least settling time among the examined controllers. For the sake of completeness, we assume that the closed-loop system is experiencing both input (Fig. 23(a)) and output disturbances due to medical interventions and physiological conditions such as hemorrhage and additional medications such as infusion of lactated ringers (LR) and sodium nitroprusside (SNP). Figure 23(b) is a typical profile of such disturbances.



(a)



(b)

Figure 23: Profile of disturbances in (a) input and (b) output channels

In order to evaluate the robustness of the proposed controllers, we consider the over/underestimation errors of 30% for the time delay value. As Fig. 25(a) suggests, in the overestimation case, the results are more conservative due to the higher assumed time delay value in the controller design processes and consequently slower closed-loop response. Additionally, for the underestimated time delay case, Fig. 25(b) presents larger overshoots than the nominal cases. However, the MAP tracking results

confirm the robustness of the proposed controllers against the parameter uncertainty.

For the case with measurement noise (white noise with intensity of  $10^{-3}$ ) and disturbances, closed-loop performance of both controllers is plotted in Fig. 24. As expected, both proposed controllers outperform the fixed structure PI controller. Moreover, the parameter-varying loop shaping controller outperforms the time-invariant PID controller with respect to the rise time and speed of the response due to its varying structure, which better handles the relatively slowly varying plant. Although the PID controller indicates a slower rise time, its performance remains acceptable because of the IMC framework's inherent robustness.

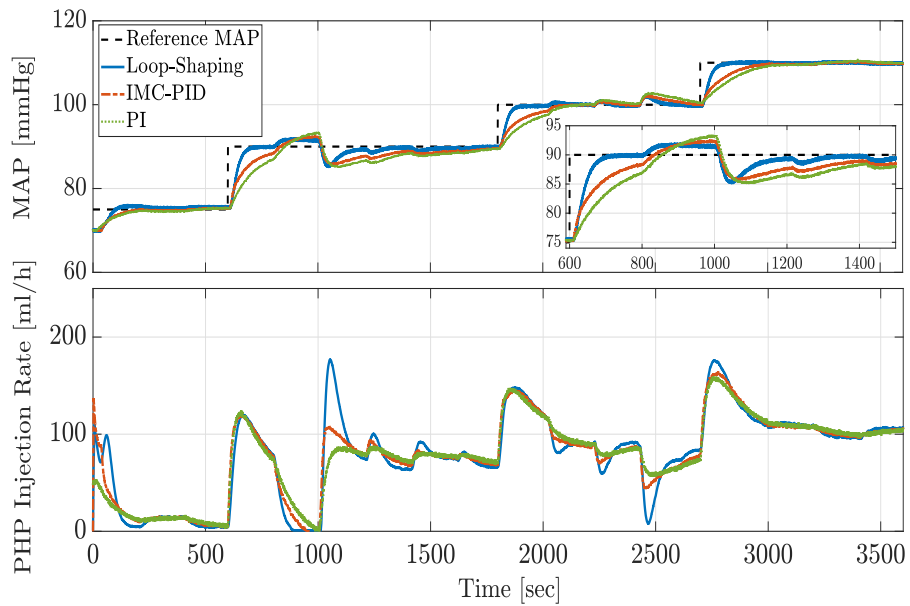
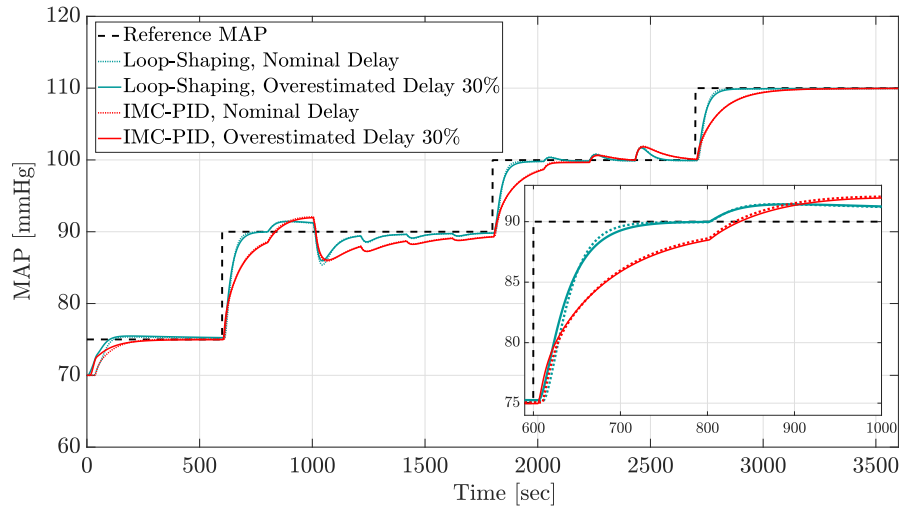
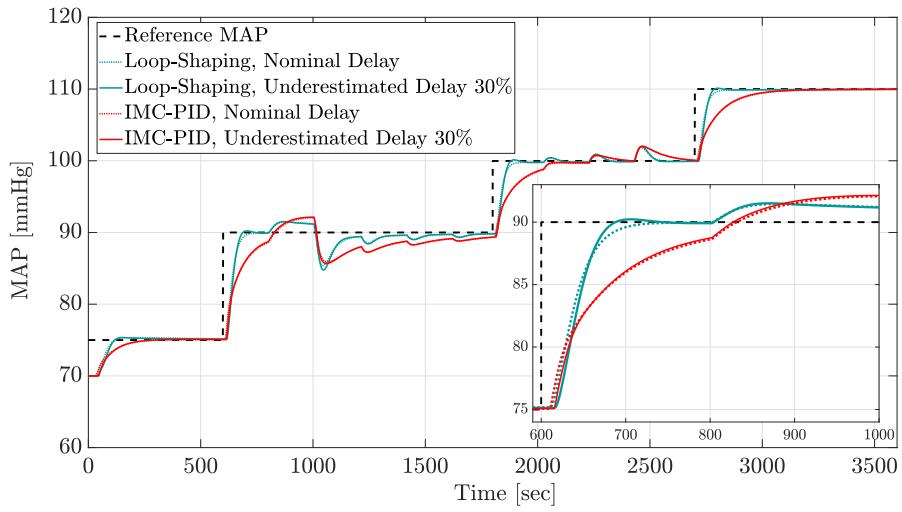


Figure 24: Tracking performance and control effort for closed-loop system with disturbances and measurement noise



(a)



(b)

Figure 25: Closed-loop performance of the parameter-varying loop-shaping and IMC-PID controllers in the presence of input and output disturbances and time delay estimation error (a) 30% overestimated time delay value , and (b) 30% underestimated time delay value

### 3.4 Chapter Conclusion

This chapter has focused on comparing robust, and parameter-varying frequency domain-based control design approaches for automatically regulating blood pressure in critical hypotensive patients using vasopressor drug infusion. The governing dynamics of the mean arterial pressure (MAP) response has been expressed by a first-order system with a time-varying delay and varying model parameters. The loop-shaping design methodology is based on the gain and phase margin stability measures, and the structure of the associated controller has been assumed to be parameter-varying based on the varying system parameters. The internal model control (IMC) design has been performed via the small-gain theorem, and a parameter-dependent stability criterion has been derived for the tuning parameter. An equivalent PID controller has been extracted whose coefficients were fixed, and system parameter variations have been assumed as unstructured uncertainties. Sensitivity analysis has then been carried out to achieve a compromise between robust stability and robust performance requirements. Furthermore, such an analysis and tuning further attenuated the overshoot, and the oscillatory response generated a less sluggish closed-loop system and maintained the bandwidth within a desirable range. Closed-loop simulations using a nonlinear patient MAP response model derived from experimental data demonstrated the proposed controllers' desirable robustness against model parameters variations and time-delay while adjusting the set-point response under disturbances and measurement noise.

## 4 Robust Control of LPV Time-Delay Systems

The following chapter appeared in:

1. Proceedings of ASME Dynamic Systems and Control Conference (DSCC), 3, 2019, pp. 1-9.

Title: Delay-Dependent Output-Feedback Control for Blood Pressure Regulation Using LPV Techniques

Authors: Shahin Tasoujian, Karolos Grigoriadis, Matthew Franchek.

Reproduced in part with permission from ASME Dynamic Systems and Control Conference Copyright 2019.

2. IET Control Theory & Applications, 2020, 14 (10), pp. 1334-1345.

Title: Robust Delay-Dependent LPV Synthesis for Blood Pressure Control with Real-Time Bayesian Parameter Estimation

Authors: Shahin Tasoujian, Saeed Salavati, Matthew A Franchek, Karolos Grigoriadis.

Reproduced in part with permission from IET Digital Library, Copyright 2020.

### 4.1 Introduction

In this chapter, first, a robust delay-dependent linear parameter varying (LPV) gain-scheduled dynamic output-feedback controller is proposed to guarantee the specified performance of the closed-loop system and its robustness in terms of the induced  $\mathcal{L}_2$ -norm characteristics when the investigated LPV time-delay system is assumed to be subject to parameter variability, varying time-delay, norm-bounded uncertainties, and disturbances that impair the closed-loop response. Next, we consider an improved parameter-dependent Lyapunov-Krasovskii functional (LKF) candidate, and the affine Jensen's inequality [14] is employed for bounding the integral cross-terms that appear in the LKF derivative. The main contribution of this section resides in the employment of affine Jensen's inequality, and hence, the conservatism that stems from the bounding of integral cross-terms in the derivation of the LKF derivative is substantially diminished. The utilized affine Jensen's inequality bounding technique considers intermediary values of delay instead of assuming the worst-case delay value. These choices of LKF and bounding method, and avoiding model transformations

have enabled us to derive less conservative conditions for the synthesis of delay-dependent dynamic output-feedback controllers for the LPV time-delay systems with large and fast-varying time delays. The proposed approach's conservativeness has been assessed and compared with previous work in the literature through a numerical example.

In the next part of this chapter, we aim to develop an efficient, robust delay-dependent dynamic control design for LPV systems with varying uncertain time delay. To this end, we utilize the proposed improved parameter-dependent LKF candidate and further enhance it with the less conservative descriptor method analysis. The input-output approach is considered to address the stability of the interconnected input-output LPV system representation under a varying uncertain delay [28]. The choices of the LKF and the bounding method and avoiding model transformations have enabled us to derive less conservative sufficient conditions for stability and performance analysis in terms of the induced  $\mathcal{L}_2$ -norm of the closed-loop system. Subsequently, we present robust gain-scheduling state-feedback and dynamic output-feedback controller design methods for the class of LPV time-delay systems with large and fast-varying uncertain time delays are derived. The merit of this work lies in the fact that the proposed approach can deal with arbitrary varying time delays without any constraints on the delay derivative, and the nominal delay is also assumed to be varying, which imposes further challenges in deriving the stability conditions. We examine the stability analysis and the worst-case disturbance amplification in terms of a prescribed induced  $\mathcal{L}_2$ -norm performance index. The final conditions are presented in a convex linear matrix inequality (LMI) format using a Lyapunov-Krasovskii functional approach. Finally, after applying a proper congruent transformation, the control synthesis results are presented in an easy-to-implement setting.

In the next section, we address the sampled-data LPV control design for the mean arterial blood pressure (MAP) response regulation problem. The input-delay technique is used to map the hybrid closed-loop system into the continuous-time domain with delay in the states. Next, delay-dependent conditions are considered to study the stability and  $\mathcal{H}_\infty$ -norm performance analysis of the hybrid closed-loop LPV system, which leads to the sampled-data output-feedback control synthesis. The proposed delay-dependent sampled-data LPV control approach demonstrates superior capability in

dealing with LPV systems with arbitrary varying time-delay and variable sampling rates.

Finally, an LPV time-delay model is assumed to represent the MAP response to PHP drug infusion dynamics as a benchmark example to evaluate the proposed LPV control design methods. Results of computer simulations utilizing collected animal experiment data and a nonlinear patient simulation model demonstrate the superiority and effectiveness of the proposed delay-dependent LPV controllers to achieve desired MAP reference tracking, transient response performance, disturbance rejection and noise attenuation.

## 4.2 Delay-Dependent Gain-Scheduling Control Synthesis for LPV Time-Delay Systems

### 4.2.1 Robust $\mathcal{H}_\infty$ Output-Feedback Control Design

Considering a time-delayed LPV system with the state-space model representation as follows

$$\begin{aligned}
\dot{\mathbf{x}}_p(t) &= \mathbf{A}(\boldsymbol{\rho}(t))\mathbf{x}_p(t) + \mathbf{A}_\tau(\boldsymbol{\rho}(t))\mathbf{x}_p(t - \tau(\boldsymbol{\rho}(t))) + \mathbf{B}_1(\boldsymbol{\rho}(t))\mathbf{w}(t) + \mathbf{B}_2(\boldsymbol{\rho}(t))\mathbf{u}(t), \\
\mathbf{z}(t) &= \mathbf{C}_1(\boldsymbol{\rho}(t))\mathbf{x}_p(t) + \mathbf{C}_{1,\tau}(\boldsymbol{\rho}(t))\mathbf{x}_p(t - \tau(\boldsymbol{\rho}(t))) + \mathbf{D}_{11}(\boldsymbol{\rho}(t))\mathbf{w}(t) + \mathbf{D}_{12}(\boldsymbol{\rho}(t))\mathbf{u}(t), \\
\mathbf{y}(t) &= \mathbf{C}_2(\boldsymbol{\rho}(t))\mathbf{x}_p(t) + \mathbf{C}_{2,\tau}(\boldsymbol{\rho}(t))\mathbf{x}_p(t - \tau(\boldsymbol{\rho}(t))) + \mathbf{D}_{21}(\boldsymbol{\rho}(t))\mathbf{w}(t), \\
\mathbf{x}_p(t_0 + \theta) &= \boldsymbol{\phi}(\theta), \quad \forall \theta \in [-\bar{\tau}, 0],
\end{aligned} \tag{57}$$

where  $\mathbf{x}_p(t) \in \mathbb{R}^{n_p}$  is the state vector,  $\mathbf{w}(t) \in \mathbb{R}^{n_w}$  is the exogenous input vector with bounded  $\mathcal{L}_2$ -norm,  $\mathbf{u}(t) \in \mathbb{R}^{n_u}$  is the control input vector,  $\mathbf{z}(t) \in \mathbb{R}^{n_z}$  is the vector of controlled outputs,  $\mathbf{y}(t) \in \mathbb{R}^{n_y}$  is the vector of measured outputs, and the state space matrices  $\mathbf{A}(\cdot)$ ,  $\mathbf{A}_\tau(\cdot)$ ,  $\mathbf{B}_1(\cdot)$ ,  $\mathbf{B}_2(\cdot)$ ,  $\mathbf{C}_1(\cdot)$ ,  $\mathbf{C}_{1,\tau}(\cdot)$ ,  $\mathbf{D}_{11}(\cdot)$ ,  $\mathbf{D}_{12}(\cdot)$ ,  $\mathbf{C}_2(\cdot)$ ,  $\mathbf{C}_{2,\tau}(\cdot)$ , and  $\mathbf{D}_{21}(\cdot)$  are real-valued matrices which are continuous functions of the time-varying scheduling parameter vector  $\boldsymbol{\rho}(\cdot)$ . This vector is assumed to be measurable in real-time with known bounds and belongs to the following set

$$\mathcal{F}_{\mathcal{P}}^\nu \triangleq \{\boldsymbol{\rho}(t) \in \mathcal{C}(\mathbb{R}_+, \mathbb{R}^{n_s}) : \boldsymbol{\rho}(t) \in \mathcal{P}, |\dot{\rho}_i(t)| \leq \nu_i, i = 1, 2, \dots, n_s\}, \tag{58}$$

where  $n_s$  is the number of parameters and  $\mathcal{P}$  is a compact subset of  $\mathbb{R}^{n_s}$ . Moreover, in LPV time-delay model representation (57),  $\phi(\theta) \in \mathcal{C}([-\bar{\tau} \ 0], \mathbb{R}^{n_p})$  is the functional system's initial condition, and  $\tau(t)$  is a differentiable scalar function representing the parameter-varying time delay which lies in the set  $\mathcal{T}^{\nu_\tau}$  defined as

$$\mathcal{T}^{\nu_\tau} \triangleq \{\tau(\boldsymbol{\rho}(t)) \in \mathcal{C}(\mathcal{P}, \mathbb{R}_+) : 0 \leq \tau(\cdot) \leq \bar{\tau} < \infty, \dot{\tau}(\cdot) \leq \nu_\tau\}. \quad (59)$$

Considering the LPV time-delay system (57), with an allowable parameter vector trajectory in  $\mathcal{F}_{\mathcal{P}}^\nu$ , and a time-delay in  $\mathcal{T}^{\nu_\tau}$ , the design objectives are as follows:

- Asymptotic stability of the LPV system with an uncertain varying time-delay in the presence of parameter variations, delay uncertainties, and disturbances, and
- Minimization of the worst-case amplification of the desired output,  $\mathbf{z}$ , to a nonzero disturbance signal,  $\mathbf{w}$ , with bounded energy, *i.e.*, solving the problem of the induced  $\mathcal{L}_2$ -norm (energy-to-energy gain) of the mapping  $\mathbf{T}_{\mathbf{z}\mathbf{w}} : \mathbf{w} \rightarrow \mathbf{z}$  given by

$$\min \|\mathbf{T}_{\mathbf{z}\mathbf{w}}\|_{i,2} = \min \sup_{\boldsymbol{\rho} \in \mathcal{F}_{\mathcal{P}}^\nu} \sup_{\|\mathbf{w}\|_2 \neq 0, \mathbf{w} \in \mathcal{L}_2} \frac{\|\mathbf{z}\|_2}{\|\mathbf{w}\|_2}. \quad (60)$$

However, instead of the optimal objective (60), we address the suboptimal problem as

$$\|\mathbf{T}_{\mathbf{z}\mathbf{w}}\|_{i,2} < \gamma, \quad (61)$$

where  $\gamma$  is a positive scalar. This means that if the condition (61) holds, the  $\mathcal{L}_2$ -norm of the desired output signal is bounded by  $\gamma\|\mathbf{w}\|_2$  for any nonzero disturbance signal with bounded energy, *i.e.*,  $\|\mathbf{w}\|_{\mathcal{L}_2} \neq 0, \mathbf{w} \in \mathcal{L}_2$ .

A full-order delay-dependent dynamic output-feedback LPV controller is considered in the following form

$$\begin{aligned}\dot{\mathbf{x}}_K(t) &= \mathbf{A}_K(\boldsymbol{\rho}(t))\mathbf{x}_K(t) + \mathbf{A}_{\tau,K}(\boldsymbol{\rho}(t))\mathbf{x}_K(t - \tau(\boldsymbol{\rho}(t))) + \mathbf{B}_K(\boldsymbol{\rho}(t))\mathbf{y}(t), \\ \mathbf{u}(t) &= \mathbf{C}_K(\boldsymbol{\rho}(t))\mathbf{x}_K(t) + \mathbf{C}_{\tau,K}(\boldsymbol{\rho}(t))\mathbf{x}_K(t - \tau(\boldsymbol{\rho}(t))) + \mathbf{D}_K(\boldsymbol{\rho}(t))\mathbf{y}(t),\end{aligned}\tag{62}$$

where  $\mathbf{x}_K(t) \in \mathbb{R}^{n_p}$  is the controller state vector and  $\mathbf{x}_K(t - \tau(\boldsymbol{\rho}(t))) \in \mathbb{R}^{n_p}$  is the delayed state of the controller, which is included in the controller structure to improve the closed-loop results compared a the memoryless controller. It should be noted that, in order to achieve convex conditions, the controller is assumed to be full order, *i.e.*, the order of the controller is equal to  $n_p$ . Considering (57) and (62), and defining the closed-loop state vector as  $\mathbf{x}_{cl}^T(t) \triangleq [\mathbf{x}_p^T(t) \quad \mathbf{x}_K^T(t)]$ , closed-loop system will be in following form

$$\begin{aligned}\dot{\mathbf{x}}_{cl}(t) &= \mathbf{A}_{cl} \mathbf{x}_{cl}(t) + \mathbf{A}_{\tau,cl} \mathbf{x}_{cl}(t - \tau(\boldsymbol{\rho}(t))) + \mathbf{B}_{cl} \mathbf{w}(t), \\ \mathbf{z}(t) &= \mathbf{C}_{cl} \mathbf{x}_{cl}(t) + \mathbf{C}_{\tau,cl} \mathbf{x}_{cl}(t - \tau(\boldsymbol{\rho}(t))) + \mathbf{D}_{cl} \mathbf{w}(t),\end{aligned}\tag{63}$$

where

$$\begin{aligned}\mathbf{A}_{cl} &= \begin{bmatrix} \mathbf{A} + \mathbf{B}_2\mathbf{D}_K\mathbf{C}_2 & \mathbf{B}_2\mathbf{C}_K \\ \mathbf{B}_K\mathbf{C}_2 & \mathbf{A}_K \end{bmatrix}, \mathbf{A}_{\tau,cl} = \begin{bmatrix} \mathbf{A}_\tau + \mathbf{B}_2\mathbf{D}_K\mathbf{C}_{2,\tau} & \mathbf{B}_2\mathbf{C}_{\tau,K} \\ \mathbf{B}_K\mathbf{C}_{2,\tau} & \mathbf{A}_{\tau,K} \end{bmatrix}, \\ \mathbf{B}_{cl} &= \begin{bmatrix} \mathbf{B}_1 + \mathbf{B}_2\mathbf{D}_K\mathbf{D}_{21} \\ \mathbf{B}_K\mathbf{D}_{21} \end{bmatrix}, \mathbf{C}_{cl} = \begin{bmatrix} \mathbf{C}_1 + \mathbf{D}_{12}\mathbf{D}_K\mathbf{C}_2 & \mathbf{D}_{12}\mathbf{C}_K \end{bmatrix}, \\ \mathbf{C}_{\tau,cl} &= \begin{bmatrix} \mathbf{C}_{1,\tau} + \mathbf{D}_{12}\mathbf{D}_K\mathbf{C}_{2,\tau} & \mathbf{D}_{12}\mathbf{C}_{\tau,K} \end{bmatrix}, \mathbf{D}_{cl} = \mathbf{D}_{11} + \mathbf{D}_{12}\mathbf{D}_K\mathbf{D}_{21},\end{aligned}\tag{64}$$

and the dependence on the scheduling parameter vector has been dropped for brevity. Now, considering the closed-loop system (63), the following result provides sufficient conditions for the synthesis of a delayed output-feedback controller to guarantee closed-loop asymptotic stability and a specified level of disturbance rejection performance according to (61).

**Theorem 2.** [15]: The system (57) is asymptotically stable over  $\boldsymbol{\rho} \in \mathcal{F}_{\mathcal{D}}^{\nu}$  and  $\tau \in \mathcal{T}^{\nu\tau}$  and satisfies the induced  $\mathcal{L}_2$ -norm performance specification (61), if there exists a continuously differentiable matrix function  $\tilde{\mathbf{P}}(\boldsymbol{\rho}(t)) : \mathcal{F}_{\mathcal{D}}^{\nu} \mapsto \mathbb{S}_{++}^{2n_p}$ , parameter dependent matrix functions  $\mathbf{X}(\boldsymbol{\rho}(t)), \mathbf{Y}(\boldsymbol{\rho}(t)) : \mathcal{F}_{\mathcal{D}}^{\nu} \mapsto \mathbb{S}_{++}^{n_p}$ , constant matrices  $\tilde{\mathbf{Q}}, \tilde{\mathbf{R}} \in \mathbb{S}_{++}^{n_p}$ , parameter dependent matrices  $\hat{\mathbf{A}}(\boldsymbol{\rho}(t)), \hat{\mathbf{A}}_{\tau}(\boldsymbol{\rho}(t)) : \mathcal{F}_{\mathcal{D}}^{\nu} \mapsto \mathbb{R}^{n_p \times n_p}$ ,  $\hat{\mathbf{B}}(\boldsymbol{\rho}(t)) : \mathcal{F}_{\mathcal{D}}^{\nu} \mapsto \mathbb{R}^{n_p \times n_y}$ ,  $\hat{\mathbf{C}}(\boldsymbol{\rho}(t)), \hat{\mathbf{C}}_{\tau}(\boldsymbol{\rho}(t)) : \mathcal{F}_{\mathcal{D}}^{\nu} \mapsto \mathbb{R}^{n_u \times n_p}$ ,  $\mathbf{D}_k(\boldsymbol{\rho}(t)) : \mathcal{F}_{\mathcal{D}}^{\nu} \mapsto \mathbb{R}^{n_u \times n_y}$ , and scalars  $\gamma > 0$ ,  $\lambda_2$ , and  $\lambda_3$  such that the following LMI condition

$$\begin{bmatrix} -2\tilde{\mathbf{V}} & \tilde{\mathbf{P}} - \lambda_2\tilde{\mathbf{V}} + \mathcal{A} & -\lambda_3\tilde{\mathbf{V}} + \mathcal{A}_{\tau} & \mathcal{B} & \mathbf{0} & \tilde{\mathbf{V}} + \bar{\tau}\tilde{\mathbf{R}} \\ * & \tilde{\Psi}_{22} + \lambda_2(\mathcal{A} + \mathcal{A}^T) & \tilde{\mathbf{R}} + \lambda_3\mathcal{A}^T + \lambda_2\mathcal{A}_{\tau} & \lambda_2\mathcal{B} & \mathcal{C}^T & \lambda_2\tilde{\mathbf{V}} - \tilde{\mathbf{P}} \\ * & * & \tilde{\Xi}_{22} + \lambda_3(\mathcal{A}_{\tau} + \mathcal{A}_{\tau}^T) & \lambda_3\mathcal{B} & \mathcal{C}_{\tau}^T & \lambda_3\tilde{\mathbf{V}} \\ * & * & * & -\gamma\mathbf{I} & \mathcal{D}^T & \mathbf{0} \\ * & * & * & * & -\gamma\mathbf{I} & \mathbf{0} \\ * & * & * & * & * & (-1 - 2\bar{\tau})\tilde{\mathbf{R}} \end{bmatrix} \prec \mathbf{0}, \quad (65)$$

holds, with

$$\begin{aligned} \tilde{\mathbf{V}} &= \begin{bmatrix} \mathbf{Y} & \mathbf{I} \\ \mathbf{I} & \mathbf{X} \end{bmatrix}, \\ \mathcal{A} &= \begin{bmatrix} \mathbf{A}\mathbf{Y} + \mathbf{B}_2\hat{\mathbf{C}} & \mathbf{A} + \mathbf{B}_2\mathbf{D}_K\mathbf{C}_2 \\ \hat{\mathbf{A}} & \mathbf{X}\mathbf{A} + \hat{\mathbf{B}}\mathbf{C}_2 \end{bmatrix}, \\ \mathcal{A}_{\tau} &= \begin{bmatrix} \mathbf{A}_{\tau}\mathbf{Y} + \mathbf{B}_2\hat{\mathbf{C}}_{\tau} & \mathbf{A}_{\tau} + \mathbf{B}_2\mathbf{D}_K\mathbf{C}_{2,\tau} \\ \hat{\mathbf{A}}_{\tau} & \mathbf{X}\mathbf{A}_{\tau} + \hat{\mathbf{B}}\mathbf{C}_{2,\tau} \end{bmatrix}, \\ \mathcal{B} &= \begin{bmatrix} \mathbf{B}_1 + \mathbf{B}_2\mathbf{D}_K\mathbf{D}_{21} \\ \mathbf{X}\mathbf{B}_1 + \hat{\mathbf{B}}\mathbf{D}_{21} \end{bmatrix}, \\ \mathcal{C} &= \begin{bmatrix} \mathbf{C}_1\mathbf{Y} + \mathbf{D}_{12}\hat{\mathbf{C}} & \mathbf{C}_1 + \mathbf{D}_{12}\mathbf{D}_K\mathbf{C}_2 \end{bmatrix}, \\ \mathcal{C}_{\tau} &= \begin{bmatrix} \mathbf{C}_{1,\tau}\mathbf{Y} + \mathbf{D}_{12}\hat{\mathbf{C}}_{\tau} & \mathbf{C}_{1,\tau} + \mathbf{D}_{12}\mathbf{D}_K\mathbf{C}_{2,\tau} \end{bmatrix}, \\ \mathcal{D} &= \begin{bmatrix} \mathbf{D}_{11} + \mathbf{D}_{12}\mathbf{D}_K\mathbf{D}_{21} \end{bmatrix}, \end{aligned}$$

$$\begin{aligned}
\tilde{\Psi}_{22} &= \sum_{i=1}^{n_s} \pm(\nu_i \frac{\partial \tilde{\mathbf{P}}}{\partial \rho_i}) + \tilde{\mathbf{Q}} - \tilde{\mathbf{R}}, \\
\tilde{\Xi}_{22} &= -\left(1 + \sum_{i=1}^{n_s} \pm(\nu_i \frac{\partial \tau}{\partial \rho_i})\right) \tilde{\mathbf{Q}} - \tilde{\mathbf{R}}.
\end{aligned} \tag{66}$$

For the robust LPV control synthesis, we consider a class of uncertain time-delay LPV systems norm-bounded uncertainties in the state and delayed state matrices as

$$\begin{aligned}
\dot{\mathbf{x}}_p(t) &= \mathbf{A}_\Delta(\boldsymbol{\rho}(t))\mathbf{x}_p(t) + \mathbf{A}_{\Delta\tau}(\boldsymbol{\rho}(t))\mathbf{x}_p(t - \tau(\boldsymbol{\rho}(t))) + \mathbf{B}_1(\boldsymbol{\rho}(t))\mathbf{w}(t) + \mathbf{B}_2(\boldsymbol{\rho}(t))\mathbf{u}(t) \\
\mathbf{z}(t) &= \mathbf{C}_1(\boldsymbol{\rho}(t))\mathbf{x}_p(t) + \mathbf{C}_{1,\tau}(\boldsymbol{\rho}(t))\mathbf{x}_p(t - \tau(\boldsymbol{\rho}(t))) + \mathbf{D}_{11}(\boldsymbol{\rho}(t))\mathbf{w}(t) + \mathbf{D}_{12}(\boldsymbol{\rho}(t))\mathbf{u}(t) \\
y(t) &= \mathbf{C}_2(\boldsymbol{\rho}(t))\mathbf{x}_p(t) + \mathbf{C}_{2,\tau}(\boldsymbol{\rho}(t))\mathbf{x}_p(t - \tau(\boldsymbol{\rho}(t))) + \mathbf{D}_{21}(\boldsymbol{\rho}(t))\mathbf{w}(t),
\end{aligned} \tag{67}$$

where  $\mathbf{A}_\Delta(\boldsymbol{\rho}(t)) = \mathbf{A}(\boldsymbol{\rho}(t)) + \Delta\mathbf{A}(t)$ ,  $\mathbf{A}_{\Delta\tau}(\boldsymbol{\rho}(t)) = \mathbf{A}_\tau(\boldsymbol{\rho}(t)) + \Delta\mathbf{A}_\tau(t)$  are bounded matrices containing parametric uncertainties. The norm-bounded uncertainties are assumed to satisfy the following relation

$$\begin{bmatrix} \Delta\mathbf{A}(t) \\ \Delta\mathbf{A}_\tau(t) \end{bmatrix} = \mathbf{H}\boldsymbol{\Delta}(t) \begin{bmatrix} \mathbf{E}_1 \\ \mathbf{E}_2 \end{bmatrix}, \tag{68}$$

where  $\mathbf{H} \in \mathbb{R}^{n_p \times i}$ ,  $\mathbf{E}_1 \in \mathbb{R}^{j \times n_p}$ ,  $\mathbf{E}_2 \in \mathbb{R}^{j \times n_p}$  are known constant matrices and  $\boldsymbol{\Delta}(t) \in \mathbb{R}^{i \times j}$  is an unknown time-varying uncertainty matrix function satisfying

$$\boldsymbol{\Delta}^T(t)\boldsymbol{\Delta}(t) \preceq \mathbf{I}. \tag{69}$$

Now, considering the uncertain delayed LPV system (67), the following result provides sufficient conditions for the synthesis of a robust time-delay output-feedback LPV controller, in the form of (62), which guarantees the asymptotic stability and a specified level of disturbance rejection performance as in (61) for the uncertain closed-loop time-delay system.

**Theorem 3.** *There exists a full-order robust output-feedback LPV controller of the form (62) which asymptotically stabilizes the uncertain LPV system (67) with all admissible uncertainties  $\Delta\mathbf{A}(t)$  and  $\Delta\mathbf{A}_\tau(t)$  of the form (68) and  $\boldsymbol{\Delta}(t)$  satisfying (69) with  $\boldsymbol{\rho} \in \mathcal{F}_\varphi^\nu$  and  $\tau \in \mathcal{T}^{\nu_\tau}$  and satisfies  $\|\mathbf{z}\|_2 \leq \gamma\|\mathbf{w}\|_2$  for the closed-loop system, if there exists a continuously differentiable matrix function*

$\tilde{\mathbf{P}}(\boldsymbol{\rho}(t)) : \mathcal{F}_{\mathcal{D}}^{\nu} \mapsto \mathbb{S}_{++}^{2n_p}$ , parameter dependent matrix functions  $\mathbf{X}(\boldsymbol{\rho}(t)), \mathbf{Y}(\boldsymbol{\rho}(t)) : \mathcal{F}_{\mathcal{D}}^{\nu} \mapsto \mathbb{S}_{++}^{n_p}$ , constant matrices  $\tilde{\mathbf{Q}}, \tilde{\mathbf{R}} \in \mathbb{S}_{++}^{n_p}$ , parameter dependent matrices  $\hat{\mathbf{A}}(\boldsymbol{\rho}(t)), \hat{\mathbf{A}}_{\tau}(\boldsymbol{\rho}(t)) : \mathcal{F}_{\mathcal{D}}^{\nu} \mapsto \mathbb{R}^{n_p \times n_p}$ ,  $\hat{\mathbf{B}}(\boldsymbol{\rho}(t)) : \mathcal{F}_{\mathcal{D}}^{\nu} \mapsto \mathbb{R}^{n_p \times n_y}$ ,  $\hat{\mathbf{C}}(\boldsymbol{\rho}(t)), \hat{\mathbf{C}}_{\tau}(\boldsymbol{\rho}(t)) : \mathcal{F}_{\mathcal{D}}^{\nu} \mapsto \mathbb{R}^{n_u \times n_p}$ ,  $\mathbf{D}_k(\boldsymbol{\rho}(t)) : \mathcal{F}_{\mathcal{D}}^{\nu} \mapsto \mathbb{R}^{n_u \times n_y}$ , and scalars  $\gamma > 0$ ,  $\epsilon > 0$ ,  $\lambda_2$ , and  $\lambda_3$  such that the following LMI

$$\left[ \begin{array}{cccc}
 -2\tilde{\mathbf{V}} & \tilde{\mathbf{P}} - \lambda_2\tilde{\mathbf{V}} + \mathcal{A} & -\lambda_3\tilde{\mathbf{V}} + \mathcal{A}_{\tau} & \mathcal{B} \\
 * & \tilde{\Psi}_{22} + \lambda_2(\mathcal{A} + \mathcal{A}^T) & \tilde{\mathbf{R}} + \lambda_3\mathcal{A}^T + \lambda_2\mathcal{A}_{\tau} & \lambda_2\mathcal{B} \\
 * & * & \tilde{\Xi}_{22} + \lambda_3(\mathcal{A}_{\tau} + \mathcal{A}_{\tau}^T) & \lambda_3\mathcal{B} \\
 * & * & * & -\gamma\mathbf{I} \\
 * & * & * & * \\
 * & * & * & * \\
 * & * & * & * \\
 * & * & * & * \\
 * & * & * & * \\
 \mathbf{0} & \tilde{\mathbf{V}} + \bar{\tau}\tilde{\mathbf{R}} & \begin{bmatrix} \mathbf{H}^T & \mathbf{H}^T\mathbf{X} \\ \mathbf{0} & \mathbf{0} \end{bmatrix} & \mathbf{0} \\
 \mathcal{C}^T & \lambda_2\tilde{\mathbf{V}} - \tilde{\mathbf{P}} & \lambda_2 \begin{bmatrix} \mathbf{H}^T & \mathbf{H}^T\mathbf{X} \\ \mathbf{0} & \mathbf{0} \end{bmatrix} & \epsilon \begin{bmatrix} \mathbf{Y}^T\mathbf{E}_1^T & \mathbf{0} \\ \mathbf{E}_1^T & \mathbf{0} \end{bmatrix} \\
 \mathcal{C}_{\tau}^T & \lambda_3\tilde{\mathbf{V}} & \lambda_3 \begin{bmatrix} \mathbf{H}^T & \mathbf{H}^T\mathbf{X} \\ \mathbf{0} & \mathbf{0} \end{bmatrix} & \epsilon \begin{bmatrix} \mathbf{Y}^T\mathbf{E}_2^T & \mathbf{0} \\ \mathbf{E}_2^T & \mathbf{0} \end{bmatrix} \\
 \mathcal{D}^T & \mathbf{0} & \mathbf{0} & \mathbf{0} \\
 -\gamma\mathbf{I} & \mathbf{0} & \mathbf{0} & \mathbf{0} \\
 * & (-1 - 2\bar{\tau})\tilde{\mathbf{R}} & \mathbf{0} & \mathbf{0} \\
 * & * & -\epsilon\mathbf{I} & \mathbf{0} \\
 * & * & * & -\epsilon\mathbf{I}
 \end{array} \right] \prec \mathbf{0}, \tag{70}$$

is feasible, with  $\tilde{\mathbf{V}}, \mathcal{A}, \mathcal{A}_{\tau}, \mathcal{B}, \mathcal{C}, \mathcal{C}_{\tau}, \mathcal{D}, \tilde{\Psi}_{22}$ , and  $\tilde{\Xi}_{22}$  as in (66).

*Proof.* By substituting the matrices with additive norm-bounded uncertainties, *i.e.*,  $\mathbf{A}_\Delta(\boldsymbol{\rho}(t)) = \mathbf{A}(\boldsymbol{\rho}(t)) + \Delta\mathbf{A}(t)$  and  $\mathbf{A}_{\Delta\tau}(\boldsymbol{\rho}(t)) = \mathbf{A}_\tau(\boldsymbol{\rho}(t)) + \Delta\mathbf{A}_\tau(t)$ , for  $\mathbf{A}(\boldsymbol{\rho}(t))$  and  $\mathbf{A}_\tau(\boldsymbol{\rho}(t))$  into the LMI condition (65) of Theorem 2, we obtain

$$\begin{bmatrix}
-2\tilde{\mathbf{V}} & & \tilde{\mathbf{P}} - \lambda_2\tilde{\mathbf{V}} + \mathcal{A} + \begin{bmatrix} \Delta\mathbf{A}\mathbf{Y} & \Delta\mathbf{A} \\ \mathbf{0} & \mathbf{X}\Delta\mathbf{A} \end{bmatrix} \\
* & \tilde{\Psi}_{22} + \lambda_2(\mathcal{A} + \mathcal{A}^\top) + \lambda_2\left(\begin{bmatrix} \Delta\mathbf{A}\mathbf{Y} & \Delta\mathbf{A} \\ \mathbf{0} & \mathbf{X}\Delta\mathbf{A} \end{bmatrix} + \begin{bmatrix} \Delta\mathbf{A}\mathbf{Y} & \Delta\mathbf{A} \\ \mathbf{0} & \mathbf{X}\Delta\mathbf{A} \end{bmatrix}^\top\right) \\
* & & * \\
* & & * \\
* & & * \\
* & & * \\
& -\lambda_3\tilde{\mathbf{V}} + \mathcal{A}_\tau + \begin{bmatrix} \Delta\mathbf{A}_\tau\mathbf{Y} & \Delta\mathbf{A}_\tau \\ \mathbf{0} & \mathbf{X}\Delta\mathbf{A}_\tau \end{bmatrix} & \mathcal{B} & \mathbf{0} & \tilde{\mathbf{V}} + \bar{\tau}\tilde{\mathbf{R}} \\
& \tilde{\mathbf{R}} + \lambda_3\mathcal{A}^\top + \lambda_2\mathcal{A}_\tau + \lambda_3\left(\begin{bmatrix} \Delta\mathbf{A}\mathbf{Y} & \Delta\mathbf{A} \\ \mathbf{0} & \mathbf{X}\Delta\mathbf{A} \end{bmatrix}^\top + \lambda_2\begin{bmatrix} \Delta\mathbf{A}_\tau\mathbf{Y} & \Delta\mathbf{A}_\tau \\ \mathbf{0} & \mathbf{X}\Delta\mathbf{A}_\tau \end{bmatrix}\right) & \lambda_2\mathcal{B} & \mathcal{C}^\top & \lambda_2\tilde{\mathbf{V}} - \tilde{\mathbf{P}} \\
& \tilde{\mathbf{E}}_{22} + \lambda_3(\mathcal{A}_\tau + \mathcal{A}_\tau^\top) + \lambda_3\left(\begin{bmatrix} \Delta\mathbf{A}_\tau\mathbf{Y} & \Delta\mathbf{A}_\tau \\ \mathbf{0} & \mathbf{X}\Delta\mathbf{A}_\tau \end{bmatrix} + \begin{bmatrix} \Delta\mathbf{A}_\tau\mathbf{Y} & \Delta\mathbf{A}_\tau \\ \mathbf{0} & \mathbf{X}\Delta\mathbf{A}_\tau \end{bmatrix}^\top\right) & \lambda_3\mathcal{B} & \mathcal{C}_\tau^\top & \lambda_3\tilde{\mathbf{V}} \\
& & * & -\gamma\mathbf{I} & \mathcal{D}^\top & \mathbf{0} \\
& & * & * & -\gamma\mathbf{I} & \mathbf{0} \\
& & * & * & * & (-1 - 2\bar{\tau})\tilde{\mathbf{R}}
\end{bmatrix} < \mathbf{0}. \tag{71}$$

This constraint can also be written as the summation of the initial LMI constraint (65) and the LMI corresponding to the uncertain parts as shown in (72). That is

$$(71) = (65) +$$

$$\begin{aligned}
 & \begin{bmatrix} 0 \\ * \\ * \\ * \\ * \\ * \end{bmatrix} \left( \begin{bmatrix} \Delta AY & \Delta A \\ 0 & X\Delta A \end{bmatrix} + \lambda_2 \left( \begin{bmatrix} \Delta AY & \Delta A \\ 0 & X\Delta A \end{bmatrix} + \begin{bmatrix} \Delta AY & \Delta A \\ 0 & X\Delta A \end{bmatrix}^T \right) \right) \\
 & \begin{bmatrix} * \\ * \\ * \\ * \end{bmatrix} \left( \begin{bmatrix} \Delta A_\tau Y & \Delta A_\tau \\ 0 & X\Delta A_\tau \end{bmatrix} + \lambda_3 \left( \begin{bmatrix} \Delta AY & \Delta A \\ 0 & X\Delta A \end{bmatrix}^T + \lambda_2 \begin{bmatrix} \Delta A_\tau Y & \Delta A_\tau \\ 0 & X\Delta A_\tau \end{bmatrix} \right) + \lambda_3 \left( \begin{bmatrix} \Delta A_\tau Y & \Delta A_\tau \\ 0 & X\Delta A_\tau \end{bmatrix} + \begin{bmatrix} \Delta A_\tau Y & \Delta A_\tau \\ 0 & X\Delta A_\tau \end{bmatrix}^T \right) \right) \\
 & \begin{bmatrix} 0 & 0 & 0 \\ 0 & 0 & 0 \\ 0 & 0 & 0 \\ * & 0 & 0 \\ * & * & 0 \end{bmatrix} \prec \mathbf{0}.
 \end{aligned} \tag{72}$$

Finally (72) can be equivalently written as

$$(71) = (65) + \text{He} \left( \begin{array}{c} \left[ \begin{array}{cc} \mathbf{H} & \mathbf{0} \\ \mathbf{XH} & \mathbf{0} \end{array} \right] \\ \lambda_2 \left[ \begin{array}{cc} \mathbf{H} & \mathbf{0} \\ \mathbf{XH} & \mathbf{0} \end{array} \right] \\ \lambda_3 \left[ \begin{array}{cc} \mathbf{H} & \mathbf{0} \\ \mathbf{XH} & \mathbf{0} \end{array} \right] \\ \mathbf{0} \\ \mathbf{0} \\ \mathbf{0} \end{array} \right) \begin{bmatrix} \Delta(t) & \mathbf{0} \\ \mathbf{0} & \Delta(t) \end{bmatrix} \quad (73)$$

$$\left( \mathbf{0}, \left[ \begin{array}{cc} \mathbf{E}_1 \mathbf{Y} & \mathbf{E}_1 \\ \mathbf{0} & \mathbf{0} \end{array} \right], \left[ \begin{array}{cc} \mathbf{E}_2 \mathbf{Y} & \mathbf{E}_2 \\ \mathbf{0} & \mathbf{0} \end{array} \right], \mathbf{0}, \mathbf{0}, \mathbf{0} \right) \prec \mathbf{0}.$$

Finally, using the following inequality [100]

$$\Theta \Delta(t) \Phi + \Phi^T \Delta^T(t) \Theta^T \leq \epsilon^{-1} \Theta \Theta^T + \epsilon \Phi^T \Phi, \quad (74)$$

which holds for all scalars  $\epsilon > 0$  and all constant matrices  $\Theta$  and  $\Phi$  of appropriate dimensions, and using the Schur complement [12], the final LMI condition (70) is obtained and it completes the proof.  $\square$

### LPV Controller Synthesis Procedure

The parameter dependent decision matrix variables  $\mathbf{X}$ ,  $\mathbf{Y}$ ,  $\widehat{A}$ ,  $\widehat{A}_\tau$ ,  $\widehat{B}$ ,  $\widehat{C}$ ,  $\widehat{C}_\tau$ , and  $\mathbf{D}_K$  are determined to minimize the performance index  $\gamma$  and to hold the LMI condition (70). Subsequently, the delayed gain-scheduling output-feedback controller (62) matrices are computed through the following steps:

1. Determine  $\mathcal{M}$  and  $\mathcal{N}$  from the factorization problem

$$\mathbf{I} - \mathbf{X}\mathbf{Y} = \mathcal{N}\mathcal{M}^T, \quad (75)$$

where the obtained  $\mathcal{M}$  and  $\mathcal{N}$  matrices are square and invertible in the case of a full-order controller.

2. Consider the following relations

$$\begin{aligned} \widehat{A} &= \mathbf{X}\mathbf{A}\mathbf{Y} + \mathbf{X}\mathbf{B}_2\mathbf{D}_K\mathbf{C}_2\mathbf{Y} + \mathcal{N}\mathbf{B}_K\mathbf{C}_2\mathbf{Y} + \mathbf{X}\mathbf{B}_2\mathbf{C}_K\mathcal{M}^T + \mathcal{N}\mathbf{A}_K\mathcal{M}^T, \\ \widehat{A}_\tau &= \mathbf{X}\mathbf{A}_\tau\mathbf{Y} + \mathbf{X}\mathbf{B}_2\mathbf{D}_K\mathbf{C}_{2,\tau}\mathbf{Y} + \mathcal{N}\mathbf{B}_K\mathbf{C}_{2,\tau}\mathbf{Y} + \mathbf{X}\mathbf{B}_2\mathbf{C}_{\tau,K}\mathcal{M}^T + \mathcal{N}\mathbf{A}_{\tau,K}\mathcal{M}^T, \\ \widehat{B} &= \mathbf{X}\mathbf{B}_2\mathbf{D}_K + \mathcal{N}\mathbf{B}_K, \\ \widehat{C} &= \mathbf{D}_K\mathbf{C}_2\mathbf{Y} + \mathbf{C}_K\mathcal{M}^T, \\ \widehat{C}_\tau &= \mathbf{D}_K\mathbf{C}_{2,\tau}\mathbf{Y} + \mathbf{C}_{\tau,K}\mathcal{M}^T. \end{aligned} \quad (76)$$

3. Finally, Compute the controller matrices in the following order

$$\begin{aligned} \mathbf{C}_{\tau,K} &= (\widehat{C}_\tau - \mathbf{D}_K\mathbf{C}_{2,\tau}\mathbf{Y})\mathcal{M}^{-T}, \\ \mathbf{C}_K &= (\widehat{C} - \mathbf{D}_K\mathbf{C}_2\mathbf{Y})\mathcal{M}^{-T}, \\ \mathbf{B}_K &= \mathcal{N}^{-1}(\widehat{B} - \mathbf{X}\mathbf{B}_2\mathbf{D}_K), \\ \mathbf{A}_{\tau,K} &= -\mathcal{N}^{-1}(\mathbf{X}\mathbf{A}_\tau\mathbf{Y} + \mathbf{X}\mathbf{B}_2\mathbf{D}_K\mathbf{C}_{2,\tau}\mathbf{Y} + \mathcal{N}\mathbf{B}_K\mathbf{C}_{2,\tau}\mathbf{Y} + \mathbf{X}\mathbf{B}_2\mathbf{C}_{\tau,K}\mathcal{M}^T - \widehat{A}_\tau)\mathcal{M}^{-T}, \\ \mathbf{A}_K &= -\mathcal{N}^{-1}(\mathbf{X}\mathbf{A}\mathbf{Y} + \mathbf{X}\mathbf{B}_2\mathbf{D}_K\mathbf{C}_2\mathbf{Y} + \mathcal{N}\mathbf{B}_K\mathbf{C}_2\mathbf{Y} + \mathbf{X}\mathbf{B}_2\mathbf{C}_K\mathcal{M}^T - \widehat{A})\mathcal{M}^{-T}. \end{aligned} \quad (77)$$

#### 4.2.2 Improved Integral Inequality for Less Conservative Control Design

In time-delay systems analysis, frequency-domain approaches are limited to systems with constant delays [58,65]. On the other hand, time-domain techniques utilizing LKFs have recently gained significant attention, primarily because of their potential in addressing the stability analysis and control synthesis of systems with arbitrary varying time-delays. In the Lyapunov-Krasovskii method, the prominent sources of conservatism are rooted in choosing the LKF, the use of model transformations (such as Newton-Leibniz [43] and Padé approximations [42]) and the use of bounding techniques required for constraining the quadratic integral terms of the form  $-\int_{t-\tau(t)}^t \dot{x}^T(s)R\dot{x}(s)ds$ , obtained from the derivative of the LKF. The authors in [64] used an LKF with the parametrized Newton-Leibniz model transformation to obtain sufficient conditions for the stability of time-delay systems. In [67], the same type of LKF, together with Park's inequality, was employed for bounding the cross-terms. Although this bounding method has helped to better address the bounding of cross-terms and hence reducing the conservatism, it still suffers from the use of model transformations that have inherent conservatism. The authors in [102] proposed a parameter-dependent LKF along with Jensen's inequality for the integral term bounding to derive delay-dependent  $\mathcal{H}_\infty$  results for LPV time-delay systems. This approach has avoided any model transformations, and therefore, no conservatism has been introduced in this regard. The resulting conditions have been derived using a more accurate and tighter bounding technique compared to previous work in the literature. Nevertheless, the presented stability and performance conditions are not guaranteed for fast varying time delays with rates greater than one. In the same work, due to the use of a simpler version of Jensen's inequality, intermediary values of delay are all neglected, and only the worst-case delay value is considered, which leads to conservative results and poor performance, especially when the actual delay value is small.

Similar to the previous section, we employ a Lyapunov-Krasovskii based strategy to derive delay-dependent gain-scheduled control synthesis conditions for LPV time-delay systems. Moreover, an improved parameter-dependent LKF candidate is proposed, followed by using an efficient bounding technique, the affine Jensen's inequality, to design an output-feedback LPV controller. These choices

of LKF and integral inequality improved the results by reducing the conservatism of the method by limiting the bounding gap in the integral cross-terms of LKF derivative. After introducing appropriate slack variables, the final relaxed synthesis conditions are formulated in terms of tractable and convex LMI conditions. Additionally, the closed-loop results of the proposed methodology are compared with past work in the literature in terms of conservatism reduction and performance improvement through a simple numerical example.

In this part of the chapter, we will take advantage of the following lemma, which plays a central role in deriving the proposed technical results for the LPV time-delay systems framework.

**Lemma 1. (Affine Jensen's inequality) [14]:** Given a matrix  $\mathbf{J} \in \mathbb{S}_{++}^n$ , a vector function  $g : \mathbb{R}_{\geq 0} \rightarrow \mathbb{R}^n$  integrable over  $[a, b]$ , where  $0 \leq a < b$ , and a vector function  $w : \mathbb{R}_{\geq 0} \times \mathbb{R}_{\geq 0} \rightarrow \mathbb{R}^{n+m}$  satisfying  $\int_a^b g(s) ds = \mathbf{M}w(a, b)$  for a constant matrix  $\mathbf{M} \in \mathbb{R}^{n \times (n+m)}$ , the following inequality

$$-\int_a^b g(s)^T \mathbf{J} g(s) ds \leq w(a, b)^T \mathbf{Q} w(a, b), \quad (78)$$

holds for all  $\mathbf{N} \in \mathbb{R}^{n \times (n+m)}$  with

$$\mathbf{Q} = \mathbf{N}^T \mathbf{M} + \mathbf{M}^T \mathbf{N} + (b - a) \mathbf{N}^T \mathbf{J}^{-1} \mathbf{N}. \quad (79)$$

To achieve less conservative results, we utilize a new extended-state based quadratic LKF candidate with modified integral terms, which depend explicitly on delay. The utilized approach avoids model transformation; hence, it leads to further conservatism reduction. Additionally, affine Jensen's inequality is used for bounding the LKF derivative's cross-terms. In order to derive tractable LMI-based results, other conservative bounding approaches, such as the rational Jensen's inequality, consider the worst-case delay value to upper-bound the rational term. On the other hand, our work's utilized inequality is affine with respect to the time-delay (hence convex), so it provides a tighter bound of the integral terms of the LKF derivative by taking all the possible intermediate time-delay values into account. The following theorem provides sufficient conditions for the synthesis of a delayed dynamic output-feedback LPV controller to meet the control design objectives, namely,

closed-loop asymptotic stability and a specified level of disturbance attenuation performance (61) for the closed-loop system.

**Theorem 4.** *There exists an output-feedback LPV controller of the form (62) to asymptotically stabilize the LPV system (57) and satisfies the induced  $\mathcal{L}_2$ -norm bound performance specification given in (61) with parameter trajectories  $\boldsymbol{\rho} \in \mathcal{F}_{\mathcal{D}}^{\nu}$  and  $\tau \in \mathcal{F}^{\nu\tau}$ , if we can find a continuously differentiable parameter dependent positive-definite matrix functions  $\tilde{\mathbf{P}}(\boldsymbol{\rho}(t)) : \mathcal{F}_{\mathcal{D}}^{\nu} \rightarrow \mathbb{S}_{++}^{2n_p}$ ,  $\mathbf{X}(\boldsymbol{\rho}(t)), \mathbf{Y}(\boldsymbol{\rho}(t)) : \mathcal{F}_{\mathcal{D}}^{\nu} \rightarrow \mathbb{S}^{n_p}$ , positive-definite matrices  $\tilde{\mathbf{Q}}, \tilde{\mathbf{R}} \in \mathbb{S}_{++}^{2n_p}$ , symmetric real matrices  $\tilde{\mathbf{W}}, \tilde{\mathbf{T}} \in \mathbb{S}_{++}^{2n_p}$ , real matrices  $\tilde{\mathbf{N}}_1, \tilde{\mathbf{N}}_2, \tilde{\mathbf{N}}_3 \in \mathbb{R}^{2n_p \times 2n_p}$ , parameter dependent real matrices  $\hat{\mathbf{A}}(\boldsymbol{\rho}(t)), \hat{\mathbf{A}}_{\tau}(\boldsymbol{\rho}(t)) : \mathcal{F}_{\mathcal{D}}^{\nu} \rightarrow \mathbb{R}^{n_p \times n_p}$ ,  $\hat{\mathbf{B}}(\boldsymbol{\rho}(t)) : \mathcal{F}_{\mathcal{D}}^{\nu} \rightarrow \mathbb{R}^{n_p \times n_y}$ ,  $\hat{\mathbf{C}}(\boldsymbol{\rho}(t)), \hat{\mathbf{C}}_{\tau}(\boldsymbol{\rho}(t)) : \mathcal{F}_{\mathcal{D}}^{\nu} \rightarrow \mathbb{R}^{n_u \times n_p}$ ,  $\mathbf{D}_K(\boldsymbol{\rho}(t)) : \mathcal{F}_{\mathcal{D}}^{\nu} \rightarrow \mathbb{R}^{n_u \times n_y}$ , a positive scalar  $\gamma$ , given scalars  $\lambda_2, \lambda_3$ , and  $\lambda_4$  such that the following LMI*

$$\begin{bmatrix} \tilde{\mathbf{E}}_{11} & \tilde{\mathbf{P}} - \tilde{\mathbf{V}} + \lambda_2 \mathcal{A}^T & \tilde{\mathbf{E}}_{13} & (1 - \dot{\tau})\tau \tilde{\mathbf{W}} + \lambda_4 \mathcal{A}^T & \mathcal{B} & \mathcal{C}^T & \mathbf{0} & \tau \tilde{\mathbf{N}}_1^T \\ * & \tau \tilde{\mathbf{R}} + \frac{\tau^2 \dot{\tau}^2}{4} \tilde{\mathbf{W}} - 2\lambda_2 \tilde{\mathbf{V}} & \lambda_2 \mathcal{A}_{\tau} - \lambda_3 \tilde{\mathbf{V}} & -\lambda_4 \tilde{\mathbf{V}} & \lambda_2 \mathcal{B} & \mathbf{0} & \mathbf{0} & \mathbf{0} \\ * & * & \tilde{\mathbf{E}}_{33} & \lambda_4 \mathcal{A}_{\tau}^T & \lambda_3 \mathcal{B} & \mathcal{C}_{\tau}^T & \mathbf{0} & \tau \tilde{\mathbf{N}}_2^T \\ * & * & * & (1 - \dot{\tau})(\tilde{\mathbf{N}}_3^T + \tilde{\mathbf{N}}_3 - \tilde{\mathbf{W}}) & \lambda_4 \mathcal{B} & \mathbf{0} & \tau \tilde{\mathbf{N}}_3^T & \mathbf{0} \\ * & * & * & * & -\gamma^2 \mathbf{I} & \mathcal{D}^T & \mathbf{0} & \mathbf{0} \\ * & * & * & * & * & -\mathbf{I} & \mathbf{0} & \mathbf{0} \\ * & * & * & * & * & * & -\tau \tilde{\mathbf{T}} & \mathbf{0} \\ * & * & * & * & * & * & * & -\tau \tilde{\mathbf{R}} \end{bmatrix} \prec \mathbf{0}, \quad (80)$$

is feasible. In the derived LMI condition (80)

$$\begin{aligned} \tilde{\mathbf{E}}_{11} &= \left[ \sum_{i=1}^{n_s} \pm \left( \nu_i \frac{\partial \tilde{\mathbf{P}}}{\partial \rho_i} \right) \right] + \tilde{\mathbf{Q}} + (\mathcal{A} + \mathcal{A}^T) + \left[ 1 - \sum_{i=1}^{n_s} \pm \left( \nu_i \frac{\partial \tau}{\partial \rho_i} \right) \right] (\tilde{\mathbf{N}}_1^T + \tilde{\mathbf{N}}_1 - \tau^2 \tilde{\mathbf{W}}) + \tau \tilde{\mathbf{T}}, \\ \tilde{\mathbf{E}}_{13} &= \left[ 1 - \sum_{i=1}^{n_s} \pm \left( \nu_i \frac{\partial \tau}{\partial \rho_i} \right) \right] (-\tilde{\mathbf{N}}_1^T + \tilde{\mathbf{N}}_2) + \mathcal{A}_{\tau} + \lambda_3 \mathcal{A}^T, \\ \tilde{\mathbf{E}}_{33} &= \left[ 1 - \sum_{i=1}^{n_s} \pm \left( \nu_i \frac{\partial \tau}{\partial \rho_i} \right) \right] (-\tilde{\mathbf{N}}_2^T - \tilde{\mathbf{N}}_2) - \tilde{\mathbf{Q}} + \lambda_3 (\mathcal{A}_{\tau} + \mathcal{A}_{\tau}^T), \end{aligned} \quad (81)$$

$\dot{\tau} = \sum_{i=1}^{n_s} \pm \left( \nu_i \frac{\partial \tau}{\partial \rho_i} \right)$  and  $\tilde{\mathbf{V}}, \mathcal{A}, \mathcal{A}_{\tau}, \mathcal{B}, \mathcal{C}, \mathcal{C}_{\tau}$ , and  $\mathcal{D}$  are as given in (66).

*Proof.* The proof relies on employing an LKF candidate of the form

$$V(\mathbf{x}_{cl_t}, \dot{\mathbf{x}}_{cl_t}, \boldsymbol{\rho}, t) = V_1(\mathbf{x}_{cl_t}, \boldsymbol{\rho}, t) + V_2(\mathbf{x}_{cl_t}, \boldsymbol{\rho}, t) + V_3(\dot{\mathbf{x}}_{cl_t}, \boldsymbol{\rho}, t) + V_4(\mathbf{x}_{cl_t}, \boldsymbol{\rho}, t) + V_5(\dot{\mathbf{x}}_{cl_t}, \boldsymbol{\rho}, t), \quad (82)$$

with

$$\begin{aligned} V_1(\mathbf{x}_{cl_t}, \boldsymbol{\rho}, t) &= \mathbf{x}_{cl_t}^\top(t) \mathbf{P}(\boldsymbol{\rho}(t)) \mathbf{x}_{cl_t}(t), \\ V_2(\mathbf{x}_{cl_t}, \boldsymbol{\rho}, t) &= \int_{t-\tau(t)}^t \mathbf{x}_{cl_t}^\top(\eta) \mathbf{Q} \mathbf{x}_{cl_t}(\eta) d\eta, \\ V_3(\dot{\mathbf{x}}_{cl_t}, \boldsymbol{\rho}, t) &= \int_{-\tau(t)}^0 \int_{t+\theta}^t \dot{\mathbf{x}}_{cl_t}^\top(\eta) \mathbf{R} \dot{\mathbf{x}}_{cl_t}(\eta) d\eta d\theta, \\ V_4(\mathbf{x}_{cl_t}, \boldsymbol{\rho}, t) &= \int_{-\tau(t)}^0 \int_{t+\theta}^t \mathbf{x}_{cl_t}^\top(\eta) \mathbf{T} \mathbf{x}_{cl_t}(\eta) d\eta d\theta, \\ V_5(\dot{\mathbf{x}}_{cl_t}, \boldsymbol{\rho}, t) &= \int_{-\tau(t)}^0 \int_{\alpha}^0 \int_{t+\theta}^t \dot{\mathbf{x}}_{cl_t}^\top(\eta) \frac{\bar{\tau}^2}{2} \mathbf{W} \dot{\mathbf{x}}_{cl_t}(\eta) d\eta d\theta d\alpha, \end{aligned}$$

The notation  $\mathbf{x}_{cl_t}(\theta)$  refers to  $\mathbf{x}_{cl_t}(t + \theta)$  for  $\theta \in [ -\bar{\tau} \ 0 ]$  where  $\mathbf{x}_{cl_t} \in \mathcal{C}([-\bar{\tau} \ 0], \mathbb{R}^{n_p})$  is the infinite-dimensional state vector of the system.

Our next task is to establish the asymptotic stability of the LPV system based on Lyapunov stability theory. Accordingly, we evaluate the time derivative of the LKF (82) along the trajectories of the closed-loop LPV system (63). After applications of the Leibniz integral rule, the time derivative of LKF is obtained as follows

$$\dot{V}(\mathbf{x}_{cl_t}, \dot{\mathbf{x}}_{cl_t}, \boldsymbol{\rho}, t) = \dot{V}_1(\mathbf{x}_{cl_t}, \boldsymbol{\rho}, t) + \dot{V}_2(\mathbf{x}_{cl_t}, \boldsymbol{\rho}, t) + \dot{V}_3(\dot{\mathbf{x}}_{cl_t}, \boldsymbol{\rho}, t) + \dot{V}_4(\mathbf{x}_{cl_t}, \boldsymbol{\rho}, t) + \dot{V}_5(\dot{\mathbf{x}}_{cl_t}, \boldsymbol{\rho}, t), \quad (83)$$

where

$$\begin{aligned}
\dot{V}_1(\mathbf{x}_{cl}, \boldsymbol{\rho}, t) &= 2\dot{\mathbf{x}}_{cl}^T(t)\mathbf{P}(\boldsymbol{\rho}(t))\mathbf{x}_{cl}(t) + \mathbf{x}_{cl}^T(t) \left[ \sum_{i=1}^{n_s} \dot{\rho}_i(t) \frac{\partial \mathbf{P}(\boldsymbol{\rho}(t))}{\partial \rho_i(t)} \right] \mathbf{x}_{cl}(t), \\
\dot{V}_2(\mathbf{x}_{cl}, \boldsymbol{\rho}, t) &= \mathbf{x}_{cl}^T(t)\mathbf{Q}\mathbf{x}_{cl}(t) - \left(1 - \sum_{i=1}^{n_s} \dot{\rho}_i(t) \frac{\partial \tau(t)}{\partial \rho_i(t)}\right) \mathbf{x}_{cl}^T(t - \tau(t))\mathbf{Q}\mathbf{x}_{cl}(t - \tau(t)), \\
\dot{V}_3(\dot{\mathbf{x}}_{cl}, \boldsymbol{\rho}, t) &= \tau(t)\dot{\mathbf{x}}_{cl}^T(t)\mathbf{R}\dot{\mathbf{x}}_{cl}(t) - \left(1 - \sum_{i=1}^{n_s} \dot{\rho}_i(t) \frac{\partial \tau(t)}{\partial \rho_i(t)}\right) \int_{t-\tau(t)}^t \dot{\mathbf{x}}_{cl}^T(\eta)\mathbf{R}\dot{\mathbf{x}}_{cl}(\eta)d\eta, \\
\dot{V}_4(\mathbf{x}_{cl}, \boldsymbol{\rho}, t) &= \tau(t)\mathbf{x}_{cl}^T(t)\mathbf{T}\mathbf{x}_{cl}(t) - \left(1 - \sum_{i=1}^{n_s} \dot{\rho}_i(t) \frac{\partial \tau(t)}{\partial \rho_i(t)}\right) \int_{t-\tau(t)}^t \mathbf{x}_{cl}^T(\eta)\mathbf{T}\mathbf{x}_{cl}(\eta)d\eta, \\
\dot{V}_5(\dot{\mathbf{x}}_{cl}, \boldsymbol{\rho}, t) &= \frac{\tau^2(t)\bar{\tau}^2}{4}\mathbf{x}_{cl}^T(t)\mathbf{W}\mathbf{x}_{cl}(t) - \left(1 - \sum_{i=1}^{n_s} \dot{\rho}_i(t) \frac{\partial \tau(t)}{\partial \rho_i(t)}\right) \int_{-\tau(t)}^0 \int_{t+\theta}^t \dot{\mathbf{x}}_{cl}^T(\eta) \frac{\bar{\tau}^2}{2} \mathbf{W}\dot{\mathbf{x}}_{cl}(\eta)d\eta d\theta.
\end{aligned}$$

The affine Jensen's inequality (Lemma 1) is used to bound the derivative terms with the negative, integral cross term. This direct bounding technique enables us to provide a delayed-scheduled tight upper bound on the time derivative of the LKF and therefore obtain less conservative results. In this context, the third derivative term is bounded as follows

$$\begin{aligned}
\dot{V}_3(\dot{\mathbf{x}}_{cl}, \boldsymbol{\rho}, t) &\leq \tau(t)\dot{\mathbf{x}}_{cl}^T(t)\mathbf{R}\dot{\mathbf{x}}_{cl}(t) + \left(1 - \sum_{i=1}^{n_s} \dot{\rho}_i(t) \frac{\partial \tau(t)}{\partial \rho_i(t)}\right) \underbrace{\left[ \mathbf{x}_{cl}^T(t) \quad \mathbf{x}_{cl}^T(t - \tau(t)) \right]}_{w(t-\tau(t), t)^T} \\
&\left( \underbrace{\begin{bmatrix} \mathbf{N}_1^T + \mathbf{N}_1 & -\mathbf{N}_1^T + \mathbf{N}_2 \\ \mathbf{N}_2^T - \mathbf{N}_1 & -\mathbf{N}_2^T - \mathbf{N}_2 \end{bmatrix}}_{\mathbf{N}^T\mathbf{M} + \mathbf{M}^T\mathbf{N}} + \tau(t) \underbrace{\begin{bmatrix} \mathbf{N}_1^T \\ \mathbf{N}_2^T \end{bmatrix}}_{\mathbf{N}^T} \underbrace{\left\{ \mathbf{J}^{-1} \begin{bmatrix} \mathbf{N}_1 & \mathbf{N}_2 \end{bmatrix} \right\}}_{\mathbf{N}} \right) \underbrace{\begin{bmatrix} \mathbf{x}_{cl}(t) \\ \mathbf{x}_{cl}(t - \tau(t)) \end{bmatrix}}_{w(t-\tau(t), t)}, \quad (84)
\end{aligned}$$

where by considering the affine Jensen's inequality (1), we choose the function  $g(t) \triangleq \dot{\mathbf{x}}_{cl}(t)$ , integrable over  $[t - \tau(t), t]$  and verifying  $\int_{t-\tau(t)}^t \dot{\mathbf{x}}_{cl}(t)dt = \mathbf{M}w(t - \tau(t), t)$ , where  $\mathbf{M} \triangleq [\mathbf{I}, -\mathbf{I}] \in \mathbb{R}^{2n_p \times 4n_p}$

and  $w(t - \tau(t), t) \triangleq \begin{bmatrix} \mathbf{x}_{cl}(t) \\ \mathbf{x}_{cl}(t - \tau(t)) \end{bmatrix} \in \mathbb{R}^{4n_p}$ . Also,  $\mathbf{J} = \mathbf{R} \in \mathbb{S}_{++}^{2n_p}$ , and  $\mathbf{N} = [\mathbf{N}_1, \mathbf{N}_2] \in \mathbb{R}^{2n_p \times 4n_p}$

where  $\mathbf{R}, \mathbf{N}_1 \in \mathbb{R}^{2n_p \times 2n_p}$ , and  $\mathbf{N}_2 \in \mathbb{R}^{2n_p \times 2n_p}$  are additional matrix variables to be determined to hold the inequality.

By employing the same bounding trick on the next derivative terms we obtain

$$\begin{aligned} \dot{V}_4(\mathbf{x}_{cl_t}, \boldsymbol{\rho}, t) &\leq \tau(t) \mathbf{x}_{cl}^T(t) \mathbf{T} \mathbf{x}_{cl}(t) + \left(1 - \sum_{i=1}^{n_s} \dot{\rho}_i(t) \frac{\partial \tau(t)}{\partial \rho_i(t)}\right) \underbrace{\int_{t-\tau(t)}^t \mathbf{x}_{cl}^T(\eta) d\eta}_{w(t-\tau(t), t)^T} \\ &\quad \left( \underbrace{\mathbf{N}_3^T + \mathbf{N}_3}_{\mathbf{N}^T \mathbf{M} + \mathbf{M}^T \mathbf{N}} + \tau(t) \underbrace{\mathbf{N}_3^T}_{\mathbf{N}^T} \underbrace{\mathbf{T}^{-1}}_{\mathbf{J}^{-1}} \underbrace{\mathbf{N}_3}_{\mathbf{N}} \right) \underbrace{\int_{t-\tau(t)}^t \mathbf{x}_{cl}(\eta) d\eta}_{w(t-\tau(t), t)}, \end{aligned} \quad (85)$$

and

$$\begin{aligned} \dot{V}_5(\dot{\mathbf{x}}_{cl_t}, \boldsymbol{\rho}, t) &\leq \frac{\tau^2(t) \bar{\tau}^2}{4} \dot{\mathbf{x}}_{cl}^T(t) \mathbf{W} \dot{\mathbf{x}}_{cl}(t) - \left(1 - \sum_{i=1}^{n_s} \dot{\rho}_i(t) \frac{\partial \tau(t)}{\partial \rho_i(t)}\right) \frac{\bar{\tau}^2}{\tau^2(t)} \\ &\quad \left[ \tau(t) \mathbf{x}_{cl}(t) - \int_{t-\tau(t)}^t \mathbf{x}_{cl}(\eta) d\eta \right]^T \mathbf{W} \left[ \tau(t) \mathbf{x}_{cl}(t) - \int_{t-\tau(t)}^t \mathbf{x}_{cl}(\eta) d\eta \right], \end{aligned} \quad (86)$$

where we choose  $\mathbf{M} \triangleq \mathbf{I} \in \mathbb{R}^{2n_p \times 2n_p}$  and  $w(t - \tau(t), t) \triangleq \int_{t-\tau(t)}^t \mathbf{x}_{cl}(\eta) d\eta \in \mathbb{R}^{2n_p}$ ,  $\mathbf{J} = \mathbf{T} \in \mathbb{S}_{++}^{2n_p}$ , and  $\mathbf{N} = \mathbf{N}_3 \in \mathbb{R}^{2n_p \times 2n_p}$  where  $\mathbf{T}, \mathbf{W} \in \mathbb{S}_{++}^{2n_p}$ , and  $\mathbf{N}_3$  are matrix variables to be determined.

Next, it remains to formulate the results as an LMI condition. Thus, the descriptor technique [28] is used, which introduces slack variables  $\mathbf{V}_1, \mathbf{V}_2, \mathbf{V}_3$ , and  $\mathbf{V}_4$  as follows

$$\begin{aligned} \mathcal{I} &\triangleq \left[ \mathbf{x}_{cl}^T(t) \mathbf{V}_1^T + \dot{\mathbf{x}}_{cl}^T(t) \mathbf{V}_2^T + \mathbf{x}_{cl}^T(t - \tau(t)) \mathbf{V}_3^T + \int_{t-\tau(t)}^t \mathbf{x}_{cl}^T(\eta) d\eta \mathbf{V}_4^T \right] \\ &\quad \left( \mathbf{A}_{cl} \mathbf{x}_{cl}(t) + \mathbf{A}_{\tau, cl} \mathbf{x}_{cl}(t - \tau(t)) + \mathbf{B}_{cl} \mathbf{w}(t) - \dot{\mathbf{x}}_{cl}(t) \right) = 0. \end{aligned} \quad (87)$$

By considering the derivative of the utilized LKF (83) and the performance index as

$$J = \int_{t_0}^{\infty} -\gamma^2 \mathbf{w}^T(t) \mathbf{w}(t) + \mathbf{z}^T(t) \mathbf{z}(t) < 0,$$

which is assumed to establish the prescribed closed-loop performance level  $\gamma$  given in (61), and by

augmenting (83) with  $2\mathcal{I}$  and  $\frac{dJ}{dt}$ , we obtain the following inequality

$$\dot{V}(\mathbf{x}_{cl_t}, \dot{\mathbf{x}}_{cl_t}, \boldsymbol{\rho}, t) + 2\mathcal{I} - \gamma^2 \mathbf{w}^T(t) \mathbf{w}(t) + \mathbf{z}^T(t) \mathbf{z}(t) \leq \boldsymbol{\zeta}^T(t) \boldsymbol{\Omega} \boldsymbol{\zeta}(t) < 0, \quad (88)$$

where the augmented state vector  $\boldsymbol{\zeta}(t)$  is defined as

$$\boldsymbol{\zeta}^T(t) \triangleq \left[ \mathbf{x}_{cl}^T(t) \quad \dot{\mathbf{x}}_{cl}^T(t) \quad \mathbf{x}_{cl}^T(t - \tau(t)) \quad \int_{t-\tau(t)}^t \mathbf{x}_{cl}^T(\eta) d\eta \quad \mathbf{w}^T(t) \right], \quad (89)$$

with

$$\boldsymbol{\Omega} = \begin{bmatrix} \boldsymbol{\Xi}_{11} & \mathbf{P} - \mathbf{V}_1^T + \mathbf{A}_{cl}^T \mathbf{V}_2 & \boldsymbol{\Xi}_{13} & (1 - \dot{\tau})\tau \mathbf{W} + \mathbf{A}_{cl}^T \mathbf{V}_4 & \mathbf{V}_1^T \mathbf{B}_{cl} \\ \star & \tau \mathbf{R} + \frac{\tau^2 \dot{\tau}^2}{4} \mathbf{W} - \mathbf{V}_2 - \mathbf{V}_2^T & \mathbf{V}_2^T \mathbf{A}_{\tau, cl} - \mathbf{V}_3 & -\mathbf{V}_4 & \mathbf{V}_2^T \mathbf{B}_{cl} \\ \star & \star & \boldsymbol{\Xi}_{33} & \mathbf{A}_{\tau, cl}^T \mathbf{V}_4 & \mathbf{V}_3^T \mathbf{B}_{cl} \\ \star & \star & \star & (1 - \dot{\tau})(\mathbf{N}_3^T + \mathbf{N}_3 - \mathbf{W}) & \mathbf{V}_4^T \mathbf{B}_{cl} \\ \star & \star & \star & \star & -\gamma^2 \end{bmatrix} \quad (90)$$

$$+ \boldsymbol{\Gamma}^T \boldsymbol{\Gamma} + \tau (\boldsymbol{\Pi}^T \mathbf{T}^{-1} \boldsymbol{\Pi} + \boldsymbol{\Phi}^T \mathbf{R}^{-1} \boldsymbol{\Phi}),$$

where

$$\begin{aligned} \boldsymbol{\Xi}_{11} &= \left[ \sum_{i=1}^{n_s} \pm \left( \nu_i \frac{\partial \mathbf{P}}{\partial \rho_i} \right) \right] + \mathbf{Q} + \mathbf{V}_1^T \mathbf{A}_{cl} + \mathbf{A}_{cl}^T \mathbf{V}_1 + \left[ 1 - \sum_{i=1}^{n_s} \pm \left( \nu_i \frac{\partial \tau}{\partial \rho_i} \right) \right] (\mathbf{N}_1^T + \mathbf{N}_1 - \tau^2 \mathbf{W}) + \tau \mathbf{T}, \\ \boldsymbol{\Xi}_{13} &= \left[ 1 - \sum_{i=1}^{n_s} \pm \left( \nu_i \frac{\partial \tau}{\partial \rho_i} \right) \right] (-\mathbf{N}_1^T + \mathbf{N}_2) + \mathbf{V}_1^T \mathbf{A}_{\tau, cl} + \mathbf{A}_{cl}^T \mathbf{V}_3, \\ \boldsymbol{\Xi}_{33} &= \left[ 1 - \sum_{i=1}^{n_s} \pm \left( \nu_i \frac{\partial \tau}{\partial \rho_i} \right) \right] (-\mathbf{N}_2^T - \mathbf{N}_2) - \mathbf{Q} + \mathbf{V}_3^T \mathbf{A}_{\tau, cl} + \mathbf{A}_{\tau, cl}^T \mathbf{V}_3, \\ \boldsymbol{\Gamma} &= \begin{bmatrix} \mathbf{C}_{cl} & \mathbf{0} & \mathbf{C}_{\tau, cl} & \mathbf{0} & \mathbf{D}_{cl} \end{bmatrix}, \\ \boldsymbol{\Pi} &= \begin{bmatrix} \mathbf{0} & \mathbf{0} & \mathbf{0} & \mathbf{N}_3 & \mathbf{0} \end{bmatrix}, \\ \boldsymbol{\Phi} &= \begin{bmatrix} \mathbf{N}_1 & \mathbf{0} & \mathbf{N}_2 & \mathbf{0} & \mathbf{0} \end{bmatrix}. \end{aligned} \quad (91)$$

Slack variables in relation (87) are chosen as  $\mathbf{V}_1 \triangleq \lambda_1 \mathbf{V} \in \mathbb{S}^{2n}$ ,  $\mathbf{V}_2 \triangleq \lambda_2 \mathbf{V}$ ,  $\mathbf{V}_3 \triangleq \lambda_3 \mathbf{V}$ , and  $\mathbf{V}_4 \triangleq \lambda_4 \mathbf{V}$ , where  $\lambda_1 = 1$ ,  $\lambda_2$ ,  $\lambda_3$ , and  $\lambda_4$  are real constants and  $\mathbf{V}$  is a real-valued symmetric matrix which is partitioned as  $\mathbf{V} \triangleq \begin{bmatrix} \mathbf{X} & \mathcal{N} \\ \mathcal{N}^T & \star \end{bmatrix}$ ,  $\mathbf{V}^{-1} \triangleq \begin{bmatrix} \mathbf{Y} & \mathcal{M} \\ \mathcal{M}^T & \star \end{bmatrix}$ , such that  $\mathbf{X}\mathbf{Y} + \mathcal{N}\mathcal{M}^T = \mathbf{I}$ . Finally, it remains to substitute closed-loop matrices (64) into (90) and then by applying the Schur complement to  $\mathbf{\Omega}$  in (90), we obtain a  $8 \times 8$  block matrix. Finally, by defining  $\mathcal{Z} \triangleq \begin{bmatrix} \mathbf{Y} & \mathbf{I} \\ \mathcal{M}^T & \mathbf{0} \end{bmatrix}$ , and performing a congruence transformation  $diag(\mathcal{Z}^T, \mathcal{Z}^T, \mathcal{Z}^T, \mathcal{Z}^T, \mathbf{I}, \mathbf{I}, \mathcal{Z}^T, \mathcal{Z}^T)$  on the  $8 \times 8$  block matrix and redefining the matrix multiplications as  $\tilde{\square} \triangleq \mathcal{Z}^T \square \mathcal{Z}$ , LMI (80) is obtained and the proof is complete.  $\square$

Finally, using the determined LMI decision variables, output-feedback LPV gain-scheduled controller can be computed following the controller synthesis steps (75)-(77).

### Numerical Example

As an illustrative example, we construct an LPV state-delayed system with the following state-space representation [107]

$$\begin{aligned}
\dot{\mathbf{x}}(t) &= \begin{bmatrix} 0 & 1 + 0.2\rho(t) \\ -2 & -3 + 0.1\rho(t) \end{bmatrix} \mathbf{x}(t) + \begin{bmatrix} 0.2\rho(t) & 0.1 \\ -0.2 + 0.1\rho(t) & -0.3 \end{bmatrix} \mathbf{x}(t - \tau(\rho(t))) \\
&+ \begin{bmatrix} 0.2 \\ 0.2 \end{bmatrix} d(t) + \begin{bmatrix} 0.2\rho(t) \\ 0.1 + 0.1\rho(t) \end{bmatrix} u(t), \\
\mathbf{z}(t) &= \begin{bmatrix} \phi & 0 \\ 0 & \xi \\ 0 & 0 \end{bmatrix} \mathbf{x}(t) + \begin{bmatrix} 0 \\ 0 \\ \psi \end{bmatrix} u(t), \\
y(t) &= \begin{bmatrix} 1 & 0 \end{bmatrix} \mathbf{x}(t),
\end{aligned} \tag{92}$$

where  $\rho(t) = \sin(t)$  is the LPV system scheduling parameter,  $\tau(\rho(t)) = \bar{\tau}|\sin(\alpha t)|$  is the parameter-dependent time-varying delay with  $0 \leq \tau(t) \leq \bar{\tau}$  and  $|\dot{\tau}| \leq \nu = \bar{\tau}\alpha$ . Weighting scalars  $\phi$ ,  $\xi$ , and  $\psi$

are selected to construct the desired controlled output vector,  $\mathbf{z}(t)$ , by penalizing the states of the system and the control input.

Based on the results of Theorem 4, an output-feedback controller of the form (62) is designed to minimize the induced  $\mathcal{L}_2$ -norm (or  $\mathcal{H}_\infty$ -norm) of the closed-loop LPV time-delay system (63). The design objective is to guarantee closed-loop stability and minimize the effect of the disturbance using the measurement information of state  $x_1$ , while maintaining the control input within reasonable limits over the entire range of the scheduling parameter and delay variations.

**Remark 4.** *The condition in Theorem 4 leads to an infinite-dimensional convex optimization problem with an infinite number of LMI constraints. To tackle this issue, we take advantage of the gridding approach to convert the infinite-dimensional problem to a finite-dimensional convex optimization problem [4]. In this regard, a quadratic parameter dependence is adopted for the parameter dependent matrices as follows:  $\mathbf{G}(\boldsymbol{\rho}(t)) = \mathbf{G}_0 + \sum_{i=1}^{n_s} \rho_i(t)\mathbf{G}_{i_1} + \frac{1}{2} \sum_{i=1}^{n_s} \rho_i^2(t)\mathbf{G}_{i_2}$ , where  $\mathbf{G}(\boldsymbol{\rho}(t))$  represents any of the involved LMI decision variables. Finally, gridding the scheduling parameter space at appropriate intervals leads to a finite set of LMIs to be solved for the unknown LMI variables and  $\gamma$ . Furthermore, in order to improve the results, a 3-dimensional search over the three scalar variables  $\lambda_2$ ,  $\lambda_3$ , and  $\lambda_4$  is performed to obtain the minimum value of  $\gamma$ . The MATLAB<sup>®</sup> toolbox YALMIP is used to solve the corresponding LMI optimization problems [51].*

In the considered numerical example (92), the weighting scalars are chosen as  $\phi = 1$ ,  $\xi = 10$ , and  $\psi = 1$ . The time delay is considered to be  $\tau(t) = 3|\sin(0.3t)|$  (i.e.,  $\bar{\tau} = 3$  and  $\alpha = 0.3$ ). The results of the proposed LPV control design approach are compared with prior results of an LPV time-delay control design with simpler LKF candidate with a conservative bounding technique [90]. Figure 26 demonstrates the closed-loop responses of (92) for the proposed control and the one in [90]. As illustrated, the proposed control scheme outperforms the one in [90] by regulating both system states to zero by minimizing the effect of the disturbance. We consider a simulation scenario where a pulse disturbance  $d(t) = 5$  for  $t \in [5 \ 8]$  sec and zero elsewhere, is assumed to affect the system. It should be noted that the same weighting scalars, parameter-dependence basis function, and the scheduling parameter grid points are considered for both approaches. The obtained optimal energy-to-energy

performance levels  $\gamma$  are 1.1786 and 3.1546 for the proposed control and the one in [90], respectively. Accordingly, Theorem 4 provides better disturbance attenuation, faster regulation, and improved induced  $\mathcal{L}_2$ -norm performance levels compared with the other controller.

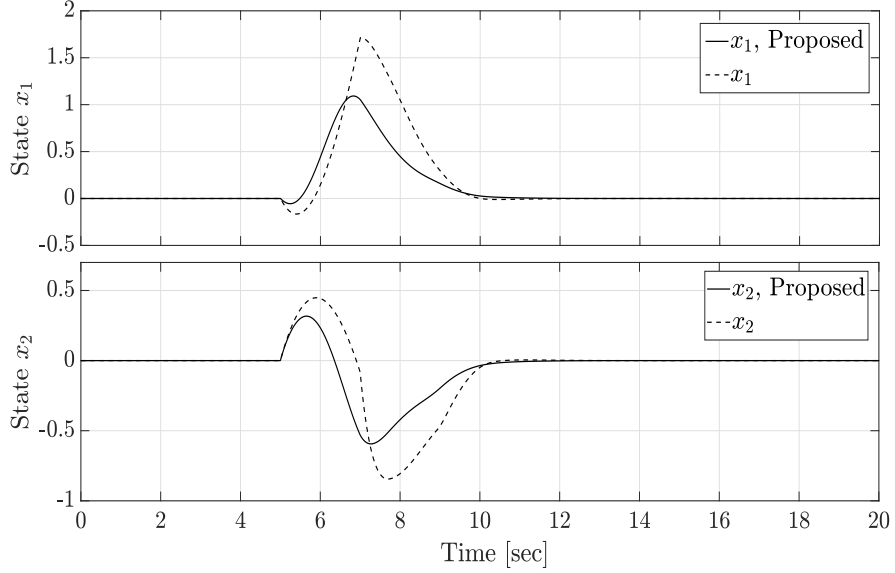


Figure 26: Closed-loop response of system states  $x_1$ , and  $x_2$  subject to disturbance

Table 3 compares the obtained performance level  $\gamma$  for both control design methods and for different maximum delay values,  $\bar{\tau}$ . It is noted that the control synthesis condition in [90] is not feasible for  $\bar{\tau} \geq 3.5$ . On the other hand, the proposed LPV delay-dependent control scheme, which utilizes the improved LKF candidate and the efficient use of the affine Jensen's inequality bounding technique, can handle much larger allowable maximum delay values and provides considerably less conservative results for a larger delay range and delay variation rates  $\nu > 1$ .

Table 3: Performance levels  $\gamma$  of both methods for different maximum delay values  $\bar{\tau}$

Method	$\bar{\tau} = 1$	$\bar{\tau} = 3$	$\bar{\tau} = 3.2$	$\bar{\tau} = 3.5$	$\bar{\tau} = 10$	$\bar{\tau} = 50$
Proposed	0.59	1.18	1.44	1.45	3.92	5.37
[90]	0.46	3.15	8.39	Inf.	Inf.	Inf.

### 4.3 Robust Control of LPV Systems with Uncertain Time-Delay

Model-based control design tools provide a systematic and practical framework for addressing closed-loop stability and performance requirements in a wide variety of real-world control problems. The mathematical modeling describing real-world systems can be carried out via either the certainty equivalence principle and physics laws or system identification techniques, which approximates the system dynamics in terms of bias and variance error on an identified model using the system's input and output data measurements [34]. However, unmodeled and hidden dynamics, problems like aging and external excursions, and generally inaccuracies and simplifications in modeling physical processes and systems make the mathematical model differ from the actual system dynamics. Consequently, robust control analysis has been introduced as an effective way of dealing with such modeling mismatch and discrepancy issues [47]. However, for such systems with varying uncertain delays, utilizing classical robust control methods or incorporating the delay uncertainty variations into the delay upper bound introduces extra conservatism and compromises the closed-loop performance.

Moreover, delay uncertainty and, in particular, uncertainty in time-varying delays further poses a robustness challenge in the model-based control design. The analysis and control of systems with uncertain time-delay is considered to be of theoretical and practical significance. It is noteworthy that in typical stability analysis of such systems, the delay is assumed to be the sum of a nominal delay, either constant or time-varying, and a perturbed uncertain part where the system with the nominal delay is regarded to be asymptotically stable. In this regard, necessary stability conditions for linear time-invariant (LTI) systems with an uncertain constant delay via a frequency-domain approach and sufficient conditions for LTI systems with an uncertain time-varying delay via Lyapunov-Krasovskii approach have been investigated in [41]. The utilized LKF has been developed to comply with a prescribed derivative expression, and it also does not explicitly depend on the bounds of the uncertainty. In [27], the author has used a complete LKF, with a particular functional form, consisting of nominal plus additional terms where the former analyzes the system under the nominal delay, and the latter addresses delay perturbations and vanishes as the perturbations disappear. Inspired by

this research, static state-feedback control of input-delay systems with an uncertain delay has been addressed in [96] where the LKF derivative is constructed based on a delay Lyapunov matrix. The work in [28] employs the small-gain theorem augmented with a scaling matrix, which provides a less conservative input-output stability analysis framework. Moreover, to handle delay uncertainties, a factor depending on the bound of the delay rate has been introduced, which can be selected *a priori* to further reduce the conservatism. By unifying the results with the LKF strategy, delay-dependent sufficient stability conditions have been derived in terms of convex LMI constraints.

On the other hand, stability analysis and control design of LPV systems with uncertain arbitrarily varying delays and external disturbances, to the best of our knowledge, has not been addressed in the LPV time-delay context. To address this problem, in this part, we develop a robust delay-dependent control design for LPV systems with uncertain time delay. We propose an improved parameter-dependent LKF candidate and further enhance it with the less conservative affine Jensen's inequality bounding technique.

#### 4.3.1 State-Feedback Control of LPV Systems with Uncertain Time-Delay

Time-delayed LPV systems with varying uncertainty in the delay are subject to performance degradation and instability. In this line, we investigate the stability of such systems invoking an input-output stability approach. By considering explicit bounds on the delay rate and time-varying delay uncertainty, the scaled small-gain theorem is adopted to form an interconnected time-delay LPV system for the uncertain dynamics.

By considering the uncertain time delay,  $\tau(t)$ , as a differentiable scalar function

$$\tau(t) = \tau_n + \eta(t), \quad |\eta(t)| \leq \mu \leq \tau_n, \quad (93)$$

where  $\tau_n$  denotes the constant nominal delay value and the time-varying uncertain part of the delay is bounded by a constant  $\mu$ . The time-varying delay lies in the set  $\mathcal{F}^{\nu\tau}$  as defined in (59).

#### Stability and $\mathcal{L}_2$ -Gain Analysis of LPV Systems with Uncertain Delay

In order to examine the stability and  $\mathcal{L}_2$ -gain analysis of the LPV system with an uncertain time-varying delay, we utilize the small-gain theorem. For this purpose, by considering the uncertain time delay (93), the delayed state of the system can be rewritten as follows

$$\mathbf{x}_p(t - \tau(t)) = \mathbf{x}_p(t - \tau_n) - \int_{-\tau_n - \eta(t)}^{-\tau_n} \dot{\mathbf{x}}_p(t + s) ds, \quad (94)$$

where the time-varying uncertain part of the delayed state is treated as a disturbance and defined as a new feedback signal

$$\mathbf{u}_1(t) \triangleq (\Delta \mathbf{y}_1)(t) = -\frac{1}{\mu \sqrt{\mathcal{F}(\nu_\tau)}} \int_{-\tau_n - \eta(t)}^{-\tau_n} \mathbf{y}_1(t + s) ds, \quad (95)$$

where  $\mathcal{F}(\nu_\tau)$  is a continuous function of the time-delay rate,  $\nu_\tau$ , which will be defined later using an extension of the small-gain theorem. By defining a new auxiliary system,  $\Delta$ , with additional input and output vectors, namely,  $\mathbf{y}_1$  and  $\mathbf{u}_1$ , the overall interconnected feedback system is constructed as shown in Fig. 27.

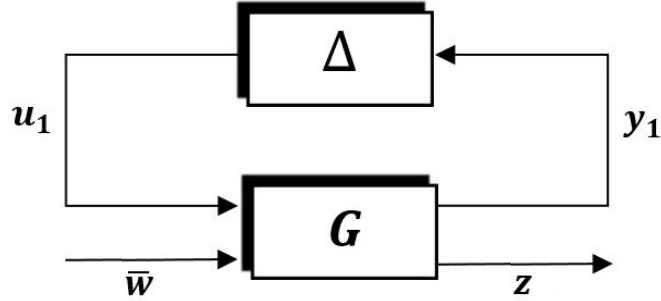


Figure 27: The overall interconnected system

Accordingly, the unforced time-delay LPV system (57), *i.e.*, no control input or  $u \equiv 0$ , is represented as a feedback interconnected system as follows

$$\begin{aligned}
\dot{\mathbf{x}}_p(t) &= \mathbf{A}(\boldsymbol{\rho}(t))\mathbf{x}_p(t) + \mathbf{A}_\tau(\boldsymbol{\rho}(t))\mathbf{x}_p(t - \tau_n) + \mu\mathbf{A}_\tau(\boldsymbol{\rho}(t))\mathbb{X}^{-1}\mathbf{u}_1(t) + \gamma^{-1}\mathbf{B}_1(\boldsymbol{\rho}(t))\bar{\mathbf{w}}(t), \\
\mathbf{y}_1(t) &= \sqrt{\mathcal{F}(\nu_\tau)}\mathbb{X}\dot{\mathbf{x}}_p(t), \\
\mathbf{z}(t) &= \mathbf{C}_1(\boldsymbol{\rho}(t))\mathbf{x}_p(t) + \mathbf{C}_{1,\tau}(\boldsymbol{\rho}(t))\mathbf{x}_p(t - \tau_n) + \mu\mathbf{C}_{1,\tau}(\boldsymbol{\rho}(t))\mathbb{X}^{-1}\mathbf{u}_1(t) + \gamma^{-1}\mathbf{D}_{11}(\boldsymbol{\rho}(t))\bar{\mathbf{w}}(t),
\end{aligned} \tag{96}$$

where  $\mathbb{X}$  denotes a scaling non-singular matrix and  $\bar{\mathbf{w}}(t) = \gamma\mathbf{w}(t)$ .

The following lemma is used to derive the delay-dependent conditions for stability and  $\mathcal{L}_2$ -gain analysis of the LPV time-delay system with an uncertain time-varying delay.

**Lemma 2. (Small-Gain Theorem for Systems with Uncertain Time-Delay) [28]:** *Considering  $\mathbf{y}_1 = \mathbf{T}_{\mathbf{y}_1\mathbf{u}_1}\mathbf{u}_1$ , and  $\mathbf{u}_1 = \Delta\mathbf{y}_1$ , where both systems  $\mathbf{T}_{\mathbf{y}_1\mathbf{u}_1} : \mathcal{L}_2[0, \infty] \rightarrow \mathcal{L}_2[0, \infty]$  and  $\Delta : \mathcal{L}_2[0, \infty] \rightarrow \mathcal{L}_2[0, \infty]$  are considered to be input-output stable. The interconnected overall system  $(\mathbf{T}_{\mathbf{y}_1\mathbf{u}_1}, \Delta)$  is input-output stable if  $\gamma_0(\Delta)\gamma_0(\mathbf{T}_{\mathbf{y}_1\mathbf{u}_1}) < 1$ , where  $\gamma_0$  is the induced  $\mathcal{L}_2$ -gain of a system. Moreover, the  $\mathcal{L}_2$ -gain of the system  $\Delta$  is found to be  $\gamma_0(\Delta) \leq \mu\sqrt{\mathcal{F}(\nu_\tau)}$  where [80]*

$$\mathcal{F}(\nu_\tau) = \begin{cases} 1, & -\infty \leq \nu_\tau \leq 1, \\ \frac{2\nu_\tau - 1}{\nu_\tau}, & 1 < \nu_\tau < 2, \\ \frac{7\nu_\tau - 8}{4\nu_\tau - 4}, & \nu_\tau \geq 2, \\ \frac{7}{4}, & \nu_\tau \text{ is unknown,} \end{cases} \tag{97}$$

with  $\|\mathbf{T}_{\mathbf{y}_1\mathbf{u}_1}\|_{i,2} < \frac{1}{\mu\sqrt{\mathcal{F}(\nu_\tau)}}$ .

Using Lemma 2, the following theorem provides a sufficient LMI condition to guarantee the stability and performance objective (61) of the LPV system (57) with an uncertain varying delay.

**Theorem 5.** *The unforced LPV system (57) with an uncertain delay and  $|\eta(t)| \leq \mu \leq \tau_n$ , over the given sets  $\mathcal{F}_\mathcal{D}^\nu$  and  $\mathcal{T}^{\nu_\tau}$  is asymptotically stable with  $\|\mathbf{z}\|_2 \leq \gamma\|\mathbf{w}\|_2$ , if there exist continuously*

differentiable parameter dependent positive-definite matrix functions  $\mathbf{P}(\boldsymbol{\rho}(t))$ ,  $\mathbf{S}(\boldsymbol{\rho}(t)) : \mathcal{F}_{\mathcal{D}}^{\nu} \rightarrow \mathbb{S}_{+++}^{n_p}$ , positive-definite matrices  $\mathbf{Q}$ ,  $\mathbf{R} \in \mathbb{S}_{+++}^{n_p}$ , parameter dependent real matrices  $\mathbf{V}_1$ ,  $\mathbf{V}_2$ ,  $\mathbf{V}_3 : \mathcal{F}_{\mathcal{D}}^{\nu} \rightarrow \mathbb{R}^{n_p \times n_p}$ , and a positive scalar  $\gamma$  satisfying the following LMI condition

$$\begin{bmatrix} \dot{\mathbf{P}} - \mathbf{R} + \mathbf{Q} + \mathbf{V}_1^T \mathbf{A} + \mathbf{A}^T \mathbf{V}_1 & \mathbf{P} - \mathbf{V}_1^T + \mathbf{A}^T \mathbf{V}_2 & \mathbf{R} + \mathbf{V}_1^T \mathbf{A}_{\tau} + \mathbf{A}^T \mathbf{V}_3 & \mu \mathbf{V}_1^T \mathbf{A}_{\tau} & \mathbf{V}_1^T \mathbf{B}_1 & \mathbf{C}_1^T \\ \star & \tau_n^2 \mathbf{R} + \mathcal{F}(\nu_{\tau}) \mathbf{S} - \mathbf{V}_2^T - \mathbf{V}_2 & \mathbf{V}_2^T \mathbf{A}_{\tau} - \mathbf{V}_3 & \mu \mathbf{V}_2^T \mathbf{A}_{\tau} & \mathbf{V}_2^T \mathbf{B}_1 & \mathbf{0} \\ \star & \star & -\mathbf{R} - \mathbf{Q} + \mathbf{V}_3^T \mathbf{A}_{\tau} + \mathbf{A}_{\tau}^T \mathbf{V}_3 & \mu \mathbf{V}_3^T \mathbf{A}_{\tau} & \mathbf{V}_3^T \mathbf{B}_1 & \mathbf{C}_{1,\tau}^T \\ \star & \star & \star & -\mathbf{S} & \mathbf{0} & \mu \mathbf{C}_{1,\tau}^T \\ \star & \star & \star & \star & -\gamma^2 \mathbf{I} & \mathbf{D}_{11}^T \\ \star & \star & \star & \star & \star & -\mathbf{I} \end{bmatrix} \prec \mathbf{0}, \quad (98)$$

where  $\dot{\mathbf{P}} = \sum_{i=1}^{n_s} \dot{\rho}_i(t) \frac{\partial \mathbf{P}(\boldsymbol{\rho}(t))}{\partial \rho_i(t)}$  and the parameter dependence of the matrices is dropped for brevity.

**Remark 5.** Considering  $\dot{\mathbf{P}} = \sum_{i=1}^{n_s} \dot{\rho}_i(t) \frac{\partial \mathbf{P}(\boldsymbol{\rho}(t))}{\partial \rho_i(t)}$ , due to affine presence of the derivative of the scheduling parameter, we may replace it by  $\dot{\mathbf{P}} = \sum_{i=1}^{n_s} \pm \nu_i \frac{\partial \mathbf{P}(\boldsymbol{\rho}(t))}{\partial \rho_i(t)}$  where the notation  $\sum_{i=1}^{n_s} \pm(\cdot)$  indicates that every combination of  $+(\cdot)$  and  $-(\cdot)$  should be included in the LMI condition (e.i., all combinations of lower and upper bounds of  $\dot{\rho}_i$ ). Consequently, it leads to  $2^{n_s}$  LMIs that must be checked simultaneously.

*Proof.*

$$V(\mathbf{x}_{p_t}, \dot{\mathbf{x}}_{p_t}, \boldsymbol{\rho}, t) = \mathbf{x}_p^T(t) \mathbf{P}(\boldsymbol{\rho}(t)) \mathbf{x}_p(t) + \int_{t-\tau_n}^t \mathbf{x}_p^T(s) \mathbf{Q} \mathbf{x}_p(s) ds + \int_{-\tau_n}^0 \int_{t+\theta}^t \dot{\mathbf{x}}_p^T(s) \mathbf{R}_0 \dot{\mathbf{x}}_p(s) ds d\theta. \quad (99)$$

We evaluate the time derivative of the LKF (99) along the trajectories of the LPV system (57)

$$\begin{aligned} \dot{V}(\mathbf{x}_{p_t}, \dot{\mathbf{x}}_{p_t}, \boldsymbol{\rho}, t) &= 2\dot{\mathbf{x}}_p^T(t) \mathbf{P}(\boldsymbol{\rho}(t)) \mathbf{x}_p(t) + \mathbf{x}_p^T(t) \dot{\mathbf{P}} \mathbf{x}_p(t) + \mathbf{x}_p^T(t) \mathbf{Q} \mathbf{x}_p(t) \\ &\quad + \mathbf{x}_p^T(t - \tau_n) \mathbf{Q} \mathbf{x}_p(t - \tau_n) + \tau_n \dot{\mathbf{x}}_p^T(t) \mathbf{R}_0 \dot{\mathbf{x}}_p - \int_{t-\tau_n}^t \dot{\mathbf{x}}_p^T(\theta) \mathbf{R}_0 \dot{\mathbf{x}}_p(\theta) d\theta. \end{aligned} \quad (100)$$

Employing the Jensen's inequality, the integral term in (100) can be upper bounded through

$$\begin{aligned} - \int_{t-\tau_n}^t \dot{\mathbf{x}}_p^T(\theta) \mathbf{R}_0 \dot{\mathbf{x}}_p(\theta) d\theta &\leq -\frac{1}{\tau_n} \left( \int_{t-\tau_n}^t \dot{\mathbf{x}}_p(\theta) d\theta \right)^T \mathbf{R}_0 \left( \int_{t-\tau_n}^t \dot{\mathbf{x}}_p(\theta) d\theta \right) \\ &= -\frac{1}{\tau_n} [\mathbf{x}_p(t) - \mathbf{x}_p(t - \tau_n)]^T \mathbf{R}_0 [\mathbf{x}_p(t) - \mathbf{x}_p(t - \tau_n)]. \end{aligned} \quad (101)$$

Next, in order to derive a relaxed final condition and be able to formulate the final results as an LMI suitable for the synthesis conditions, we use the descriptor technique [28]. Introducing three slack variables  $\mathbf{V}_1$ ,  $\mathbf{V}_2$ , and  $\mathbf{V}_3$  and using the LPV system dynamics (96), we define  $\mathcal{I}$  as

$$\begin{aligned} \mathcal{I} &= \left[ \mathbf{x}_p^T(t) \mathbf{V}_1^T + \dot{\mathbf{x}}_p^T(t) \mathbf{V}_2^T + \mathbf{x}_p^T(t - \tau_n) \mathbf{V}_3^T \right] \\ &\quad \left( \mathbf{A} \mathbf{x}_p(t) + \mathbf{A}_\tau \mathbf{x}_p(t - \tau_n) + \mu \mathbf{A}_\tau \mathbb{X}^{-1} \mathbf{u}_1(t) + \gamma^{-1} \mathbf{B}_1 \bar{\mathbf{w}}(t) - \dot{\mathbf{x}}_p(t) \right) = 0. \end{aligned} \quad (102)$$

Considering the augmented forward system with all input and output vectors, *i.e.*,  $\begin{bmatrix} \mathbf{y}_1 \\ \mathbf{z} \end{bmatrix} = \mathbf{G} \begin{bmatrix} \mathbf{u}_1 \\ \bar{\mathbf{w}} \end{bmatrix}$  as in Fig. 27, the assumption  $\|\mathbf{G}\|_{i,2} < 1$  is equivalent to [28]

$$\|\mathbf{y}_1\|_{\mathcal{L}_2}^2 + \|\mathbf{z}\|_{\mathcal{L}_2}^2 < \|\mathbf{u}_1\|_{\mathcal{L}_2}^2 + \|\bar{\mathbf{w}}\|_{\mathcal{L}_2}^2. \quad (103)$$

Inequality (103) satisfies both the condition given in Lemma 2 for the input-output stability of the LPV system with uncertain time-delay, *i.e.*,  $\|\mathbf{T}_{\mathbf{y}_1 \mathbf{u}_1}\|_{i,2} < \frac{1}{\mu \sqrt{\mathcal{F}(\nu_\tau)}}$ , and also the prescribed performance level given in (61), *i.e.*,  $\|\mathbf{T}_{\mathbf{z} \mathbf{w}}\|_{i,2} < \gamma$ . Finally, by augmenting the derivative of the LKF given in (100) by the descriptor method's result and (103) is

$$\dot{V}(\mathbf{x}_{p_t}, \dot{\mathbf{x}}_{p_t}, \boldsymbol{\rho}, t) + 2\mathcal{I} + \mathbf{y}_1^T(t) \mathbf{y}_1(t) + \mathbf{z}^T(t) \mathbf{z}(t) - \mathbf{u}_1^T(t) \mathbf{u}_1(t) - \bar{\mathbf{w}}^T(t) \bar{\mathbf{w}}(t) \leq \boldsymbol{\zeta}^T(t) \boldsymbol{\Omega} \boldsymbol{\zeta}(t) < 0, \quad (104)$$

where the augmented state vector  $\boldsymbol{\zeta}(t)$  is defined as

$$\boldsymbol{\zeta}^T(t) \triangleq \left[ \mathbf{x}_p^T(t) \quad \dot{\mathbf{x}}_p^T(t) \quad \mathbf{x}_p^T(t - \tau_n) \quad \mathbf{u}_1^T(t) \mathbb{X}^{-T} \quad \bar{\mathbf{w}}^T(t) \right]. \quad (105)$$

Using the bound computed for the integral term in the LKF time-derivative (101), and substituting the dynamics vectors from (96) in (104),  $\mathbf{\Omega}$  is obtained as

$$\left[ \begin{array}{ccc} \dot{\mathbf{P}} - \mathbf{R} + \mathbf{Q} + \mathbf{V}_1^T \mathbf{A} + \mathbf{A}^T \mathbf{V}_1 + \mathbf{C}_1^T \mathbf{C}_1 & \mathbf{P} - \mathbf{V}_1^T + \mathbf{A}^T \mathbf{V}_2 & \\ & \star & \tau_n^2 \mathbf{R} + \mathcal{F}(\nu_\tau) \mathbf{S} - \mathbf{V}_2^T - \mathbf{V}_2 \\ & \star & \star \\ & \star & \star \\ & \star & \star \\ \mathbf{R} + \mathbf{V}_1^T \mathbf{A}_\tau + \mathbf{A}^T \mathbf{V}_3 + \mathbf{C}_{1,\tau}^T \mathbf{C}_{1,\tau} & \mu(\mathbf{V}_1^T \mathbf{A}_\tau + \mathbf{C}_{1,\tau}^T \mathbf{C}_{1,\tau}) & \gamma^{-1}(\mathbf{V}_1^T \mathbf{B}_1 + \mathbf{C}_{1,\tau}^T \mathbf{D}_{11}) \\ & \mathbf{V}_2^T \mathbf{A}_\tau - \mathbf{V}_3 & \mu \mathbf{V}_2^T \mathbf{A}_\tau & \mathbf{V}_2^T \mathbf{B}_1 \\ -\mathbf{R} - \mathbf{Q} + \mathbf{V}_3^T \mathbf{A}_\tau + \mathbf{A}_\tau^T \mathbf{V}_3 + \mathbf{C}_{1,\tau}^T \mathbf{C}_{1,\tau} & \mu(\mathbf{V}_3^T \mathbf{A}_\tau + \mathbf{C}_{1,\tau}^T \mathbf{C}_{1,\tau}) & \gamma^{-1}(\mathbf{V}_3^T \mathbf{B}_1 + \mathbf{C}_{1,\tau}^T \mathbf{D}_{11}) & \\ & \star & -\mathbf{S} + \mu^2 \mathbf{C}_{1,\tau}^T \mathbf{C}_{1,\tau} & \gamma^{-1} \mu \mathbf{C}_{1,\tau}^T \mathbf{D}_{11} \\ & \star & \star & \gamma^{-2} \mathbf{D}_{11}^T \mathbf{D}_{11} - \mathbf{I} \end{array} \right], \quad (106)$$

where  $\mathbf{S}(\boldsymbol{\rho}(t)) \triangleq \mathbb{X}^T \mathbb{X}$ , and  $\mathbf{R} \triangleq \frac{\mathbf{R}_0}{\tau_n}$ . By pre- and post-multiplying (106) by  $\text{diag}(\mathbf{I}, \mathbf{I}, \mathbf{I}, \mathbf{I}, \gamma \mathbf{I})$  and its transpose, and applying the Schur complement, LMI (98) is obtained and the proof is accomplished.  $\square$

### State-Feedback LPV Controller Design Process

We extend the results of Theorem 5 for the synthesis of a robust state-feedback gain-scheduling controller for the case of general LPV systems (57) with an uncertain varying time-delay as in (93). Such a parameter-dependent controller is proposed in the following format:

$$\mathbf{u}(t) = \mathbf{K}(\boldsymbol{\rho}(t)) \mathbf{x}_p(t), \quad (107)$$

where the controller utilizes full-state information and aims to meet the design objectives as mentioned in Section 4.2.1. Feeding back the control law (107) into the LPV system dynamics (57), the

resultant closed-loop system will be

$$\begin{aligned}\dot{\mathbf{x}}_p(t) &= \mathbf{A}_{cl}(\boldsymbol{\rho}(t))\mathbf{x}_p(t) + \mathbf{A}_\tau(\boldsymbol{\rho}(t))\mathbf{x}_p(t - \tau(t)) + \mathbf{B}_1(\boldsymbol{\rho}(t))\mathbf{w}(t), \\ \mathbf{z}(t) &= \mathbf{C}_{1,cl}(\boldsymbol{\rho}(t))\mathbf{x}_p(t) + \mathbf{C}_{1,\tau}(\boldsymbol{\rho}(t))\mathbf{x}_p(t - \tau(t)) + \mathbf{D}_{11}(\boldsymbol{\rho}(t))\mathbf{w}(t),\end{aligned}\tag{108}$$

where  $\mathbf{A}_{cl}(\boldsymbol{\rho}(t)) = \mathbf{A}(\boldsymbol{\rho}(t)) + \mathbf{B}_2(\boldsymbol{\rho}(t))\mathbf{K}(\boldsymbol{\rho}(t))$ ,  $\mathbf{C}_{1,cl}(\boldsymbol{\rho}(t)) = \mathbf{C}_1(\boldsymbol{\rho}(t)) + \mathbf{D}_{12}(\boldsymbol{\rho}(t))\mathbf{K}(\boldsymbol{\rho}(t))$ . By substituting  $\mathbf{A}_{cl}(\boldsymbol{\rho}(t))$  and  $\mathbf{C}_{1,cl}(\boldsymbol{\rho}(t))$  for  $\mathbf{A}$  and  $\mathbf{C}_1$  in (98), the following theorem presents a sufficient condition for investigating the closed-loop stability and performance with an uncertain delay implementing a state-feedback LPV controller.

**Theorem 6.** *There exists a state-feedback gain-scheduling LPV controller (107), over the sets  $\mathcal{F}_{\mathcal{D}}^\nu$  and  $\mathcal{T}^{\nu\tau}$ , to provide the closed-loop system (108) with asymptotic stability and the induced  $\mathcal{L}_2$ -norm performance index given in (61), if there exist continuously differentiable parameter dependent positive-definite matrix functions  $\tilde{\mathbf{P}}(\boldsymbol{\rho}(t))$ ,  $\tilde{\mathbf{S}}(\boldsymbol{\rho}(t)) : \mathcal{F}_{\mathcal{D}}^\nu \rightarrow \mathbb{S}_{++}^{n_p}$ , positive-definite matrices  $\tilde{\mathbf{Q}}$ ,  $\tilde{\mathbf{R}} \in \mathbb{S}_{++}^{n_p}$ , parameter dependent real matrix functions  $\mathbf{U}(\boldsymbol{\rho}(t)) : \mathcal{F}_{\mathcal{D}}^\nu \rightarrow \mathbb{R}^{n_p \times n_p}$ ,  $\mathbf{Y}(\boldsymbol{\rho}(t)) : \mathcal{F}_{\mathcal{D}}^\nu \rightarrow \mathbb{R}^{n_u \times n_p}$ , a positive scalar  $\gamma$ , and real scalars  $\lambda_2$  and  $\lambda_3$  such that the LMI (110) is feasible and such a control law can then be computed as follows*

$$\mathbf{u}(t) = \mathbf{Y}(\boldsymbol{\rho}(t))\mathbf{U}^{-1}(\boldsymbol{\rho}(t))\mathbf{x}(t).\tag{109}$$



where  $\tau_n(t)$  denotes the nominal time-varying delay and  $\eta(t)$  stands for the time-varying uncertain part of the delay which is bounded by  $\mu$ . The major difference compared to the uncertain time delay (93) discussed in Section 4.3.1 is that (111) considers the nominal delay to be time-varying. Moreover, the time-varying delay is considered to be dependent on the scheduling parameter vector and lies in the set  $\mathcal{F}^{\nu_\tau}$  as defined in (59).

### Input-Output Approach: Stability and $\mathcal{L}_2$ -Gain Analysis of LPV Systems with Uncertain Delay

By considering the uncertain time delay (111), the delayed state of the system can be rewritten as follows

$$\mathbf{x}_p(t - \tau(t)) = \mathbf{x}_p(t - \tau_n(t)) - \int_{-\tau_n(t) - \eta(t)}^{-\tau_n(t)} \dot{\mathbf{x}}_p(t + s) ds, \quad (112)$$

where the time-varying uncertain part of the delayed state is treated as a disturbance and defined as a new feedback signal

$$\mathfrak{U}_p(t) \triangleq (\Delta \eta_p)(t) = -\frac{1}{\mu \sqrt{\mathcal{F}(\nu_\tau)}} \int_{-\tau_n(t) - \eta(t)}^{-\tau_n(t)} \eta_p(t + s) ds. \quad (113)$$

We define a new auxiliary system,  $\Delta$ , with additional input and output vectors, namely,  $\eta_p$  and  $\mathfrak{U}_p$ , and the overall interconnected feedback system can be shown as in Fig. 28.

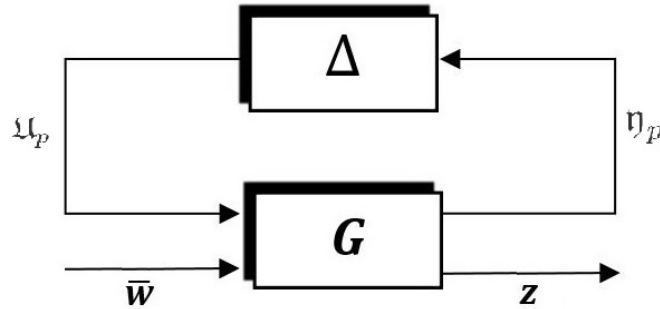


Figure 28: The overall interconnected system

The unforced LPV time-delay system is represented in the form of an interconnected feedback system as

$$\begin{aligned}
\dot{\mathbf{x}}_p(t) &= \mathbf{A}(\boldsymbol{\rho}(t))\mathbf{x}_p(t) + \mathbf{A}_\tau(\boldsymbol{\rho}(t))\mathbf{x}_p(t - \tau_n) + \mu\mathbf{A}_\tau(\boldsymbol{\rho}(t))\mathbb{X}_p^{-1}\mathfrak{U}_p(t) + \gamma^{-1}\mathbf{B}_1(\boldsymbol{\rho}(t))\bar{\mathbf{w}}(t), \\
\mathbf{z}(t) &= \mathbf{C}_1(\boldsymbol{\rho}(t))\mathbf{x}_p(t) + \mathbf{C}_{1,\tau}(\boldsymbol{\rho}(t))\mathbf{x}_p(t - \tau_n) + \mu\mathbf{C}_{1,\tau}(\boldsymbol{\rho}(t))\mathbb{X}_p^{-1}\mathfrak{U}_p(t) + \gamma^{-1}\mathbf{D}_{11}(\boldsymbol{\rho}(t))\bar{\mathbf{w}}(t), \\
\mathbf{y}(t) &= \mathbf{C}_2(\boldsymbol{\rho}(t))\mathbf{x}_p(t) + \mathbf{C}_{2,\tau}(\boldsymbol{\rho}(t))\mathbf{x}_p(t - \tau_n) + \mu\mathbf{C}_{2,\tau}(\boldsymbol{\rho}(t))\mathbb{X}_p^{-1}\mathfrak{U}_p(t) + \gamma^{-1}\mathbf{D}_{21}(\boldsymbol{\rho}(t))\bar{\mathbf{w}}(t), \\
\boldsymbol{\eta}_p(t) &= \sqrt{\mathcal{F}(\nu_\tau)}\mathbb{X}_p\dot{\mathbf{x}}_p(t).
\end{aligned} \tag{114}$$

Next, the small-gain theorem (Lemma 2) is used to derive the stability conditions for the auxiliary system with additional input and output signals. Accordingly, by considering  $\boldsymbol{\eta}_p = \mathbf{T}_{\boldsymbol{\eta}_p\mathfrak{U}_p}\mathfrak{U}_p$ , and  $\mathfrak{U}_p = \Delta\boldsymbol{\eta}_p$ , where both operators  $\mathbf{T}_{\boldsymbol{\eta}_p\mathfrak{U}_p} : \mathcal{L}_2[0, \infty] \rightarrow \mathcal{L}_2[0, \infty]$  and  $\Delta : \mathcal{L}_2[0, \infty] \rightarrow \mathcal{L}_2[0, \infty]$  are considered to be input-output stable. The interconnected overall system  $(\mathbf{T}_{\boldsymbol{\eta}_p\mathfrak{U}_p}, \Delta)$  is input-output stable if  $\gamma_0(\Delta)\gamma_0(\mathbf{T}_{\boldsymbol{\eta}_p\mathfrak{U}_p}) < 1$ , where  $\gamma_0$  is the induced  $\mathcal{L}_2$  gain. The induced  $\mathcal{L}_2$ -gain of the operator  $\Delta$  is found to be bounded as  $\gamma_0(\Delta) \leq \mu\sqrt{\mathcal{F}(\nu_\tau)}$ , hence

$$\|\mathbf{T}_{\boldsymbol{\eta}_p\mathfrak{U}_p}\|_{i,2} < \frac{1}{\mu\sqrt{\mathcal{F}(\nu_\tau)}}. \tag{115}$$

The following theorem summarizes the main results to derive a sufficient condition to investigate the stability and performance analysis of the unforced LPV time-delay system with an uncertain time-varying delay. To reduce the conservatism, we take the benefit of the Lyapunov-Krasovskii approach and a quadratic LKF candidate with modified integral terms, which depend explicitly on the time delay function. The utilized approach avoids model transformation; hence, it leads to further conservatism reduction on this level. Additionally, the affine Jensen's inequality (see Lemma 1), as an efficient class of integral inequality bounding technique, is employed for bounding the cross-terms in the derivative of the functional. The utilized inequality bounding is affine with respect to time-delay and takes all the possible intermediate time-delay values into account, so, unlike traditional bounding techniques, it can provide tighter bounds for the integral cross-terms.

**Theorem 7.** *The unforced LPV system (57) with an uncertain delay and  $|\eta(t)| \leq \mu \leq \bar{\tau}_n$ , over the defined sets  $\mathcal{F}_{\mathcal{D}}^{\nu}$  and  $\mathcal{T}^{\nu\tau}$  is asymptotically stable and satisfies the induced  $\mathcal{L}_2$ -norm performance requirement given by (61), if there exist a continuously differentiable parameter dependent positive-definite matrix function  $\mathbf{P}(\boldsymbol{\rho}(t)) : \mathcal{F}_{\mathcal{D}}^{\nu} \rightarrow \mathbb{S}_{++}^{n_p}$ , a parameter dependent symmetric matrix function  $\mathbf{S}_p(\boldsymbol{\rho}(t)) : \mathcal{F}_{\mathcal{D}}^{\nu} \rightarrow \mathbb{S}^{n_p}$ , positive-definite matrices  $\mathbf{Q}, \mathbf{R}, \mathbf{T} \in \mathbb{S}_{++}^{n_p}$ , real valued matrices  $\mathbf{V}_1, \mathbf{V}_2, \mathbf{V}_3, \mathbf{V}_4, \mathbf{N}_1, \mathbf{N}_2, \mathbf{N}_3 \in \mathbb{R}^{n_p \times n_p}$ , and a positive scalar  $\gamma$ , such that the following LMI condition (116)*

$$\begin{bmatrix}
 \Sigma_{11} & \mathbf{P} - \mathbf{V}_1^T + \mathbf{A}^T \mathbf{V}_2 & \Sigma_{13} & \mathbf{A}^T \mathbf{V}_4 \\
 * & \Sigma_{22} & \mathbf{V}_2^T \mathbf{A}_{\tau} - \mathbf{V}_3 & -\mathbf{V}_4 \\
 * & * & \Sigma_{33} & \mathbf{A}_{\tau}^T \mathbf{V}_4 \\
 * & * & * & (1 - \dot{\tau})(\mathbf{N}_3^T + \mathbf{N}_3) \\
 * & * & * & * \\
 * & * & * & * \\
 * & * & * & * \\
 * & * & * & * \\
 * & * & * & *
 \end{bmatrix}
 \begin{bmatrix}
 \mu \mathbf{V}_1^T \mathbf{A}_{\tau} & \mathbf{V}_1^T \mathbf{B}_1 & \mathbf{C}_1^T & \mathbf{0} & \tau_n(t) \mathbf{N}_1^T \\
 \mu \mathbf{V}_2^T \mathbf{A}_{\tau} & \mathbf{V}_2^T \mathbf{B}_1 & \mathbf{0} & \mathbf{0} & \mathbf{0} \\
 \mu \mathbf{V}_3^T \mathbf{A}_{\tau} & \mathbf{V}_3^T \mathbf{B}_1 & \mathbf{C}_{1,\tau}^T & \mathbf{0} & \tau_n(t) \mathbf{N}_2^T \\
 \mu \mathbf{V}_4^T \mathbf{A}_{\tau} & \mathbf{V}_4^T \mathbf{B}_1 & \mathbf{0} & \tau_n(t) \mathbf{N}_3^T & \mathbf{0} \\
 -\mathbf{S}_p & \mathbf{0} & \mu \mathbf{C}_{1,\tau}^T & \mathbf{0} & \mathbf{0} \\
 * & -\gamma \mathbf{I} & \mathbf{D}_{11}^T & \mathbf{0} & \mathbf{0} \\
 * & * & -\gamma \mathbf{I} & \mathbf{0} & \mathbf{0} \\
 * & * & * & -\tau_n(t) \mathbf{T} & \mathbf{0} \\
 * & * & * & * & -\tau_n(t) \mathbf{R}
 \end{bmatrix} \prec \mathbf{0}, \tag{116}$$

holds, with the variables as

$$\begin{aligned}
\Sigma_{11} &= \dot{\mathbf{P}} + \mathbf{Q} + \left[1 - \sum_{i=1}^{n_s} \pm(\nu_i \frac{\partial \tau}{\partial \rho_i})\right] (\mathbf{N}_1^T + \mathbf{N}_1) + \tau_n(t) \mathbf{T} + \mathbf{V}_1^T \mathbf{A} + \mathbf{A}^T \mathbf{V}_1, \\
\Sigma_{13} &= \left[1 - \sum_{i=1}^{n_s} \pm(\nu_i \frac{\partial \tau}{\partial \rho_i})\right] (-\mathbf{N}_1^T + \mathbf{N}_2) + \mathbf{V}_1^T \mathbf{A}_\tau + \mathbf{A}^T \mathbf{V}_3, \\
\Sigma_{22} &= \tau_n(t) \mathbf{R} + \mathcal{F}(\nu_\tau) \mathbf{S}_p - \mathbf{V}_2^T - \mathbf{V}_2, \\
\Sigma_{33} &= -\left[1 - \sum_{i=1}^{n_s} \pm(\nu_i \frac{\partial \tau}{\partial \rho_i})\right] (\mathbf{N}_2^T + \mathbf{N}_2) - \mathbf{Q} + \mathbf{V}_3^T \mathbf{A}_\tau + \mathbf{A}_\tau^T \mathbf{V}_3.
\end{aligned} \tag{117}$$

*Proof.* The proof begins by suggesting the LKF candidate in the form of

$$V(\mathbf{x}_{p_t}, \dot{\mathbf{x}}_{p_t}, \boldsymbol{\rho}, t) = V_1(\mathbf{x}_p, \boldsymbol{\rho}, t) + V_2(\mathbf{x}_{p_t}, \boldsymbol{\rho}, t) + V_3(\dot{\mathbf{x}}_{p_t}, \boldsymbol{\rho}, t) + V_4(\mathbf{x}_{p_t}, \boldsymbol{\rho}, t), \tag{118}$$

where

$$\begin{aligned}
V_1(\mathbf{x}_p, \boldsymbol{\rho}, t) &= \mathbf{x}_p^T(t) \mathbf{P}(\boldsymbol{\rho}(t)) \mathbf{x}_p(t), \\
V_2(\mathbf{x}_{p_t}, \boldsymbol{\rho}, t) &= \int_{t-\tau_n(t)}^t \mathbf{x}_p^T(\eta) \mathbf{Q} \mathbf{x}_p(\eta) d\eta, \\
V_3(\dot{\mathbf{x}}_{p_t}, \boldsymbol{\rho}, t) &= \int_{-\tau_n(t)}^0 \int_{t+\theta}^t \dot{\mathbf{x}}_p^T(\eta) \mathbf{R} \dot{\mathbf{x}}_p(\eta) d\eta d\theta, \\
V_4(\mathbf{x}_{p_t}, \boldsymbol{\rho}, t) &= \int_{-\tau_n(t)}^0 \int_{t+\theta}^t \mathbf{x}_p^T(\eta) \mathbf{T} \mathbf{x}_p(\eta) d\eta d\theta.
\end{aligned}$$

We evaluate the derivative of LKF (118) along the trajectories of the system (114), that is

$$\dot{V}(\mathbf{x}_{p_t}, \dot{\mathbf{x}}_{p_t}, \boldsymbol{\rho}, t) = \dot{V}_1(\mathbf{x}_p, \boldsymbol{\rho}, t) + \dot{V}_2(\mathbf{x}_{p_t}, \boldsymbol{\rho}, t) + \dot{V}_3(\dot{\mathbf{x}}_{p_t}, \boldsymbol{\rho}, t) + \dot{V}_4(\mathbf{x}_{p_t}, \boldsymbol{\rho}, t), \tag{119}$$

where the derivative terms are

$$\begin{aligned}
\dot{V}_1(\mathbf{x}_p, \boldsymbol{\rho}, t) &= 2\dot{\mathbf{x}}_p^T(t) \mathbf{P}(\boldsymbol{\rho}(t)) \mathbf{x}_p(t) + \mathbf{x}_p^T(t) \left[ \sum_{i=1}^{n_s} \dot{\rho}_i(t) \frac{\partial \mathbf{P}(\boldsymbol{\rho}(t))}{\partial \rho_i(t)} \right] \mathbf{x}_p(t), \\
\dot{V}_2(\mathbf{x}_{p_t}, \boldsymbol{\rho}, t) &= \mathbf{x}_p^T(t) \mathbf{Q} \mathbf{x}_p(t) - \left(1 - \sum_{i=1}^{n_s} \dot{\rho}_i(t) \frac{\partial \tau_n(t)}{\partial \rho_i(t)}\right) \mathbf{x}_p^T(t - \tau_n(t)) \mathbf{Q} \mathbf{x}_p(t - \tau_n(t)),
\end{aligned}$$

$$\begin{aligned}\dot{V}_3(\dot{\mathbf{x}}_{p_t}, \boldsymbol{\rho}, t) &= \tau_n(t) \dot{\mathbf{x}}_p^T(t) \mathbf{R} \dot{\mathbf{x}}_p(t) - \left(1 - \sum_{i=1}^{n_s} \dot{\rho}_i(t) \frac{\partial \tau_n(t)}{\partial \rho_i(t)}\right) \int_{t-\tau_n(t)}^t \dot{\mathbf{x}}_p^T(\eta) \mathbf{R} \dot{\mathbf{x}}_p(\eta) d\eta, \\ \dot{V}_4(\mathbf{x}_{p_t}, \boldsymbol{\rho}, t) &= \tau_n(t) \mathbf{x}_p^T(t) \mathbf{T} \mathbf{x}_p(t) - \left(1 - \sum_{i=1}^{n_s} \dot{\rho}_i(t) \frac{\partial \tau_n(t)}{\partial \rho_i(t)}\right) \int_{t-\tau_n(t)}^t \mathbf{x}_p^T(\eta) \mathbf{T} \mathbf{x}_p(\eta) d\eta.\end{aligned}$$

Using Lemma 1, we bound the integral cross-term appeared in the third and fourth derivative terms. The affine Jensen's inequality is a direct bounding technique which enables us to provide a delayed-scheduled tight upper bound on the time derivative of the LKF and therefore obtain less conservative results (see (84) and (85)). Next, to derive a relaxed final condition and formulate the final results in an LMI form suitable for the controller synthesis, we apply the descriptor technique [28]. To this end, by using the LPV system dynamics (114),  $\mathcal{I}$  is defined as

$$\begin{aligned}2\mathcal{I} &= 2 \left[ \mathbf{x}_p^T(t) \mathbf{V}_1^T + \dot{\mathbf{x}}_p^T(t) \mathbf{V}_2^T + \mathbf{x}_p^T(t - \tau_n(t)) \mathbf{V}_3^T + \int_{t-\tau_n(t)}^t \mathbf{x}_p^T(\eta) d\eta \mathbf{V}_4^T \right] \\ &\left( \mathbf{A}(\boldsymbol{\rho}(t)) \mathbf{x}_p(t) + \mathbf{A}_\tau(\boldsymbol{\rho}(t)) \mathbf{x}_p(t - \tau_n) + \mu \mathbf{A}_\tau(\boldsymbol{\rho}(t)) \mathbb{X}_p^{-1} \mathfrak{U}_p(t) + \gamma^{-1} \mathbf{B}_1(\boldsymbol{\rho}(t)) \bar{\mathbf{w}}(t) - \dot{\mathbf{x}}_p(t) \right) = 0, \quad (120)\end{aligned}$$

where four slack variables  $\mathbf{V}_i \in \mathbb{R}^{n_p \times n_p}$ ,  $i = 1, \dots, 4$  are introduced through the descriptor technique [28]. Moreover, the other reason to augment  $2\mathcal{I}$  descriptor method's expression with the derivative of LKF is that we want  $\dot{V}_{aug}$  to depend on  $\dot{\mathbf{x}}_{p_t}$  which enables the design to treat the fast-varying delay more effectively.

Consider the augmented forward system, *i.e.*,  $\begin{bmatrix} \mathfrak{y}_p \\ \mathbf{z} \end{bmatrix} = \mathbf{G} \begin{bmatrix} \mathfrak{U}_p \\ \bar{\mathbf{w}} \end{bmatrix}$  as shown in Fig. 28, the assumption  $\|\mathbf{G}\|_{i,2} < 1$  is equivalent to [28]

$$\|\mathfrak{y}_p\|_{\mathcal{L}_2}^2 + \|\mathbf{z}\|_{\mathcal{L}_2}^2 < \|\mathfrak{U}_p\|_{\mathcal{L}_2}^2 + \|\bar{\mathbf{w}}\|_{\mathcal{L}_2}^2. \quad (121)$$

Inequality (121) satisfies both conditions, the one given in Lemma 2 for the input-output stability of the LPV system with uncertain time-delay, *i.e.*,  $\|\mathbf{T}_{\mathfrak{y}_p \mathfrak{U}_p}\|_{i,2} < \frac{1}{\mu \sqrt{\mathcal{F}(\nu_\tau)}}$ , and the condition for the prescribed performance index given in (61). Finally, augmenting the derivative of the LKF by

descriptor approach's term (120) and (121) will supply

$$\dot{V}_{aug} = \dot{V}(\mathbf{x}_{p_t}, \dot{\mathbf{x}}_{p_t}, \boldsymbol{\rho}, t) + 2\mathcal{L} + \boldsymbol{\eta}_p^T(t)\boldsymbol{\eta}_p(t) + \mathbf{z}^T(t)\mathbf{z}(t) - \boldsymbol{\mathfrak{U}}_p^T(t)\boldsymbol{\mathfrak{U}}_p(t) - \bar{\mathbf{w}}^T(t)\bar{\mathbf{w}}(t) \leq \boldsymbol{\zeta}^T(t)\boldsymbol{\Omega}\boldsymbol{\zeta}(t) < 0, \quad (122)$$

where the augmented state vector  $\boldsymbol{\zeta}(t)$  is defined as

$$\boldsymbol{\zeta}^T(t) \triangleq \left[ \mathbf{x}_p^T(t) \quad \dot{\mathbf{x}}_p^T(t) \quad \mathbf{x}_p^T(t - \tau_n(t)) \quad \int_{t-\tau_n(t)}^t \mathbf{x}_p^T(\eta) d\eta \quad \boldsymbol{\mathfrak{U}}_p^T(t)\mathbb{X}_p^T \quad \bar{\mathbf{w}}^T(t) \right]. \quad (123)$$

Using the upper bounds for the derivative of the LKF, and substituting the dynamics vectors from (114) in (122),  $\boldsymbol{\Omega}$  is obtained as

$$\left[ \begin{array}{cccc} \boldsymbol{\Sigma}_{11} + \mathbf{C}_1^T \mathbf{C}_1 & \mathbf{P} - \mathbf{V}_1^T + \mathbf{A}^T \mathbf{V}_2 & \boldsymbol{\Sigma}_{13} + \mathbf{C}_1^T \mathbf{C}_{1,\tau} & \mathbf{A}^T \mathbf{V}_4 \\ \star & \boldsymbol{\Sigma}_{22} & \mathbf{V}_2^T \mathbf{A}_\tau - \mathbf{V}_3 & -\mathbf{V}_4 \\ \star & \star & \boldsymbol{\Sigma}_{33} + \mathbf{C}_{1,\tau}^T \mathbf{C}_{1,\tau} & \mathbf{A}_\tau^T \mathbf{V}_4 \\ \star & \star & \star & (1 - \dot{\tau})(\mathbf{N}_3^T + \mathbf{N}_3) \\ \star & \star & \star & \star \\ \star & \star & \star & \star \\ \mu(\mathbf{V}_1^T \mathbf{A}_\tau + \mathbf{C}_1^T \mathbf{C}_{1,\tau}) & \gamma^{-1}(\mathbf{V}_1^T \mathbf{B}_1 + \mathbf{C}_1^T \mathbf{D}_{11}) & & \\ \mu \mathbf{V}_2^T \mathbf{A}_\tau & \gamma^{-1} \mathbf{V}_2^T \mathbf{B}_1 & & \\ \mu(\mathbf{V}_3^T \mathbf{A}_\tau + \mathbf{C}_{1,\tau}^T \mathbf{C}_{1,\tau}) & \gamma^{-1}(\mathbf{V}_3^T \mathbf{B}_1 + \mathbf{C}_{1,\tau}^T \mathbf{D}_{11}) & & \\ \mu \mathbf{V}_4^T \mathbf{A}_\tau & \gamma^{-1} \mathbf{V}_4^T \mathbf{B}_1 & & \\ -\mathbf{S}_p + \mu^2 \mathbf{C}_{1,\tau}^T \mathbf{C}_{1,\tau} & \mu \gamma^{-1} \mathbf{C}_{1,\tau}^T \mathbf{D}_{11} & & \\ \star & -\mathbf{I} + \gamma^{-2} \mathbf{D}_{11}^T \mathbf{D}_{11} & & \end{array} \right] \quad (124)$$

$$+ \tau_n (\boldsymbol{\Gamma}^T \mathbf{R}^{-1} \boldsymbol{\Gamma} + \boldsymbol{\Pi}^T \mathbf{T}^{-1} \boldsymbol{\Pi}),$$

where  $\mathbf{S}_p(\boldsymbol{\rho}(t)) \triangleq \mathbb{X}_p^T \mathbb{X}_p$ ,  $\boldsymbol{\Gamma} = \left[ \mathbf{N}_1 \quad \mathbf{0} \quad \mathbf{N}_2 \quad \mathbf{0} \quad \mathbf{0} \quad \mathbf{0} \right]$ , and  $\boldsymbol{\Pi} = \left[ \mathbf{0} \quad \mathbf{0} \quad \mathbf{0} \quad \mathbf{N}_3 \quad \mathbf{0} \quad \mathbf{0} \right]$ . We

then pre- and post-multiply (124) by  $\text{diag}\{\mathbf{I}, \mathbf{I}, \mathbf{I}, \mathbf{I}, \mathbf{I}, \gamma \mathbf{I}\}$  and apply the Schur complement lemma, LMI (116) is resulted and the proof is complete.  $\square$

### Dynamic Output-Feedback Gain-Scheduled LPV Controller Design

In this part, we extend the results of Theorem 7 for the synthesis of a robust output-feedback gain-scheduling  $\mathcal{H}_\infty$  controller for the case of LPV systems with varying uncertain time-delay. Such a delay-dependent output-feedback controller is sought to accomplish design objectives, namely, asymptotic internal stability and desired performance index (61) of the closed-loop LPV time-delay system. To this end, a full-order ( $n_K = n_p$ ) dynamic output-feedback controller is considered with following structure

$$\begin{aligned}\dot{\mathbf{x}}_K(t) &= \mathbf{A}_K(\boldsymbol{\rho}(t))\mathbf{x}_K(t) + \mathbf{A}_{\tau,K}(\boldsymbol{\rho}(t))\mathbf{x}_K(t - \tau_n) + \mu\mathbf{A}_{\tau,K}(\boldsymbol{\rho}(t))\mathbb{X}_K^{-1}\mathfrak{U}_K(t) + \mathbf{B}_K(\boldsymbol{\rho}(t))\mathbf{y}(t), \\ \mathbf{u}(t) &= \mathbf{C}_K(\boldsymbol{\rho}(t))\mathbf{x}_K(t) + \mathbf{C}_{\tau,K}(\boldsymbol{\rho}(t))\mathbf{x}_K(t - \tau_n) + \mu\mathbf{C}_{\tau,K}(\boldsymbol{\rho}(t))\mathbb{X}_K^{-1}\mathfrak{U}_K(t) + \mathbf{D}_K(\boldsymbol{\rho}(t))\mathbf{y}(t), \\ \boldsymbol{\eta}_K(t) &= \sqrt{\mathcal{F}(\nu_\tau)}\mathbb{X}_K\dot{\mathbf{x}}_K(t),\end{aligned}\tag{125}$$

where  $\mathbb{X}_K$  denotes a scaling non-singular matrix. In the controller dynamics (125), the uncertain part of the delayed state of the controller is treated as a disturbance and defined as a feedback signal

$$\mathfrak{U}_K(t) = (\Delta\boldsymbol{\eta}_K)(t) = -\frac{1}{\mu\sqrt{\mathcal{F}(\nu_\tau)}} \int_{-\tau_n(t)-\eta(t)}^{-\tau_n(t)} \boldsymbol{\eta}_K(t+s)ds.\tag{126}$$

Feeding back the control dynamics (125) into the LPV system dynamics (57), the resultant closed-loop system will be

$$\begin{aligned}\dot{\mathbf{x}}_{cl}(t) &= \mathbf{A}_{cl}\mathbf{x}_{cl}(t) + \mathbf{A}_{\tau,cl}\mathbf{x}_{cl}(t - \tau_n) + \mu\mathbf{A}_{\tau,cl}\mathbb{X}^{-1}\mathfrak{U}(t) + \gamma^{-1}\mathbf{B}_{cl}\bar{\mathbf{w}}(t), \\ \mathbf{z}(t) &= \mathbf{C}_{cl}\mathbf{x}_{cl}(t) + \mathbf{C}_{\tau,cl}\mathbf{x}_{cl}(t - \tau_n) + \mu\mathbf{C}_{\tau,cl}\mathbb{X}^{-1}\mathfrak{U}(t) + \gamma^{-1}\mathbf{D}_{cl}\bar{\mathbf{w}}(t), \\ \boldsymbol{\eta}(t) &= \sqrt{\mathcal{F}(\nu_\tau)}\mathbb{X}\dot{\mathbf{x}}_{cl}(t),\end{aligned}\tag{127}$$

where the closed-loop state vector is defined as  $\mathbf{x}_{cl}(t) \triangleq \begin{bmatrix} \mathbf{x}_p(t) \\ \mathbf{x}_K(t) \end{bmatrix}$ ,  $\mathfrak{U}(t) \triangleq \begin{bmatrix} \mathfrak{U}_p(t) \\ \mathfrak{U}_K(t) \end{bmatrix}$ ,  $\mathfrak{Y}(t) \triangleq \begin{bmatrix} \mathfrak{Y}_p(t) \\ \mathfrak{Y}_K(t) \end{bmatrix}$ ,

$\mathbb{X}^{-1} \triangleq \begin{bmatrix} \mathbb{X}_p^{-1} & \mathbf{0} \\ \mathbf{0} & \mathbb{X}_K^{-1} \end{bmatrix}$ , and closed-loop state-space matrices are as defined in (64).

The following theorem provides sufficient conditions for the synthesis of a delayed dynamic output-feedback controller to meet the control design objectives, namely, closed-loop asymptotic stabilization and a specified level of disturbance attenuation performance (61) for the closed-loop LPV system with varying uncertain time-delay (127).

**Theorem 8.** *There exists an output-feedback gain-scheduled LPV controller (62) over  $\boldsymbol{\rho} \in \mathcal{F}_{\mathcal{D}}^{\nu}$  and  $\tau \in \mathcal{T}^{\nu\tau}$ , to provide the closed-loop system with asymptotic stability and the induced  $\mathcal{L}_2$ -norm performance specification given in (61), if there are continuously differentiable parameter dependent positive-definite matrix functions  $\tilde{\mathbf{P}}(\boldsymbol{\rho}(t)) : \mathcal{F}_{\mathcal{D}}^{\nu} \rightarrow \mathbb{S}_{++}^{2n_p}$ ,  $\mathbf{X}(\boldsymbol{\rho}(t)), \mathbf{Y}(\boldsymbol{\rho}(t)) : \mathcal{F}_{\mathcal{D}}^{\nu} \rightarrow \mathbb{S}^{n_p}$ ,  $\tilde{\mathbf{S}}(\boldsymbol{\rho}(t)) : \mathcal{F}_{\mathcal{D}}^{\nu} \rightarrow \mathbb{S}^{2n_p}$ , positive-definite matrices  $\tilde{\mathbf{Q}}, \tilde{\mathbf{R}}, \tilde{\mathbf{T}} \in \mathbb{S}_{++}^{2n_p}$ , real matrices  $\tilde{\mathbf{N}}_1, \tilde{\mathbf{N}}_2, \tilde{\mathbf{N}}_3 \in \mathbb{R}^{2n_p \times 2n_p}$ , parameter dependent real matrices  $\hat{\mathbf{A}}(\boldsymbol{\rho}(t)), \hat{\mathbf{A}}_{\tau}(\boldsymbol{\rho}(t)) : \mathcal{F}_{\mathcal{D}}^{\nu} \rightarrow \mathbb{R}^{n_p \times n_p}$ ,  $\hat{\mathbf{B}}(\boldsymbol{\rho}(t)) : \mathcal{F}_{\mathcal{D}}^{\nu} \rightarrow \mathbb{R}^{n_p \times n_y}$ ,  $\hat{\mathbf{C}}(\boldsymbol{\rho}(t)), \hat{\mathbf{C}}_{\tau}(\boldsymbol{\rho}(t)) : \mathcal{F}_{\mathcal{D}}^{\nu} \rightarrow \mathbb{R}^{n_u \times n_p}$ ,  $\mathbf{D}_K(\boldsymbol{\rho}(t)) : \mathcal{F}_{\mathcal{D}}^{\nu} \rightarrow \mathbb{R}^{n_u \times n_y}$ , a positive scalar  $\gamma$ , given scalars  $\lambda_2, \lambda_3$ , and  $\lambda_4$  such that the following LMI*

$$\begin{bmatrix} \tilde{\mathbf{\Xi}}_{11} & \tilde{\mathbf{P}} - \tilde{\mathbf{V}} + \lambda_2 \mathcal{A}^T & \tilde{\mathbf{\Xi}}_{13} & \lambda_4 \mathcal{A}^T & \mu \mathcal{A}_{\tau} & \mathcal{B} & \mathcal{C}^T & \mathbf{0} & \tau_n(t) \tilde{\mathbf{N}}_1^T \\ * & \tilde{\mathbf{\Xi}}_{22} & \lambda_2 \mathcal{A}_{\tau} - \lambda_3 \tilde{\mathbf{V}} & -\lambda_4 \tilde{\mathbf{V}} & \mu \lambda_2 \mathcal{A}_{\tau} & \lambda_2 \mathcal{B} & \mathbf{0} & \mathbf{0} & \mathbf{0} \\ * & * & \tilde{\mathbf{\Xi}}_{33} & \lambda_4 \mathcal{A}_{\tau}^T & \mu \lambda_3 \mathcal{A}_{\tau} & \lambda_3 \mathcal{B} & \mathcal{C}_{\tau}^T & \mathbf{0} & \tau_n(t) \tilde{\mathbf{N}}_2^T \\ * & * & * & \tilde{\mathbf{N}}_3^T + \tilde{\mathbf{N}}_3 & \mu \lambda_4 \mathcal{A}_{\tau} & \lambda_4 \mathcal{B} & \mathbf{0} & \tau_n(t) \tilde{\mathbf{N}}_3^T & \mathbf{0} \\ * & * & * & * & -\tilde{\mathbf{S}} & \mathbf{0} & \mu \mathcal{C}_{\tau}^T & \mathbf{0} & \mathbf{0} \\ * & * & * & * & * & -\gamma \mathbf{I} & \mathcal{D}^T & \mathbf{0} & \mathbf{0} \\ * & * & * & * & * & * & -\gamma \mathbf{I} & \mathbf{0} & \mathbf{0} \\ * & * & * & * & * & * & * & -\tau_n(t) \tilde{\mathbf{T}} & \mathbf{0} \\ * & * & * & * & * & * & * & * & -\tau_n(t) \tilde{\mathbf{R}} \end{bmatrix} \prec \mathbf{0}, \quad (128)$$

is feasible, with

$$\begin{aligned}
\tilde{\mathbf{E}}_{11} &= \tilde{\mathbf{P}} + \tilde{\mathbf{Q}} + \left[1 - \sum_{i=1}^{n_s} \pm(\nu_i \frac{\partial \tau}{\partial \rho_i})\right] (\tilde{\mathbf{N}}_1^T + \tilde{\mathbf{N}}_1) + \tau_n(t) \tilde{\mathbf{T}} + \mathcal{A} + \mathcal{A}^T, \\
\tilde{\mathbf{E}}_{13} &= \left[1 - \sum_{i=1}^{n_s} \pm(\nu_i \frac{\partial \tau}{\partial \rho_i})\right] (-\tilde{\mathbf{N}}_1^T + \tilde{\mathbf{N}}_2) + \mathcal{A}_\tau + \lambda_3 \mathcal{A}^T, \\
\tilde{\mathbf{E}}_{22} &= \tau_n(t) \tilde{\mathbf{R}} + \mathcal{F}(\nu_\tau) \tilde{\mathbf{S}}_p - 2\lambda_2 \tilde{\mathbf{V}}, \\
\tilde{\mathbf{E}}_{33} &= -\left[1 - \sum_{i=1}^{n_s} \pm(\nu_i \frac{\partial \tau}{\partial \rho_i})\right] (\tilde{\mathbf{N}}_2^T + \tilde{\mathbf{N}}_2) - \tilde{\mathbf{Q}} + \lambda_3 (\mathcal{A}_\tau + \mathcal{A}_\tau^T),
\end{aligned}$$

and  $\tilde{\mathbf{V}}$ ,  $\mathcal{A}$ ,  $\mathcal{A}_\tau$ ,  $\mathcal{B}$ ,  $\mathcal{C}$ ,  $\mathcal{C}_\tau$ , and  $\mathcal{D}$  are as given in (66).

*Proof.* By substituting the closed-loop system state vector  $\mathbf{x}_{cl}$  for  $\mathbf{x}_p$ , and using the LKF candidate (118) and its derivative (119), applying the affine Jensen's bounding method, and finally substituting the closed-loops system dynamics (127), we achieve

$$\dot{V}_{aug} = \dot{V}(\mathbf{x}_{cl_t}, \dot{\mathbf{x}}_{cl_t}, \boldsymbol{\rho}, t) + 2\mathcal{I} + \boldsymbol{\eta}^T(t) \boldsymbol{\eta}(t) + \mathbf{z}^T(t) \mathbf{z}(t) - \boldsymbol{\mathfrak{U}}^T(t) \boldsymbol{\mathfrak{U}}(t) - \bar{\mathbf{w}}^T(t) \bar{\mathbf{w}}(t) \leq \boldsymbol{\zeta}_{cl}^T(t) \boldsymbol{\Omega}_{cl} \boldsymbol{\zeta}_{cl}(t) < 0, \quad (129)$$

where the augmented closed-loop state vector  $\boldsymbol{\zeta}_{cl}(t)$  is defined as

$$\boldsymbol{\zeta}_{cl}^T(t) \triangleq \left[ \mathbf{x}_{cl}^T(t) \quad \dot{\mathbf{x}}_{cl}^T(t) \quad \mathbf{x}_{cl}^T(t - \tau_n(t)) \quad \int_{t-\tau_n(t)}^t \mathbf{x}_{cl}^T(\eta) d\eta \quad \boldsymbol{\mathfrak{U}}^T(t) \mathbb{X}^{-T} \quad \bar{\mathbf{w}}^T(t) \right]. \quad (130)$$

Now, we just need to substitute the closed dynamics (127) in  $\dot{V}_{aug}$  (129), and  $\boldsymbol{\Omega}_{cl}$  is obtained as given in (124), where closed-loop system matrices  $\mathbf{A}_{cl}$ ,  $\mathbf{A}_{\tau,cl}$ ,  $\mathbf{B}_{cl}$ ,  $\mathbf{C}_{cl}$ ,  $\mathbf{C}_{\tau,cl}$ ,  $\mathbf{D}_{cl}$  are replaced for  $\mathbf{A}$ ,  $\mathbf{A}_\tau$ ,  $\mathbf{B}_1$ ,  $\mathbf{C}_1$ ,  $\mathbf{C}_\tau$ , and  $\mathbf{D}_{11}$ , respectively, and  $\mathbf{S}(\boldsymbol{\rho}(t)) \triangleq \mathbb{X}^T \mathbb{X}$ .

Next, in order to obtain tractable convex results, we select slack variables in (120) as  $\mathbf{V}_1 \triangleq \lambda_1 \mathbf{V} \in \mathbb{R}^{2n_p \times 2n_p}$ ,  $\mathbf{V}_2 \triangleq \lambda_2 \mathbf{V}$ ,  $\mathbf{V}_3 \triangleq \lambda_3 \mathbf{V}$ , and  $\mathbf{V}_4 \triangleq \lambda_4 \mathbf{V}$  where  $\lambda_1 = 1$ ,  $\lambda_2$ ,  $\lambda_3$ , and  $\lambda_4$  are real constants. Accordingly,  $\mathbf{V}$  and its inverse are partitioned as  $\mathbf{V} \triangleq \begin{bmatrix} \mathbf{X} & \mathcal{N} \\ \mathcal{N}^T & \star \end{bmatrix}$ ,  $\mathbf{V}^{-1} \triangleq \begin{bmatrix} \mathbf{Y} & \mathcal{M} \\ \mathcal{M}^T & \star \end{bmatrix}$ , such that  $\mathbf{X}\mathbf{Y} + \mathcal{N}\mathcal{M}^T = \mathbf{I}$ . After substituting the closed-loop matrices (64) into  $\boldsymbol{\Omega}_{cl}$ , we apply the

Schur complement to the resulting  $9 \times 9$  block matrix. Finally, by defining  $\mathcal{Z} \triangleq \begin{bmatrix} \mathbf{Y} & \mathbf{I} \\ \mathcal{M}^T & \mathbf{0} \end{bmatrix}$ , and performing a congruence transformation  $\text{diag}\{\mathcal{Z}^T, \mathcal{Z}^T, \mathcal{Z}^T, \mathcal{Z}^T, \mathcal{Z}^T, \mathbf{I}, \mathbf{I}, \mathcal{Z}^T, \mathcal{Z}^T\}$  on the  $9 \times 9$  block matrix and redefining the matrix multiplications as  $\tilde{\square} \triangleq \mathcal{Z}^T \square \mathcal{Z}$ , LMI (128) is obtained and the proof is accomplished. □

### Numerical Example

In this part, we investigate LPV systems with varying uncertain time delays as given in (111). That is, both nominal and uncertain parts of the delay are considered to be time-varying. Figure 29 presents such case where  $|\eta(t)| \leq \mu \leq \bar{\tau}_n$ .

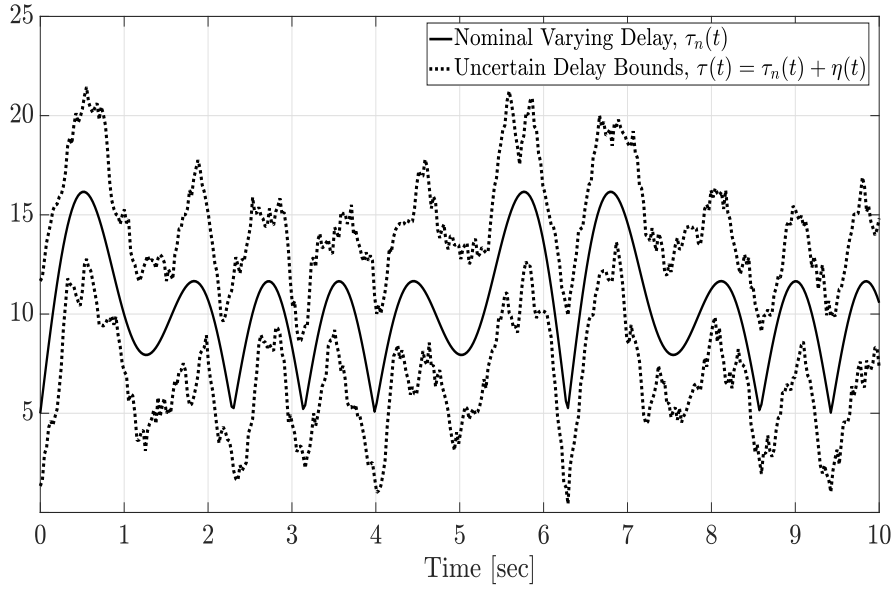


Figure 29: Varying uncertain time delay profile example

As an illustrative example, we consider an LPV state-delayed system (92), where the LPV system

scheduling parameter is  $\rho(t) = \sin(t)$ , and varying uncertain time delay of the system is

$$\tau(\rho(t)) = \underbrace{\tau_0 + \tau_n |\sin(\alpha t)|}_{\tau_n(t)} + \eta(t) \leq \bar{\tau}, \quad |\eta(t)| \leq \mu \leq \bar{\tau}_n, \quad (131)$$

and  $|\dot{\tau}| \leq \nu_\tau = \tau_n \alpha$ .

Now, we apply the results of Theorem 8 to find an output-feedback controller of the form (125) to minimize the induced  $\mathcal{L}_2$ -norm for the considered LPV system with varying uncertain time delay (92). The results of the proposed robust LPV control design are compared with another LPV time-delay control design, in which a relatively simpler and unimproved LKF candidate, along with a conservative bounding technique has been utilized. For  $\tau_0 = \tau_n = 2$ ,  $\alpha = 0.25$ , and  $|\eta(t)| \leq \mu \leq \bar{\tau}_n = 4$ , *i.e.*,  $\tau(t) = 2 + 2|\sin(0.25t)| + \eta(t)$ , Table 4 lists the obtained optimal energy-to-energy performance levels  $\gamma$  of the proposed design and the one in [90] for different maximum time delay uncertainty values. As expected, due to considering the time-delay uncertainty explicitly in the design process, employing an improved LKF candidate and the efficient affine Jensen's inequality bounding technique, the proposed approach (Theorem 8) is capable of handling much larger allowable delay uncertainties and provides improved induced  $\mathcal{L}_2$ -norm performance levels compared with the other controller. Moreover, control design in [90] leads to infeasible results for  $\mu > 3.1$

Table 4: Performance levels  $\gamma$  of both methods for different delay uncertainty values  $\mu$

Method \ $\mu$	0.5	1	2	3.1	4
[90]	6.42	19.61	54.42	554.77	Inf.
Theorem 2	2.15	2.18	2.24	2.35	2.56

**Remark 6.** *Unlike other methods for time-delay systems analysis, which handle the varying time-delay uncertainty by considering the largest time-delay value [44], the proposed method (Theorem 8) addresses the time-delay uncertainty explicitly in the design process; thus, it provides better disturbance attenuation, an improved induced  $\mathcal{L}_2$ -norm performance level, and less conservative results for a larger delay uncertainty range and delay variation rates  $\nu_\tau > 1$ .*

## 4.4 Sampled-Data LPV Control Design

In this part, we propose a delay-dependent sampled-data output-feedback LPV control technique to address the MAP control problem. The patient's MAP response dynamics have been captured by a continuous-time LPV system with varying time-delay. The interconnection of the continuous-time plant and a digital controller through converter devices forms a hybrid closed-loop configuration. Therefore, to benefit the wealth of continuous-time control synthesis tools, the input-delay method has been employed to transfer the hybrid closed-loop system into the continuous-time domain with system inherent time delay and a delay imposed by the mapping approach. The designed sampled-data gain-scheduled output-feedback controller is required to establish the closed-loop asymptotic stability and a prescribed level of performance for the LPV system with an arbitrarily varying time delay and sampling time, where the final results are provided in a convex LMI constraint setting.

Due to the simplicity and availability of control approaches, the literature on the continuous-time control system design is rich [74, 91, 92]. However, the controller implementation is usually fulfilled by a digital instrument in discrete-time. This combination of the continuous-time plant and the discrete-time digital controller along with the sampling analog-to-digital (A/D) and the holding digital-to-analog (D/A) converter devices will form sampled-data closed-loop system representation with a hybrid nature [69]. To this end, the designer is required to find an appropriate discrete-time controller to provide a guarantee for the stability and the prescribed performance of the closed-loop hybrid system while taking the converter devices and intersample behavior into account [19]. The sampled-data control design process is even more demanding when the studied continuous-time plant is a nonlinear or an LPV system [88]. A general intuitive approach, also known as the indirect digital controller design, is to discretize the plant and then find a discrete-time controller and then cascade the digital controller with the continuous-time plant along with the converter devices [19]. Another indirect method is to take advantage of well-established continuous-time control design methods to design a controller and then use conventional methods such as trapezoidal approximation [3] to come up with the controller in the discrete-time domain [69, 94]. Despite the simplicity in the design process, traditionally utilized indirect sampled-data control design approaches fail to guarantee

stability and desired performance for the closed-loop hybrid dynamical system and also disregard the effect of sampling/hold rate of converter devices implicitly in the design process, which may result in the degraded performance of the control design and instability [68]. On the other hand, authors in [69, 88] used the lifting technique [9] to come up with a direct sampled-data filter or control design methods for the LPV systems. In the lifting method, first, the continuous-time plant and the sample and hold converter devices are augmented, and then the augmented plant is mapped to an equivalent discrete-time system representation followed by a digital control design process. However, the sampled-data control design methods relying on the lifting approach are computationally complex and cumbersome [87].

### Sampled-Data Controller Design Procedure

We consider the general LPV time-delay system with the state-space representation as in (57), where the time-varying scheduling parameter vector  $\boldsymbol{\rho} \in \mathcal{F}_{\mathcal{D}}^{\nu}$  (58), and  $\tau \in \mathcal{T}^{\nu\tau}$  (59).

Due to the digital nature of controllers, in this section, we seek to design a full-order discrete-time parameter-varying controller of the form

$$\begin{aligned}\mathbf{x}_d(k+1) &= \mathbf{A}_d(\boldsymbol{\rho}(k))\mathbf{x}_d(k) + \sum_{i=1}^N \mathbf{A}_{\tau d_i} \mathbf{x}_d(k-i) + \mathbf{B}_d(\boldsymbol{\rho}(k))\mathbf{y}(k), \\ \mathbf{u}_d(k) &= \mathbf{C}_d(\boldsymbol{\rho}(k))\mathbf{x}_d(k) + \sum_{i=1}^N \mathbf{C}_{\tau d_i} \mathbf{x}_d(k-i) + \mathbf{D}_d(\boldsymbol{\rho}(k))\mathbf{y}(k),\end{aligned}\tag{132}$$

that uses the sampled measurements of the continuous plant to generate a discrete control action, goes through a zero-order hold device before being inputted to the continuous-time plant.  $\mathbf{x}_d(k)$ ,  $\mathbf{y}(k)$ , and  $\mathbf{u}_d(k)$  are the discrete-time signals of controller state vector, measurement, and control input, respectively. For the sake of brevity, the counter  $k$  is chosen to show the sampling instances,  $t_k$ , and  $N$  denotes the number of back samples of the controller state vector. Figure 30 demonstrates the configuration of the hybrid sampled-data closed-loop system, which shows the interconnection of the open-loop continuous-time system and a digital controller along with the signal converter devices.

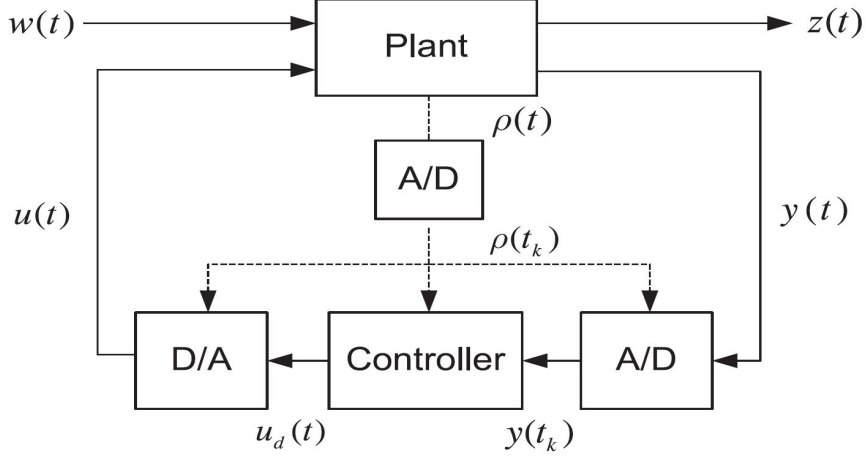


Figure 30: Sampled-data closed-loop system configuration

Unlike continuous-time LPV system in which scheduling parameter vector  $\boldsymbol{\rho}(t) \in \mathcal{F}_{\mathcal{P}}^{\nu}$  is continuously being measured in real-time, in sampled-data control design framework, parameter vector is only measured at sampling instances. Hence, in the continuous-time system, we assume that the parameter vector does not change in between two consecutive samples and the set of all admissible parameter trajectories is redefined for the sampled-data system as

$$\varepsilon_{\mathcal{P}}^{\nu} \triangleq \{\boldsymbol{\rho}(t) \in \mathcal{P}, \boldsymbol{\rho}(t_k + t) = \boldsymbol{\rho}(t_k), |\rho_i(t_{k+1}) - \rho_i(t_k)| \leq \nu_i, k \in \mathbb{Z}_+, i = 1, 2, \dots, n_s, \forall t \in [0, \mathcal{T}_k]\}, \quad (133)$$

where  $\mathcal{T}_k$  denotes the varying sampling period, *i.e.*, the length of time interval  $[t_k, t_{k+1}]$ . Interconnection of the system (57), the controller (132), and the converters form a closed-loop system  $\mathbf{T}_{\mathbf{z}\mathbf{w}}$  which maps the disturbance signal  $\mathbf{w}(t)$  to the desired control signal  $\mathbf{z}(t)$ . Considering the allowable parameter trajectories in  $\varepsilon_{\mathcal{P}}^{\nu}$ , the designed sampled-data controller is required to satisfy the asymptotic stability of the closed-loop system in the face of the parameters and delay variations, and disturbances to maintain the boundedness of the closed-loop system trajectories, and minimize the worst case amplification of the desired output,  $\mathbf{z}$ , to a nonzero disturbance signal,  $\mathbf{w}$ , with bounded energy, *i.e.*, solving the problem of  $\gamma$ -suboptimal induced  $\mathcal{L}_2$ -norm (energy-to-energy gain) of the

mapping  $\mathbf{T}_{\mathbf{zw}} : \mathbf{w} \rightarrow \mathbf{z}$  given by (61).

Considering a continuous-time full-order controller with a state-space representation as follows

$$\begin{aligned}
\dot{\mathbf{x}}_K(t) &= \mathbf{A}_K(\boldsymbol{\rho}(t))\mathbf{x}_K(t) + \mathbf{A}_{\tau,K}(\boldsymbol{\rho}(t))\mathbf{x}_K(t - \tau(\boldsymbol{\rho}(t))) + \mathbf{A}_{\mathcal{T},K}(\boldsymbol{\rho}(t))\mathbf{x}_K(t_k) + \mathbf{B}_K(\boldsymbol{\rho}(t))\mathbf{y}(t_k), \\
\mathbf{u}_K(t_k) &= \mathbf{C}_K(\boldsymbol{\rho}(t))\mathbf{x}_K(t_k) + \mathbf{D}_K(\boldsymbol{\rho}(t))\mathbf{y}(t_k), \\
\mathbf{u}(t) &= \mathbf{u}_K(t_k), \quad t_k \leq t < t_{k+1},
\end{aligned} \tag{134}$$

where  $\boldsymbol{\rho} \in \varepsilon'_{\mathcal{D}}$  and  $\boldsymbol{\rho}(t_k)$  is replaced with  $\boldsymbol{\rho}(t)$  for  $t_k \leq t < t_{k+1}$  for the simplicity, emphasizing the fact that the continuous-time scheduling parameter vector is considered to be piecewise constant and does not vary in between sampling instances. It should be noted that unlike conventional approaches where a continuous-time controller is discretized without taking the converter devices into account, in the proposed sampled-data controller design approach (134), the effects of sampling and holding devices are taken into consideration. In the sampled-data framework, as shown in Fig. 30, controller (134) uses discrete-time signals of measurement and the scheduling parameter vector. In order to obtain a unified state-space continuous-time domain representation, the input-delay approach is utilized as follows [28]:

$$u(t_k) = t \underbrace{\left( t - t_k \right)}_{\mathcal{T}_k(t)} = u(t - \mathcal{T}_k(t)), \quad t_k \leq t < t_{k+1}, \tag{135}$$

where  $\mathcal{T}_k \leq t_{k+1} - t_k \leq \bar{\mathcal{T}}$  and  $\bar{\mathcal{T}}$  denotes the maximum sampling interval value. Taking the advantage of the input-delay approach, the sampling/holding characteristics are captured by defining a new delay term,  $\mathcal{T}_k$ . By substituting (135) in (134) the controller state-space model is transferred into a continuous-time representation as follows

$$\begin{aligned}
\dot{\mathbf{x}}_K(t) &= \mathbf{A}_K(\boldsymbol{\rho}(t))\mathbf{x}_K(t) + \mathbf{A}_{\tau,K}(\boldsymbol{\rho}(t))\mathbf{x}_K(t - \tau(\boldsymbol{\rho}(t))) + \mathbf{A}_{\mathcal{T},K}(\boldsymbol{\rho}(t))\mathbf{x}_K(t - \mathcal{T}_k) \\
&+ \mathbf{B}_K(\boldsymbol{\rho}(t))\mathbf{C}_2(\boldsymbol{\rho}(t))\mathbf{x}_p(t - \mathcal{T}_k), \\
\mathbf{u}(t) &= \mathbf{C}_K(\boldsymbol{\rho}(t))\mathbf{x}_K(t - \mathcal{T}_k) + \mathbf{D}_K(\boldsymbol{\rho}(t))\mathbf{C}_2(\boldsymbol{\rho}(t))\mathbf{x}_p(t - \mathcal{T}_k).
\end{aligned} \tag{136}$$

Finally, by augmenting the controller (136) and the LPV system (57) and defining the closed-loop state vector as  $\mathbf{x}_{cl}^T(t) = [ \mathbf{x}_p^T(t) \quad \mathbf{x}_K^T(t) ]$ , closed-loop sampled-data system is in the following form

$$\begin{aligned}\dot{\mathbf{x}}_{cl}(t) &= \mathbf{A}_{cl} \mathbf{x}_{cl}(t) + \mathbf{A}_{\tau,cl} \mathbf{x}_{cl}(t - \tau(t)) + \mathbf{A}_{\mathcal{I},cl} \mathbf{x}_{cl}(t - \mathcal{I}(t)) + \mathbf{B}_{cl} \mathbf{w}(t), \\ \mathbf{z}(t) &= \mathbf{C}_{cl} \mathbf{x}_{cl}(t) + \mathbf{C}_{\tau,cl} \mathbf{x}_{cl}(t - \tau(t)) + \mathbf{C}_{\mathcal{I},cl} \mathbf{x}_{cl}(t - \mathcal{I}(t)) + \mathbf{D}_{cl} \mathbf{w}(t),\end{aligned}\tag{137}$$

with closed-loop system matrices

$$\begin{aligned}\mathbf{A}_{cl} &= \begin{bmatrix} \mathbf{A} & \mathbf{0} \\ \mathbf{0} & \mathbf{A}_K \end{bmatrix}, \mathbf{A}_{\tau,cl} = \begin{bmatrix} \mathbf{A}_\tau & \mathbf{0} \\ \mathbf{0} & \mathbf{A}_{\tau,K} \end{bmatrix}, \mathbf{A}_{\mathcal{I},cl} = \begin{bmatrix} \mathbf{B}_2 \mathbf{D}_K \mathbf{C}_2 & \mathbf{B}_2 \mathbf{C}_K \\ \mathbf{B}_K \mathbf{C}_2 & \mathbf{A}_{\mathcal{I},K} \end{bmatrix}, \mathbf{B}_{cl} = \begin{bmatrix} \mathbf{B}_1 \\ \mathbf{0} \end{bmatrix}, \\ \mathbf{C}_{cl} &= \begin{bmatrix} \mathbf{C}_1 & \mathbf{0} \end{bmatrix}, \mathbf{C}_{\tau,cl} = \begin{bmatrix} \mathbf{C}_{1,\tau} & \mathbf{0} \end{bmatrix}, \mathbf{C}_{\mathcal{I},cl} = \begin{bmatrix} \mathbf{D}_{12} \mathbf{D}_K \mathbf{C}_2 & \mathbf{D}_{12} \mathbf{C}_K \end{bmatrix}, \mathbf{D}_{cl} = \mathbf{D}_{11}.\end{aligned}\tag{138}$$

The closed-loop LPV system (137) has two delays: the first one is the inherent system delay, and the other delay term is imposed using the input-delay approach and the sampling. In the following, we employ the Lyapunov-Krasovskii approach by using an extended quadratic LKF candidate, which results in sufficient delay-dependent conditions to guarantee the closed-loop stability and  $\mathcal{L}_2$ -gain performance of the sampled-data LPV system with arbitrary varying time-delay and sampling rate.

**Theorem 9.** : *There exists a full-order output-feedback gain-scheduled LPV controller (134), over the sets  $\varepsilon_{\mathcal{D}}^\nu$  and  $\mathcal{T}^{\nu\tau}$ , to asymptotically stabilizes the closed-loop LPV system (137) and satisfies the induced  $\mathcal{L}_2$  norm performance level given in (61), with the sampling time  $\mathcal{T}_k \leq \bar{\mathcal{T}}$ , if there exists a continuously differentiable parameter dependent positive-definite matrix function  $\tilde{\mathbf{P}}(\boldsymbol{\rho}(t)) : \mathbb{R}^s \rightarrow \mathbb{S}_{+++}^{2n_p}$ , parameter dependent matrix functions  $\mathbf{X}(\boldsymbol{\rho}(t)), \mathbf{Y}(\boldsymbol{\rho}(t)) : \mathbb{R}^s \rightarrow \mathbb{S}^{n_p}$ , positive-definite matrices  $\tilde{\mathbf{Q}}_\tau, \tilde{\mathbf{Q}}_{\mathcal{I}}, \tilde{\mathbf{R}}_\tau, \tilde{\mathbf{R}}_{\mathcal{I}}, \tilde{\mathbf{T}}_\tau \in \mathbb{S}_{+++}^{2n_p}$ , parameter dependent real matrix functions  $\hat{\mathbf{A}}(\boldsymbol{\rho}(t)), \hat{\mathbf{A}}_\tau(\boldsymbol{\rho}(t)), \hat{\mathbf{A}}_{\mathcal{I}}(\boldsymbol{\rho}(t)) : \mathbb{R}^s \rightarrow \mathbb{R}^{n_p \times n_p}$ ,  $\hat{\mathbf{B}}(\boldsymbol{\rho}(t)) : \mathbb{R}^s \rightarrow \mathbb{R}^{n_p \times n_u}$ ,  $\hat{\mathbf{C}}(\boldsymbol{\rho}(t)) : \mathbb{R}^s \rightarrow \mathbb{R}^{n_u \times n_p}$ ,  $\hat{\mathbf{C}}_d(\boldsymbol{\rho}(t)), \mathbf{D}_K(\boldsymbol{\rho}(t)) : \mathbb{R}^s \rightarrow \mathbb{R}^{n_u \times n_y}$ , a positive scalar  $\gamma$ , and real scalars  $\lambda_2, \lambda_3, \lambda_4, \lambda_5 \in \mathbb{R}$  such that*

$$\begin{bmatrix}
\tilde{\mathbf{E}}_{11} & \tilde{\mathbf{P}} - \tilde{\mathbf{V}} + \lambda_2 \mathcal{A}^T & \tilde{\mathbf{R}}_\tau + \mathcal{A}_\tau + \lambda_3 \mathcal{A}^T & \tilde{\mathbf{R}}_{\mathcal{G}} + \mathcal{A}_{\mathcal{G}} + \lambda_4 \mathcal{A}^T & \lambda_5 \mathcal{A}^T & \mathcal{B} & \mathcal{C}^T \\
\star & \bar{\tau}^2 \tilde{\mathbf{R}}_\tau + \bar{\mathcal{F}}^2 \tilde{\mathbf{R}}_{\mathcal{G}} - 2\lambda_2 \tilde{\mathbf{V}} & \lambda_2 \mathcal{A}_\tau - \lambda_3 \tilde{\mathbf{V}} & \lambda_2 \mathcal{A}_{\mathcal{G}} - \lambda_4 \tilde{\mathbf{V}} & -\lambda_5 \tilde{\mathbf{V}} & \lambda_2 \mathcal{B} & \mathbf{0} \\
\star & \star & \tilde{\mathbf{E}}_{33} & \lambda_3 \mathcal{A}_{\mathcal{G}} + \lambda_4 \mathcal{A}_\tau^T & \lambda_5 \mathcal{A}_\tau^T & \lambda_3 \mathcal{B} & \mathcal{C}_\tau^T \\
\star & \star & \star & \tilde{\mathbf{E}}_{44} & \lambda_5 \mathcal{A}_{\mathcal{G}}^T & \lambda_4 \mathcal{B} & \mathcal{C}_{\mathcal{G}}^T \\
\star & \star & \star & \star & -\tilde{\mathbf{T}}_\tau & \lambda_5 \mathcal{B} & \mathbf{0} \\
\star & \star & \star & \star & \star & -\gamma \mathbf{I} & \mathbf{D}_{11}^T \\
\star & \star & \star & \star & \star & \star & -\gamma \mathbf{I}
\end{bmatrix} \prec \mathbf{0}, \quad (139)$$

is feasible, and the variables in (139) are as follows

$$\begin{aligned}
\tilde{\mathbf{V}} &= \begin{bmatrix} \mathbf{Y} & \mathbf{I} \\ \mathbf{I} & \mathbf{X} \end{bmatrix}, \mathcal{A} = \begin{bmatrix} \mathbf{A}\mathbf{Y} & \mathbf{A} \\ \mathbf{X}\mathbf{A}\mathbf{Y} + \mathcal{N}\mathbf{A}_K\mathcal{M}^T & \mathbf{X}\mathbf{A} \end{bmatrix} = \begin{bmatrix} \mathbf{A}\mathbf{Y} & \mathbf{A} \\ \hat{\mathbf{A}} & \mathbf{X}\mathbf{A} \end{bmatrix}, \\
\mathcal{A}_\tau &= \begin{bmatrix} \mathbf{A}_\tau\mathbf{Y} & \mathbf{A}_\tau \\ \mathbf{X}\mathbf{A}_\tau\mathbf{Y} + \mathcal{N}\mathbf{A}_{\tau,K}\mathcal{M}^T & \mathbf{X}\mathbf{A}_\tau \end{bmatrix} = \begin{bmatrix} \mathbf{A}_\tau\mathbf{Y} & \mathbf{A}_\tau \\ \hat{\mathbf{A}}_\tau & \mathbf{X}\mathbf{A}_\tau \end{bmatrix}, \\
\mathcal{A}_{\mathcal{G}} &= \begin{bmatrix} \mathbf{B}_2(\mathbf{D}_K\mathbf{C}_2\mathbf{Y} + \mathbf{C}_K\mathcal{M}^T) & \mathbf{B}_2\mathbf{D}_K\mathbf{C}_2 \\ \mathbf{X}\mathbf{B}_2\mathbf{D}_K\mathbf{C}_2\mathbf{Y} + \mathcal{N}\mathbf{B}_K\mathbf{C}_2\mathbf{Y} & (\mathbf{X}\mathbf{B}_2\mathbf{D}_K + \mathcal{N}\mathbf{B}_K)\mathbf{C}_2 \\ +\mathbf{X}\mathbf{B}_2\mathbf{C}_K\mathcal{M}^T + \mathcal{N}\mathbf{A}_{\mathcal{G},K}\mathcal{M}^T & \end{bmatrix} = \begin{bmatrix} \mathbf{B}_2\hat{\mathbf{C}} & \mathbf{B}_2\mathbf{D}_K\mathbf{C}_2 \\ \hat{\mathbf{A}}_{\mathcal{G}} & \hat{\mathbf{B}}\mathbf{C}_2 \end{bmatrix}, \\
\mathcal{B} &= \begin{bmatrix} \mathbf{B}_1 \\ \mathbf{X}\mathbf{B}_1 \end{bmatrix}, \mathcal{C} = \begin{bmatrix} \mathbf{C}_1\mathbf{Y} & \mathbf{C}_1 \end{bmatrix}, \mathcal{C}_\tau = \begin{bmatrix} \mathbf{C}_{1,\tau}\mathbf{Y} & \mathbf{C}_{1,\tau} \end{bmatrix}, \\
\mathcal{C}_{\mathcal{G}} &= \begin{bmatrix} \mathbf{D}_{12}(\mathbf{D}_K\mathbf{C}_2\mathbf{Y} + \mathbf{C}_K\mathcal{M}^T) & \mathbf{D}_{12}\mathbf{D}_K\mathbf{C}_2 \end{bmatrix} = \begin{bmatrix} \mathbf{D}_{12}\hat{\mathbf{C}} & \mathbf{D}_{12}\mathbf{D}_K\mathbf{C}_2 \end{bmatrix}, \\
\tilde{\mathbf{E}}_{11} &= \left[ \sum_{i=1}^s \pm \left( \nu_i \frac{\partial \tilde{\mathbf{P}}}{\partial \rho_i} \right) \right] + \tilde{\mathbf{Q}}_\tau - \tilde{\mathbf{R}}_\tau + \bar{\tau}^2 \tilde{\mathbf{T}}_\tau + \tilde{\mathbf{Q}}_{\mathcal{G}} - \tilde{\mathbf{R}}_{\mathcal{G}} + \mathcal{A} + \mathcal{A}^T, \\
\tilde{\mathbf{E}}_{33} &= - \left[ 1 - \sum_{i=1}^s \pm \left( \nu_i \frac{\partial \tau}{\partial \rho_i} \right) \right] \tilde{\mathbf{Q}}_\tau - \tilde{\mathbf{R}}_\tau + \lambda_3(\mathcal{A}_\tau + \mathcal{A}_\tau^T),
\end{aligned}$$

$$\tilde{\mathbf{E}}_{44} = - \left[ 1 - \sum_{i=1}^s \pm \left( \nu_i \frac{\partial \mathcal{J}}{\partial \rho_i} \right) \right] \tilde{\mathbf{Q}}_{\mathcal{J}} - \tilde{\mathbf{R}}_{\mathcal{J}} + \lambda_4 (\mathcal{A}_{\mathcal{J}} + \mathcal{A}_{\mathcal{J}}^T). \quad (140)$$

*Proof.* The proof relies on employing an LKF candidate of the form

$$V(\mathbf{x}_{cl_t}, \dot{\mathbf{x}}_{cl_t}, \boldsymbol{\rho}, t) = V_0(\mathbf{x}_{cl}, \boldsymbol{\rho}, t) + V_{\tau}(\mathbf{x}_{cl_t}, \dot{\mathbf{x}}_{cl_t}, \boldsymbol{\rho}, t) + V_{\mathcal{J}}(\mathbf{x}_{cl_t}, \dot{\mathbf{x}}_{cl_t}, \boldsymbol{\rho}, t), \quad (141)$$

with

$$\begin{aligned} V_0(\mathbf{x}_{cl}, \boldsymbol{\rho}, t) &= \mathbf{x}_{cl}^T(t) \mathbf{P}(\boldsymbol{\rho}(t)) \mathbf{x}_{cl}(t), \\ V_{\tau}(\mathbf{x}_{cl_t}, \dot{\mathbf{x}}_{cl_t}, \boldsymbol{\rho}, t) &= \int_{t-\tau(t)}^t \mathbf{x}_{cl}^T(\eta) \mathbf{Q}_{\tau} \mathbf{x}_{cl}(\eta) d\eta + \int_{-\bar{\tau}}^0 \int_{t+\theta}^t \dot{\mathbf{x}}_{cl}^T(\eta) \bar{\mathbf{R}}_{\tau} \dot{\mathbf{x}}_{cl}(\eta) d\eta d\theta \\ &\quad + \int_{-\bar{\tau}}^0 \int_{t+\theta}^t \mathbf{x}_{cl}^T(\eta) \bar{\mathbf{T}}_{\tau} \mathbf{x}_{cl}(\eta) d\eta d\theta, \\ V_{\mathcal{J}}(\mathbf{x}_{cl_t}, \dot{\mathbf{x}}_{cl_t}, \boldsymbol{\rho}, t) &= \int_{t-\mathcal{J}(t)}^t \mathbf{x}_{cl}^T(\eta) \mathbf{Q}_{\mathcal{J}} \mathbf{x}_{cl}(\eta) d\eta + \int_{-\bar{\mathcal{J}}}^0 \int_{t+\theta}^t \dot{\mathbf{x}}_{cl}^T(\eta) \bar{\mathcal{T}}_{\mathcal{J}} \dot{\mathbf{x}}_{cl}(\eta) d\eta d\theta, \end{aligned}$$

and the time derivative of LKF is as follows

$$\dot{V}(\mathbf{x}_{cl_t}, \dot{\mathbf{x}}_{cl_t}, \boldsymbol{\rho}, t) = \dot{V}_0(\mathbf{x}_{cl}, \boldsymbol{\rho}, t) + \dot{V}_{\tau}(\mathbf{x}_{cl_t}, \dot{\mathbf{x}}_{cl_t}, \boldsymbol{\rho}, t) + \dot{V}_{\mathcal{J}}(\mathbf{x}_{cl_t}, \dot{\mathbf{x}}_{cl_t}, \boldsymbol{\rho}, t), \quad (142)$$

where

$$\begin{aligned} \dot{V}_0(\mathbf{x}_{cl}, \boldsymbol{\rho}, t) &= 2\dot{\mathbf{x}}_{cl}^T(t) \mathbf{P}(\boldsymbol{\rho}(t)) \mathbf{x}_{cl}(t) + \mathbf{x}_{cl}^T(t) \left[ \sum_{i=1}^{n_s} \dot{\rho}_i(t) \frac{\partial \mathbf{P}(\boldsymbol{\rho}(t))}{\partial \rho_i(t)} \right] \mathbf{x}_{cl}(t), \\ \dot{V}_{\tau}(\mathbf{x}_{cl_t}, \dot{\mathbf{x}}_{cl_t}, \boldsymbol{\rho}, t) &= \mathbf{x}_{cl}^T(t) \mathbf{Q}_{\tau} \mathbf{x}_{cl}(t) - (1 - \dot{\rho}_i(t) \frac{\partial \tau(t)}{\partial \rho_i(t)}) \mathbf{x}_{cl}^T(t - \tau(t)) \mathbf{Q}_{\tau} \mathbf{x}_{cl}(t - \tau(t)) \\ &\quad + \bar{\tau}^2 \dot{\mathbf{x}}_{cl}^T(t) \mathbf{R}_{\tau} \dot{\mathbf{x}}_{cl}(t) - \int_{t-\bar{\tau}}^t \dot{\mathbf{x}}_{cl}^T(\eta) \bar{\mathbf{R}}_{\tau} \dot{\mathbf{x}}_{cl}(\eta) d\eta + \bar{\tau}^2 \mathbf{x}_{cl}^T(t) \mathbf{T}_{\tau} \mathbf{x}_{cl}(t) - \int_{t-\bar{\tau}}^t \mathbf{x}_{cl}^T(\eta) \bar{\mathbf{T}}_{\tau} \mathbf{x}_{cl}(\eta) d\eta, \\ \dot{V}_{\mathcal{J}}(\mathbf{x}_{cl_t}, \dot{\mathbf{x}}_{cl_t}, \boldsymbol{\rho}, t) &= \mathbf{x}_{cl}^T(t) \mathbf{Q}_{\mathcal{J}} \mathbf{x}_{cl}(t) - (1 - \dot{\rho}_i(t) \frac{\partial \mathcal{J}(t)}{\partial \rho_i(t)}) \mathbf{x}_{cl}^T(t - \mathcal{J}(t)) \mathbf{Q}_{\mathcal{J}} \mathbf{x}_{cl}(t - \mathcal{J}(t)) \\ &\quad + \bar{\mathcal{J}}^2 \dot{\mathbf{x}}_{cl}^T(t) \mathbf{R}_{\mathcal{J}} \dot{\mathbf{x}}_{cl}(t) - \int_{t-\bar{\mathcal{J}}}^t \dot{\mathbf{x}}_{cl}^T(\eta) \bar{\mathcal{T}}_{\mathcal{J}} \dot{\mathbf{x}}_{cl}(\eta) d\eta. \end{aligned}$$

The time derivative of LKF (142) will be upper-bounded as follows

$$\begin{aligned}
\dot{V}(\mathbf{x}_{cl_t}, \dot{\mathbf{x}}_{cl_t}, \boldsymbol{\rho}, t) &\leq \dot{V}_0(\mathbf{x}_{cl}, \boldsymbol{\rho}, t) + \mathbf{x}_{cl}^T(t) \mathbf{Q}_\tau \mathbf{x}_{cl}(t) - (1 - \dot{\rho}_i(t) \frac{\partial \tau(t)}{\partial \rho_i(t)}) \mathbf{x}_{cl}^T(t - \tau(t)) \mathbf{Q}_\tau \mathbf{x}_{cl}(t - \tau(t)) \\
&+ \bar{\tau}^2 \dot{\mathbf{x}}_{cl}^T(t) \mathbf{R}_\tau \dot{\mathbf{x}}_{cl}(t) - [\mathbf{x}_{cl}(t) - \mathbf{x}_{cl}(t - \tau(t))]^T \mathbf{R}_\tau [\mathbf{x}_{cl}(t) - \mathbf{x}_{cl}(t - \tau(t))] + \bar{\tau}^2 \mathbf{x}_{cl}^T(t) \mathbf{T}_\tau \mathbf{x}_{cl}(t) \\
&- \left( \int_{t-\tau(t)}^t \mathbf{x}_{cl}(\eta) d\eta \right)^T \mathbf{T}_\tau \left( \int_{t-\tau(t)}^t \mathbf{x}_{cl}(\eta) d\eta \right) + \mathbf{x}_{cl}^T(t) \mathbf{Q}_{\mathcal{I}} \mathbf{x}_{cl}(t) \\
&- (1 - \dot{\rho}_i(t) \frac{\partial \mathcal{I}(t)}{\partial \rho_i(t)}) \mathbf{x}_{cl}^T(t - \mathcal{I}(t)) \mathbf{Q}_{\mathcal{I}} \mathbf{x}_{cl}(t - \mathcal{I}(t)) + \bar{\mathcal{I}}^2 \dot{\mathbf{x}}_{cl}^T(t) \mathbf{R}_{\mathcal{I}} \dot{\mathbf{x}}_{cl}(t) \\
&- [\mathbf{x}_{cl}(t) - \mathbf{x}_{cl}(t - \mathcal{I}(t))]^T \mathbf{R}_{\mathcal{I}} [\mathbf{x}_{cl}(t) - \mathbf{x}_{cl}(t - \mathcal{I}(t))]. \tag{143}
\end{aligned}$$

Next, to derive relaxed LMI conditions appropriate for the synthesis conditions, we use the descriptor technique [28], which introduces slack variables  $\mathbf{V}_1$ ,  $\mathbf{V}_2$ ,  $\mathbf{V}_3$ ,  $\mathbf{V}_4$ , and  $\mathbf{V}_5$  as follows

$$\begin{aligned}
\mathcal{I} &= \left[ \mathbf{x}_{cl}^T(t) \mathbf{V}_1^T + \dot{\mathbf{x}}_{cl}^T(t) \mathbf{V}_2^T + \mathbf{x}_{cl}^T(t - \tau(t)) \mathbf{V}_3^T + \mathbf{x}_{cl}^T(t - \mathcal{I}(t)) \mathbf{V}_4^T + \int_{t-\tau(t)}^t \mathbf{x}_{cl}(\eta) d\eta \mathbf{V}_5^T \right] \\
&\left( \mathbf{A}_{cl} \mathbf{x}_{cl}(t) + \mathbf{A}_{\tau,cl} \mathbf{x}_{cl}(t - \tau(t)) + \mathbf{A}_{\mathcal{I},cl} \mathbf{x}_{cl}(t - \mathcal{I}(t)) + \mathbf{B}_{cl} \mathbf{w}(t) - \dot{\mathbf{x}}_{cl}(t) \right) = 0. \tag{144}
\end{aligned}$$

To establish the prescribed performance requirement, we consider the performance index as  $J = \int_{t_0}^{\infty} -\gamma^2 \mathbf{w}^T(t) \mathbf{w}(t) + \mathbf{z}^T(t) \mathbf{z}(t) < 0$ , and by augmenting (143) with  $2\mathcal{I}$  and  $\frac{dJ}{dt}$  the final inequality is obtained as follows

$$\dot{V}(\mathbf{x}_{cl_t}, \dot{\mathbf{x}}_{cl_t}, \boldsymbol{\rho}, t) + 2\mathcal{I} - \gamma^2 \mathbf{w}^T(t) \mathbf{w}(t) + \mathbf{z}^T(t) \mathbf{z}(t) \leq \boldsymbol{\zeta}^T(t) \boldsymbol{\Omega} \boldsymbol{\zeta}(t) < 0, \tag{145}$$

where the augmented state vector  $\boldsymbol{\zeta}(t)$  is defined as

$$\boldsymbol{\zeta}^T(t) \triangleq \left[ \mathbf{x}_{cl}^T(t), \dot{\mathbf{x}}_{cl}^T(t), \mathbf{x}_{cl}^T(t - \tau(t)), \mathbf{x}_{cl}^T(t - \mathcal{I}(t)), \int_{t-\tau(t)}^t \mathbf{x}_{cl}^T(\eta) d\eta, \mathbf{w}^T(t) \right], \tag{146}$$

and

$$\begin{aligned}
\Omega = & \begin{bmatrix} \Xi_{11} & \mathbf{P} - \mathbf{V}_1^T + \mathbf{A}_{cl}^T \mathbf{V}_2 & \mathbf{R}_\tau + \mathbf{V}_1^T \mathbf{A}_{\tau,cl} + \mathbf{A}_{cl}^T \mathbf{V}_3 \\ \star & \bar{\tau}^2 \mathbf{R}_\tau + \bar{\mathcal{F}}^2 \mathbf{R}_{\mathcal{J}} - \mathbf{V}_2 - \mathbf{V}_2^T & \mathbf{V}_2^T \mathbf{A}_{\tau,cl} - \mathbf{V}_3 \\ \star & \star & \Xi_{33} \\ \star & \star & \star \\ \star & \star & \star \\ \star & \star & \star \end{bmatrix} \\
& \begin{bmatrix} \mathbf{R}_{\mathcal{J}} + \mathbf{V}_1^T \mathbf{A}_{\mathcal{J},cl} + \mathbf{A}_{cl}^T \mathbf{V}_4 & \mathbf{A}_{cl}^T \mathbf{V}_5 & \mathbf{V}_1^T \mathbf{B}_{cl} \\ \mathbf{V}_2^T \mathbf{A}_{\mathcal{J},cl} - \mathbf{V}_4 & -\mathbf{V}_5 & \mathbf{V}_2^T \mathbf{B}_{cl} \\ \mathbf{V}_3^T \mathbf{A}_{\mathcal{J},cl} + \mathbf{A}_{\tau,cl}^T \mathbf{V}_4 & \mathbf{A}_{\tau,cl}^T \mathbf{V}_5 & \mathbf{V}_3^T \mathbf{B}_{cl} \\ \Xi_{44} & \mathbf{A}_{\mathcal{J},cl}^T \mathbf{V}_5 & \mathbf{V}_4^T \mathbf{B}_{cl} \\ \star & -\mathbf{T}_\tau & \mathbf{V}_5^T \mathbf{B}_{cl} \\ \star & \star & -\gamma^2 \mathbf{I} \end{bmatrix} + \mathbf{\Gamma}^T \mathbf{\Gamma}, \tag{147}
\end{aligned}$$

where

$$\begin{aligned}
\Xi_{11} &= \left[ \sum_{i=1}^{n_s} \pm \left( \nu_i \frac{\partial \mathbf{P}}{\partial \rho_i} \right) \right] + \mathbf{Q}_\tau - \mathbf{R}_\tau + \bar{\tau}^2 \mathbf{T}_\tau + \mathbf{Q}_{\mathcal{J}} - \mathbf{R}_{\mathcal{J}} + \mathbf{V}_1^T \mathbf{A}_{cl} + \mathbf{A}_{cl}^T \mathbf{V}_1, \\
\Xi_{33} &= - \left[ 1 - \sum_{i=1}^{n_s} \pm \left( \nu_i \frac{\partial \tau}{\partial \rho_i} \right) \right] \mathbf{Q}_\tau - \mathbf{R}_\tau + \mathbf{V}_3^T \mathbf{A}_{\tau,cl} + \mathbf{A}_{\tau,cl}^T \mathbf{V}_3, \\
\Xi_{44} &= - \left[ 1 - \sum_{i=1}^{n_s} \pm \left( \nu_i \frac{\partial \mathcal{J}}{\partial \rho_i} \right) \right] \mathbf{Q}_{\mathcal{J}} - \mathbf{R}_{\mathcal{J}} + \mathbf{V}_4^T \mathbf{A}_{\mathcal{J},cl} + \mathbf{A}_{\mathcal{J},cl}^T \mathbf{V}_4, \\
\mathbf{\Gamma} &= \begin{bmatrix} \mathbf{C}_{cl} & \mathbf{0} & \mathbf{C}_{\tau,cl} & \mathbf{C}_{\mathcal{J},cl} & \mathbf{0} & \mathbf{D}_{cl} \end{bmatrix}. \tag{148}
\end{aligned}$$

By choosing the four slack variable matrices in (87) as  $\mathbf{V}_1 \triangleq \lambda_1 \mathbf{V} \in \mathbb{S}^{2n_p}$ ,  $\mathbf{V}_2 \triangleq \lambda_2 \mathbf{V}$ ,  $\mathbf{V}_3 \triangleq \lambda_3 \mathbf{V}$ ,  $\mathbf{V}_4 \triangleq \lambda_4 \mathbf{V}$ , and  $\mathbf{V}_5 \triangleq \lambda_5 \mathbf{V}$ , where  $\lambda_1 = 1$ ,  $\lambda_2$ ,  $\lambda_3$ ,  $\lambda_4$ , and  $\lambda_5$  are scalars and  $\mathbf{V}$  matrix and its inverse are partitioned as  $\mathbf{V} \triangleq \begin{bmatrix} \mathbf{X} & \mathcal{N} \\ \mathcal{N}^T & \star \end{bmatrix}$ ,  $\mathbf{V}^{-1} \triangleq \begin{bmatrix} \mathbf{Y} & \mathcal{M} \\ \mathcal{M}^T & \star \end{bmatrix}$ , such that  $\mathbf{X}\mathbf{Y} + \mathcal{N}\mathcal{M}^T = \mathbf{I}$ . Next, we

substitute closed-loop matrices (138) into (147) and then we apply Schur complement formula to the  $\Omega$  (147), resulting a  $7 \times 7$  block matrix. Finally, by defining  $\mathcal{Z} \triangleq \begin{bmatrix} \mathbf{Y} & \mathbf{I} \\ \mathcal{M}^T & \mathbf{0} \end{bmatrix}$ , and performing a congruence transformation  $diag(\mathcal{Z}^T, \mathcal{Z}^T, \mathcal{Z}^T, \mathcal{Z}^T, \mathcal{Z}^T, \mathbf{I}, \mathbf{I})$  on the  $7 \times 7$  block matrix and redefining the matrix multiplications as  $\tilde{\square} \triangleq \mathcal{Z}^T \square \mathcal{Z}$ , final LMI condition (139) is obtained and the proof is complete.  $\square$

#### 4.4.1 Digital Controller Derivation

Once the parameter dependent matrices  $\mathbf{X}$ ,  $\mathbf{Y}$ ,  $\hat{A}$ ,  $\hat{A}_\tau$ ,  $\hat{A}_{\mathcal{G}}$ ,  $\hat{B}$ ,  $\hat{C}$ , and  $\mathbf{D}_K$  satisfying the mentioned LMI condition (139) are obtained, we compute the square and invertible matrices  $\mathcal{M}$  and  $\mathcal{N}$  from the factorization problem

$$\mathbf{I} - \mathbf{X}\mathbf{Y} = \mathcal{N}\mathcal{M}^T,$$

and finally the continuous-time practically valid gain-scheduled controller matrices of (134) are computed in the following order

$$\begin{aligned} \mathbf{A}_K &= \mathcal{N}^{-1}(\hat{A} - \mathbf{X}\mathbf{A}\mathbf{Y})\mathcal{M}^T, \\ \mathbf{A}_{\tau,K} &= \mathcal{N}^{-1}(\hat{A}_\tau - \mathbf{X}\mathbf{A}_\tau\mathbf{Y})\mathcal{M}^T, \\ \mathbf{B}_K &= \mathcal{N}^{-1}(\hat{B} - \mathbf{X}\mathbf{B}_2\mathbf{D}_K), \\ \mathbf{C}_K &= (\hat{C} - \mathbf{D}_K\mathbf{C}_2\mathbf{Y})\mathcal{M}^{-T}, \\ \mathbf{A}_{\mathcal{G},K} &= \mathcal{N}^{-1}(\hat{A}_{\mathcal{G}} - \mathbf{X}\mathbf{B}_2\mathbf{D}_K\mathbf{C}_2\mathbf{Y} - \mathcal{N}\mathbf{B}_K\mathbf{C}_2\mathbf{Y} - \mathbf{X}\mathbf{B}_2\mathbf{C}_K\mathcal{M}^T)\mathcal{M}^{-T}. \end{aligned} \tag{149}$$

For the implementation purpose, we need to find a discretized equivalence of the designed continuous-time LPV control design (134) as follows

$$\begin{aligned} \mathbf{x}_d(k+1) &= \mathbf{A}_d(\boldsymbol{\rho}(k))\mathbf{x}_d(k) + \sum_{i=l}^{l+2} \mathbf{A}_{\tau d_i}\mathbf{x}_d(k-i) + \mathbf{B}_d(\boldsymbol{\rho}(k))\mathbf{y}(k), \\ \mathbf{u}_d(k) &= \mathbf{C}_d(\boldsymbol{\rho}(k))\mathbf{x}_d(k) + \mathbf{D}_d(\boldsymbol{\rho}(k))\mathbf{y}(k). \end{aligned} \tag{150}$$

By using the approach suggested in [68], discrete-time controller matrices are computed as follows

$$\begin{aligned}
\mathbf{A}_d &= e^{(t_{k+1}-t_k)\mathbf{A}_K(\boldsymbol{\rho}(t_k))} + (e^{(t_{k+1}-t_k)\mathbf{A}_K(\boldsymbol{\rho}(t_k))} - \mathbf{I})\mathbf{A}_K^{-1}(\boldsymbol{\rho}(t_k))\mathbf{A}_{\mathcal{T},K}(\boldsymbol{\rho}(t_k)), \\
\mathbf{B}_d &= (e^{(t_{k+1}-t_k)\mathbf{A}_K(\boldsymbol{\rho}(t_k))} - \mathbf{I})\mathbf{A}_K^{-1}(\boldsymbol{\rho}(t_k))\mathbf{B}_K(\boldsymbol{\rho}(t_k)), \\
\mathbf{C}_d &= \mathbf{C}_K(\boldsymbol{\rho}(t_k)), \\
\mathbf{D}_d &= \mathbf{D}_K(\boldsymbol{\rho}(t_k)), \\
\mathbf{A}_{\tau d_l} &= \frac{c_1}{2}(e^{(t_{k+1}-t_k)\mathbf{A}_K(\boldsymbol{\rho}(t_k))} - e^{(t_{k+1}-\tau_k-t_{l+1})\mathbf{A}_K(\boldsymbol{\rho}(t_k))})\mathbf{A}_K^{-1}(\boldsymbol{\rho}(t_k))\mathbf{A}_{\tau,K}(\boldsymbol{\rho}(t_k)), \\
\mathbf{A}_{\tau d_{l+1}} &= \left(\frac{1+c_2}{2}e^{(t_{k+1}-t_k)\mathbf{A}_K(\boldsymbol{\rho}(t_k))} - \frac{c_2-c_3}{2}e^{(t_{k+1}-\tau_k-t_{l+1})\mathbf{A}_K(\boldsymbol{\rho}(t_k))} - \frac{1+c_3}{2}\mathbf{I}\right)\mathbf{A}_K^{-1}(\boldsymbol{\rho}(t_k))\mathbf{A}_{\tau,K}(\boldsymbol{\rho}(t_k)), \\
\mathbf{A}_{\tau d_{l+2}} &= \frac{c_4}{2}(e^{(t_{k+1}-\tau_k-t_{l+1})\mathbf{A}_K(\boldsymbol{\rho}(t_k))} - \mathbf{I})\mathbf{A}_K^{-1}(\boldsymbol{\rho}(t_k))\mathbf{A}_{\tau,K}(\boldsymbol{\rho}(t_k)),
\end{aligned} \tag{151}$$

with

$$c_1 = \frac{t_{l+1} - (t_k - \tau_k)}{t_{l+1} - t_l}, c_2 = \frac{(t_k - \tau_k) - t_l}{t_{l+1} - t_l}, c_3 = \frac{t_{l+2} - (t_{k+1} - \tau_k)}{t_{l+2} - t_{l+1}}, c_4 = \frac{(t_{k+1} - \tau_k) - t_{l+1}}{t_{l+2} - t_{l+1}}.$$

Thus far, designing the LPV controllers is accomplished. In the next part, the blood pressure regulation and control problem is introduced as a real-life case study to illustrate the efficiency and assess the closed-loop performance and the improvements of the proposed gain-scheduling LPV control scheme in several simulation scenarios.

## 4.5 Closed-Loop MAP Regulation

### 4.5.1 MAP Response Continuous-Time LPV Modeling

By considering continuous-time MAP response dynamics (1), the following LPV model is utilized to capture the MAP response dynamics subject to PHP drug infusion [92, 93]

$$\begin{aligned}
\dot{x}(t) &= -\frac{1}{T(t)}x(t) + \frac{K(t)}{T(t)}u(t - \tau(t)), \\
y(t) &= x(t) + d_o(t),
\end{aligned} \tag{152}$$

where the state variable is considered to capture the MAP variations in *mmHg* from its baseline value, *i.e.*,  $x(t) = \Delta MAP(t) = MAP(t) - MAP_b(t)$ ,  $u(t)$  is the drug infusion rate in *ml/h*,  $y(t)$  is the patient's measured MAP response output in *mmHg*, and  $d_o(t)$  denotes the disturbance signal.

Next, in order to utilize the proposed time-delay LPV control design tools introduced in Section 4, we need to transform the input delay system dynamics (152) into a tractable state-delay LPV representation (57). For this purpose, we introduce a low-pass input dynamics

$$u(s) = \frac{\Omega}{s + \Lambda} u_a(s), \quad (153)$$

where  $\Omega$  and  $\Lambda$  are positive scalars that are selected based on the bandwidth of the actuators. Then, the state-space state-delay LPV representation of the MAP response dynamics takes the standard time-delay LPV representation (57) with the augmented state vector of the system defined as  $\mathbf{x}(t) \triangleq \mathbf{x}_a(t) = [x(t) \quad u(t) \quad x_e(t)]^T$ .  $\mathbf{w}(t) = [r(t) \quad d_o(t)]^T$  stands for the exogenous disturbance vector including the reference MAP command,  $r(t)$ , and output disturbance signals.  $x_e(t)$  is defined for command tracking purposes, *i.e.*,  $\dot{x}_e(t) \triangleq e(t) = r(t) - y(t)$ , and thus the state space matrices of the MAP response dynamics in the LPV system representation (57) are as follows:

$$\begin{aligned} \mathbf{A}(\boldsymbol{\rho}(t)) &= \begin{bmatrix} -\frac{1}{T(t)} & 0 & 0 \\ 0 & -\Lambda & 0 \\ -1 & 0 & 0 \end{bmatrix}, \mathbf{A}_\tau(\boldsymbol{\rho}(t)) = \begin{bmatrix} 0 & \frac{K(t)}{T(t)} & 0 \\ 0 & 0 & 0 \\ 0 & 0 & 0 \end{bmatrix}, \mathbf{B}_1 = \begin{bmatrix} 0 & 0 \\ 0 & 0 \\ 1 & -1 \end{bmatrix}, \\ \mathbf{B}_2 &= \begin{bmatrix} 0 \\ \Omega \\ 0 \end{bmatrix}, \mathbf{C}_1 = \begin{bmatrix} 0 & 0 & \phi \\ 0 & 0 & 0 \end{bmatrix}, \mathbf{C}_{1,\tau} = \mathbf{0}_{2 \times 3}, \mathbf{D}_{11} = \mathbf{0}_{2 \times 2}, \mathbf{D}_{12} = \begin{bmatrix} 0 \\ \psi \end{bmatrix}, \end{aligned} \quad (154)$$

where the LPV scheduling parameter vector takes the form  $\boldsymbol{\rho}(t) = [K(t) \quad T(t) \quad \tau(t)]^T$ , which is not known *a priori*; however, it is supposed to be measured or estimated in real time. In a practical scenario, the Bayesian-based square-root cubature Kalman filtering algorithm can be used to estimate the scheduling parameters (see chapter 2).

#### 4.5.2 Automated LPV MAP Control Simulation Results and Discussions

The nonlinear patient simulation model developed in Section 1.1.1 is utilized along with the real-time model parameter estimations provided by the multiple-model square-root cubature Kalman filtering (MMSRCKF) algorithm (see chapter 2), to validate the proposed robust time-delay LPV control approaches in the closed-loop simulations. MMSRCKF estimates the model parameters of the nonlinear patient in real-time and feeds them to the LPV controller as the scheduling parameter vector, as shown in Fig. 16.

The closed-loop MAP tracking results of the proposed LPV control design methodologies have been compared against the conventionally implemented fixed-gain PI controller (see [98]) in various one-hour-long simulation scenarios. Given the following nominal values of the model parameters and time-delay,  $\bar{K} = 0.55$ ,  $\bar{T} = 150$ , and  $\bar{\tau} = 40$ , the tuned PI controller transfer function will be in the following form

$$G_c(s) = 3 + \frac{0.017}{s}, \quad (155)$$

which is computed based on the desired gain and phase margin control design constraints [105].

For the investigated MAP control task, the controlled output vector,  $\mathbf{z}(t)$ , in (57) is defined to be  $\mathbf{z}(t) = [\phi \cdot x_e(t) \quad \psi \cdot u(t)]^T$  as (154) suggests. The weighting scalars  $\phi$  and  $\psi$  penalize the tracking error,  $x_e(t)$ , and the control effort,  $u(t)$ , respectively to fulfill desired performance objectives.

By employing the LPV controller synthesis results presented in chapter 4, robust delay-dependent gain-scheduling LPV controllers are designed for systems with either parametric uncertainties or varying uncertain delay. Such control design is sought to guarantee closed-loop asymptotic stability and desired energy-to-energy (induced  $\mathcal{L}_2$ -norm) over the entire range of model parameter trajectories,  $\boldsymbol{\rho} \in \mathcal{F}_{\boldsymbol{\rho}}^{\nu}$ , and time-delay variation,  $\tau \in \mathcal{T}^{\nu\tau}$ , with the varying time-delay uncertainty lies in the range given in (111).

For this purpose, the results of Theorem 8 have been implemented to design a gain-scheduled LPV controller for calculating the drug injection rate in the computerized MAP regulation case

study. The first scenario has been generated in the simulation environment in the absence of disturbances and measurement noise to investigate the controllers' ability to respond to reference command changes. Accordingly, the MAP tracking profiles and the associated control efforts are depicted in Fig. 31, where the favorable controller is sought to regulate the MAP response to desirably track the commanded MAP profile with a minimal settling time and zero steady-state error while keeping the response overshoot within a narrow allowable range. As shown, the MAP reference to be tracked consists of sharp stepwise and ramp changes. According to this figure, the proposed gain-scheduling controller outperforms the fixed-gain control design in fulfilling the resuscitation goals.

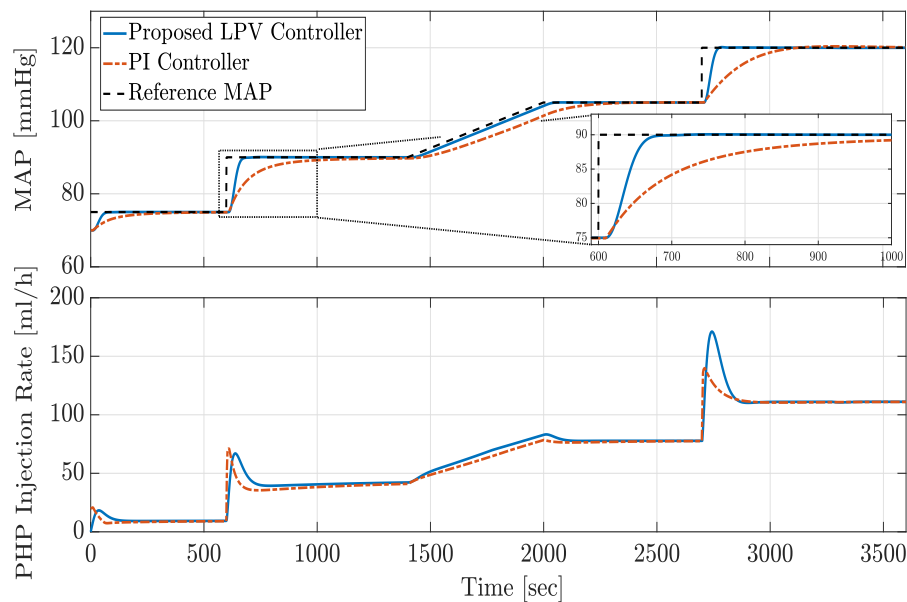


Figure 31: Closed-loop response and PHP injection rate of proposed LPV controller against fixed structure PI controller for disturbance and noise free case

In the next scenario, we assume that the closed-loop system is subject to measurement noise and output disturbances. During the resuscitation, a patient's blood pressure could be influenced by factors other than the vasoactive drug administration such as hemorrhage, unmodeled physiological variations, medications interference like lactated ringers (LR) or sodium nitroprusside (SNP), and any other medical interventions. Figure 23(b) shows a typical profile of such incidents modeled as a

disturbance signal. The closed-loop simulation results of the proposed LPV control design and PI controller are shown in Fig. 32 where the closed-loop system is subject to measurement noise and output disturbances. The considered measurement noise is assumed to be a white noise signal with an intensity of  $10^{-3}$ .

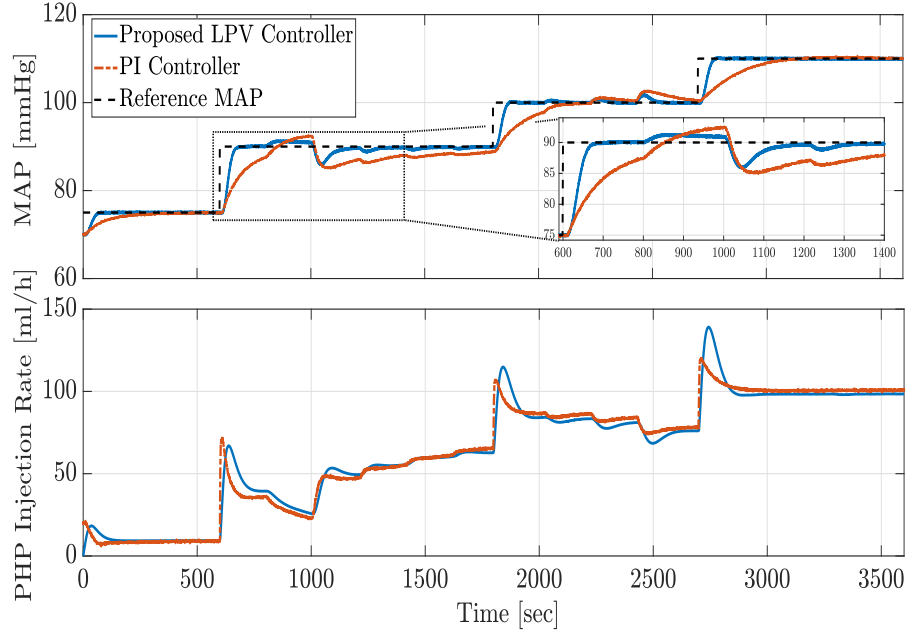


Figure 32: Closed-loop response and PHP injection rate of proposed LPV controller against fixed structure PI controller subject to disturbance and measurement noise

As illustrated in Fig. 32, the proposed LPV control method, due to its scheduling structure and robustness in the design, demonstrates a superior MAP command tracking performance with respect to the rise time and speed of the response while desirably rejecting the disturbances and measurement noise. The design parameters are given in Table 5 where the MATLAB<sup>®</sup> toolbox YALMIP with MOSEK solver has been used to solve the LMI optimization problems.

Table 5: Design parameters and performance index

$\lambda_2$	$\lambda_3$	$\lambda_4$	$\phi$	$\psi$	$\Lambda$	$\Omega$	$\gamma$
22.3	0.26	-0.10	1.6	1.1	50	50	26.4

To evaluate the robustness of the proposed LPV control design (Theorem 3), we investigate the closed-loop response in the presence of uncertainties on the model parameters. Accordingly, the time-delay and the sensitivity are considered to be under-estimated by 30%, and the time constant is considered to be over-estimated by 30%, which corresponds to the worst-case perturbation scenario. The closed-loop MAP response of the system with the proposed robust LPV control design is compared to the response of the LPV controller designed without considering uncertainty obtained using the results of Theorem 2. As per Fig. 33, the control without considering uncertainty in the design demonstrates oscillatory behavior and higher overshoots both in the closed-loop MAP response and also in the PHP injection control input signal, which are undesirable. As the results suggest, the proposed robust LPV control design is capable of compensating for parameter uncertainties.

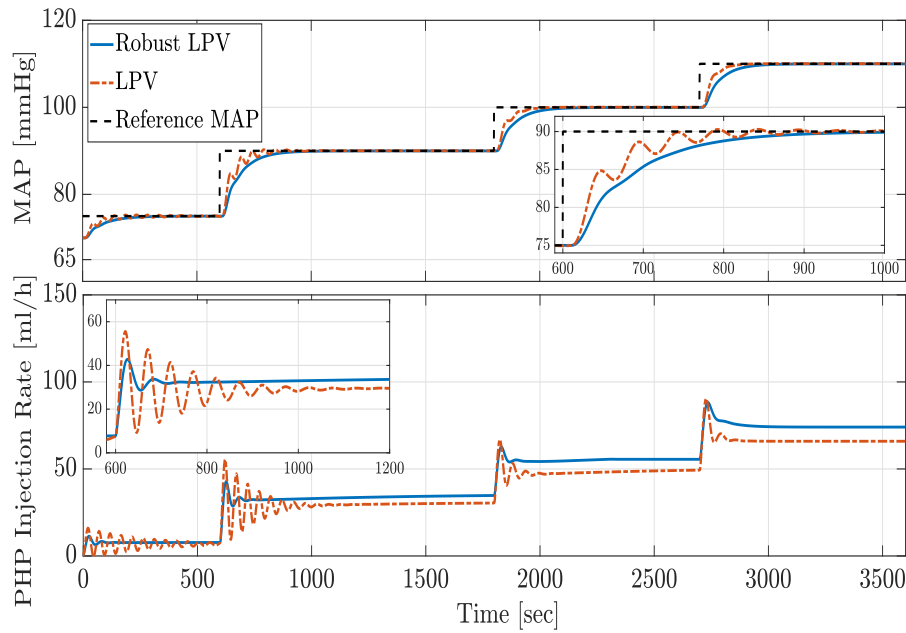


Figure 33: Closed-loop MAP response and control effort (PHP injection rate) of robust LPV controller in the presence of model parameter uncertainty

Moreover, to examine the robustness of the proposed control scheme in handling the time-varying delay uncertainty, we created a scenario in which the model's varying time-delay has been underestimated by 50%. The closed-loop MAP response of the system with the proposed robust state-feedback LPV controller (Theorem 6) has been compared with the response of a fixed-gain PI controller. Fig. 34 depicts the MAP tracking result of both controllers in this scenario and shows that the PI controller, which is designed without considering the time-varying delay uncertainty, demonstrates undesirable oscillatory performance and higher overshoots both in the closed-loop MAP response tracking and also in the PHP injection control input signal.

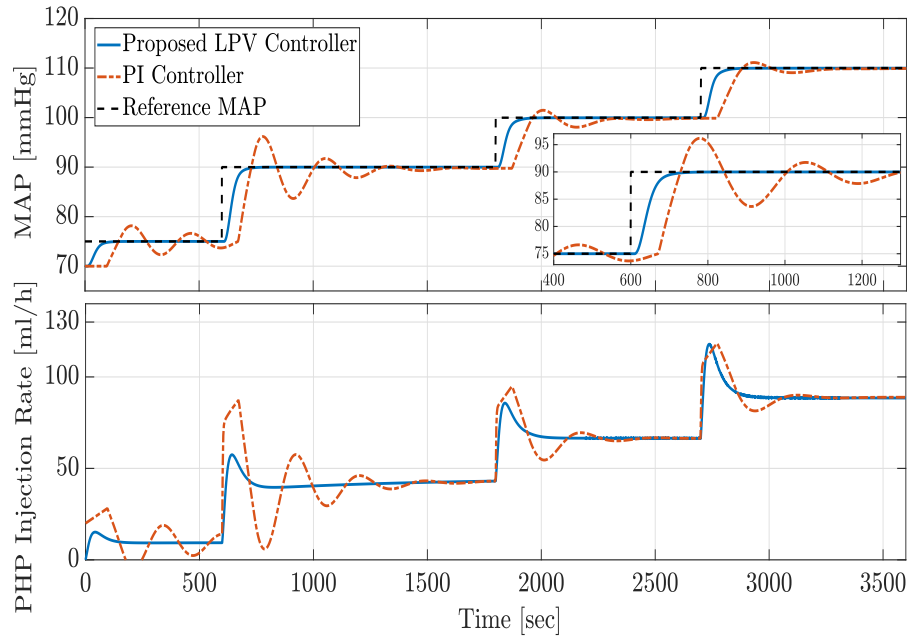


Figure 34: MAP response tracking performance and PHP injection rate of LPV controller against fixed structure PI controller under time delay uncertainty

Finally, we assess the proposed sampled-data controller (discussed in Section 4.4) in MAP reference tracking while rejecting disturbances. For this purpose, the results of Theorem 9 have been employed to design a gain-scheduled sampled-data controller (132) for calculating the drug injection rate in the automated MAP regulation task. To have an effective discrete control design, the choice

of sampling frequency is crucial and is a trade-off between the quality of the closed-loop system response and the implementation costs. In the presented simulation scenario, we consider one sample per two seconds, *i.e.*, 0.5 Hz. Figure 35 depicts the closed-loop performance of the proposed sampled-data LPV control design, where the closed-loop system is subject to output disturbances (as shown in Fig. 23(b)). As illustrated, the sampled-data LPV control, due to its scheduling structure and direct discrete-time synthesis, takes the sampling/hold times into account, has a superior MAP tracking performance with respect to the rise time and speed of the response while desirably rejecting the external disturbances.

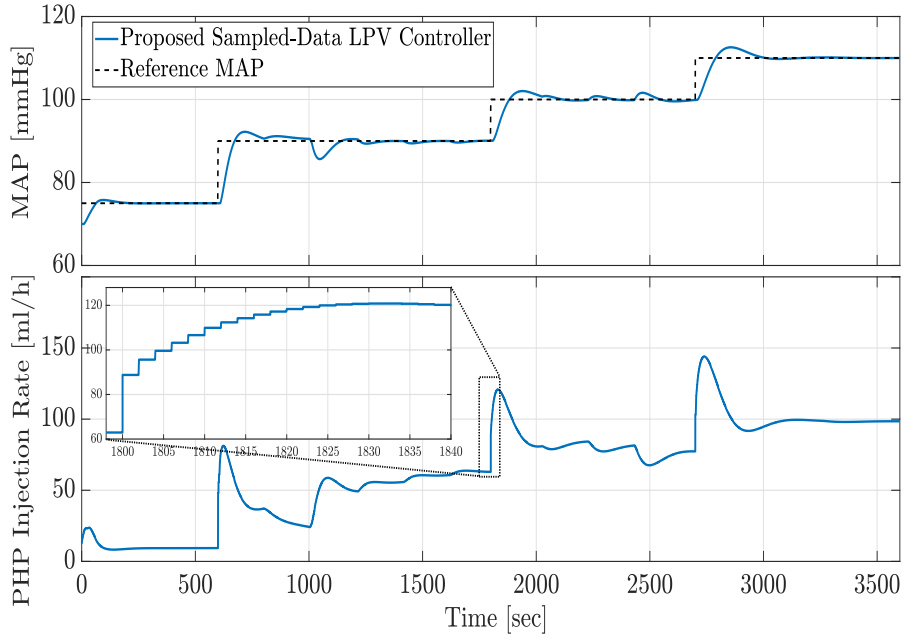


Figure 35: MAP response tracking performance and PHP injection rate of the proposed sample-data LPV controller under output disturbance

## 4.6 Chapter Conclusion

This chapter has proposed sufficient stability and control synthesis conditions for linear parameter varying (LPV) systems with time-varying uncertain delays affected by external disturbances. The uncertain delay has been examined as a nominal varying delay plus a perturbed function, and

in order to confine the perturbation in a stable domain, an input-output stability approach via the small-gain theorem results has been investigated. To this end, a Lyapunov-Krasovskii based approach has been employed, and by utilizing an improved parameter-dependent Lyapunov Krasovskii functional (LKF) candidate and applying an efficient bounding technique, the affine Jensen's inequality, sufficient stability, and performance conditions have been derived and formulated in terms of tractable and convex linear matrix inequality (LMI) conditions. Next, by introducing appropriate slack variables, the final relaxed synthesis conditions have been developed to provide closed-loop stability and minimize the disturbance amplification in terms of the induced  $\mathcal{L}_2$ -norm performance specification. The mean arterial blood pressure (MAP) regulation via automated drug administration example has been studied to assess the proposed control algorithm's effectiveness compared to the traditional control tools. To this end, MAP response dynamics to drug infusion has been characterized in an LPV state-delay representation. The final closed-loop simulations have been conducted to prove the potential adopted methodologies. As the results suggest, the proposed robust gain-scheduled LPV control design methods have significantly improved the MAP tracking accuracy over previous tools in the literature. Moreover, the proposed design favorably regulated the hypotensive patient's MAP response to the commanded MAP values while rejecting disturbances and measurement noises. Furthermore, developed control strategies in this chapter demonstrated a superior potential in handling model parameter variations, large time-delay and sampling time, and compensating for fast-varying sampling rates and delay uncertainties.

## 5 Conclusion, Contributions and Future Work

In this chapter, the important results and contributions of the dissertation are summarized, and we make recommendations for future research.

### 5.1 Summary of the Dissertation

This dissertation's primary focus was to develop and implement novel Bayesian-based parameter estimation and advanced gain-scheduling control techniques to be implemented on the automated blood pressure regulation task in clinical hypotensive patients. Most importantly, considerable effort has been devoted to study linear parameter varying (LPV) time-delay systems. Accordingly, various robust delay-dependent control design strategies have been introduced and assessed for such complex systems in cases of fast parameter variations, uncertainties, modeling mismatches, input and output disturbances, and measurement noise.

In the first chapter of the dissertation, the importance, necessity, and objectives of the mean arterial blood pressure (MAP) regulation in critical patient resuscitation scenarios have been discussed in detail. In this regard, a first-order continuous-time linear time-varying model with adjustable parameters and a varying input delay was considered to characterize patients' MAP response dynamics subject to vasoactive drug infusion. The utilized mathematical model effectively addressed the complexity, pharmacological variability, and the intra- and inter-patient variability of the physiological response to vasoactive drugs.

Chapter 2 proposed a Bayesian-based square root cubature Kalman filtering (SRCKF) approach for real-time model parameter estimation. Moreover, we used a multiple-model module with a posterior probability estimation to provide the time delay estimation. The proposed MMSRCKF estimation algorithm has been implemented on the MAP response model. To this end, we discretized the model and augmented the state vector with model parameters as unknown states of the system. Simulated nonlinear patient and swine animal experimental data have been used to verify the effectiveness of the developed identification algorithm.

Chapter 3 has proposed and compared two frequency-domain based control design methods,

namely, parameter-varying loop-shaping and internal model control (IMC), to regulate the blood pressure in critical patients via vasopressor drug administration. The first method has transformed the infinite-dimensional time-delay problem into a finite-dimensional but non-minimum phase (NMP) one through using the Padé approximation. The parameter-varying loop-shaping controller has been designed to make the closed-loop system meet bandwidth requirements in a straightforward manner while carefully dealing with the limitations imposed by the internal dynamics of the NMP system. In the IMC control design method, the small-gain theorem has been used to characterize necessary and sufficient conditions for robust stability of the closed-loop system.

In chapter 4, we addressed the stability analysis and control synthesis problem for LPV time-delay systems with norm-bounded parametric and/or time-delay uncertainties. First, by considering a class of LPV systems with additive norm-bounded uncertainties in the state and delayed state matrices and employing Lyapunov-Krasovskii functionals (LKFs), delay-dependent sufficient conditions were derived and formulated in terms of linear matrix inequalities (LMIs) to ensure the robust stability and a prescribed energy-to-energy gain performance level. In the next section of the same chapter, an improved parameter-dependent LKF candidate and an efficient bounding technique, the affine Jensen's inequality, were proposed to design a less conservative output-feedback LPV controller. A numerical example was provided and compared the proposed less conservative controller design scheme to another method in the literature. We further extended the research to address the robust control synthesis for the class of LPV systems with varying uncertain delays. To this end, we encountered the problem by considering the uncertain time delay as a nominal varying delay plus a perturbed function, and in order to confine the uncertainty in a stable domain, an input-output stability approach via the small-gain theorem results has been examined. Then, stability analysis, along with robust control synthesis conditions, characterized via a prescribed induced  $\mathcal{L}_2$ -norm of the closed-loop system, are derived via bounding the derivative of LKF, and the final results have been formulated in a relaxed parameter-dependent LMI frame. The next section of chapter 4 focused on the direct sampled-data LPV control design for continuous-time LPV time-delay systems. A combination of a digital controller and a continuous-time system resulted in a hybrid closed-loop system

that is challenging to analyze mathematically and needs to be encountered using advanced control methods that take the sampling behavior into account. We applied the input-delay approach to map the hybrid closed-loop system into a unified continuous-time domain. The mapping introduced another delay into the system dynamics other than the system's inherent time-delay. To complete the discussion, by employing the Krasovskii method of Lyapunov functionals, we proposed sampled-data output-feedback LPV synthesis conditions to ensure the asymptotic parameter-dependent quadratic (PDQ) stability and induced  $\mathcal{L}_2$ -norm performance index of the hybrid closed-loop LPV system. The investigated approach provided a less conservative approach in handling LPV systems with fast-varying time-delay and potentially large variable sampling rates. Finally, as a benchmark, we examined the automated MAP control in a hypotensive patient resuscitation where the MAP response dynamics to drug infusion was characterized in a time-delay LPV representation. The effectiveness of the proposed gain-scheduling LPV control design tools was evaluated in terms of MAP command tracking, disturbance rejection, and robustness against uncertainties. The closed-loop simulation results have been provided to verify the proposed LPV methodology's performance and superior potential.

## 5.2 Future Research Direction

Here are the list of some future research directions to extend the LPV time-delay control design:

- The developed real-time parameter estimation tool (2) and the proposed feedback control design methods (chapters 3 and 4) can ultimately be implemented and tested on an actual clinical patient resuscitation after passing the medical standards and safety protocols.
- The application of the proposed LPV time-delay systems analysis and control synthesis approaches could be extended to the LPV modeling and control of fluid resuscitation in burn patients.
- The results in chapter 4 were based on satisfying a prescribed energy-to-energy gain (or equivalently induced  $\mathcal{L}_2$ -norm) of the closed-loop system. In future research, we will study designing

gain-scheduling LPV controllers with different performance objectives, such as energy-to-peak, peak-to-peak, and multi-objective problems.

- In this dissertation, we derived the delay-dependent output-feedback synthesis conditions based on the improved LKFs and a less conservative affine Jensen's inequality bounding technique. This research could be further extended by examining more complete LKFs to improve the results and further reduce the conservatism. Additionally, we might examine and compare the results of other bounding techniques such as Wirtinger inequality to limit the bounding gap in the integral cross-terms of the LKF derivative.
- Future research will aim to address the sampled-data gain-scheduling LPV control problem in the presence of time-delay uncertainties and actuator saturation constraints.
- In future research, convergence analysis and the sensitivity of the proposed MMSRCKF algorithm to different initial conditions will be addressed and compared to other available estimations tools, such as EKF, UKF, and PF.
- Finally, future work will focus on the real-time testing and closed-loop implementation of the proposed MMSRCKF and automated LPV control methodologies for real animal and human cases.

## Bibliography

- [1] AHMED, S., AND ÖZBAY, H. Design of a switched robust control scheme for drug delivery in blood pressure regulation. *IFAC-PapersOnLine* 49, 10 (2016), 252–257.
- [2] ALBERTOS, P. Phase-conditionally stable systems. *Systems & control letters* 55, 10 (2006), 803–808.
- [3] APKARIAN, P. On the discretization of LMI-synthesized linear parameter-varying controllers. *Automatica* 33, 4 (1997), 655–661.
- [4] APKARIAN, P., AND ADAMS, R. J. Advanced gain-scheduling techniques for uncertain systems. *IEEE Transactions on Control Systems Technology* 6, 1 (1998), 21–32.
- [5] ARASARATNAM, I., AND HAYKIN, S. Cubature Kalman filters. *IEEE Transactions on Automatic Control* 54, 6 (2009), 1254–1269.
- [6] ARNSPARGER, J. M., MCINNIS, B. C., GLOVER, J. R., AND NORMANN, N. A. Adaptive control of blood pressure. *IEEE Transactions on Biomedical Engineering*, 3 (1983), 168–176.
- [7] ÅSTRÖM, K. J. Limitations on control system performance. *European Journal of Control* 6, 1 (2000), 2–20.
- [8] BAILEY, J. M., AND HADDAD, W. M. Drug dosing control in clinical pharmacology. *IEEE Control Systems Magazine* 25, 2 (2005), 35–51.
- [9] BAMIEH, B. A., AND PEARSON, J. B. A general framework for linear periodic systems with applications to  $\mathcal{H}_\infty$  sampled-data control. *IEEE transactions on automatic control* 37, 4 (1992), 418–435.
- [10] BIANCHI, F. D., DE BATTISTA, H., AND MANTZ, R. J. *Wind Turbine Control Systems: Principles, Modelling and Gain Scheduling Design*. Springer Science & Business Media, 2006.

- [11] BIANCHI, F. D., MANTZ, R. J., AND CHRISTIANSEN, C. F. Gain scheduling control of variable-speed wind energy conversion systems using quasi-LPV models. *Control Engineering Practice* 13, 2 (2005), 247–255.
- [12] BOYD, S., EL GHAOU, L., FERON, E., AND BALAKRISHNAN, V. *Linear Matrix Inequalities in System and Control Theory*, vol. 15. Siam, 1994.
- [13] BOZORG, M., AND DAVISON, E. J. Control of time delay processes with uncertain delays: Time delay stability margins. *Journal of Process Control* 16, 4 (2006), 403–408.
- [14] BRIAT, C. Convergence and equivalence results for the Jensen’s inequality—application to time-delay and sampled-data systems. *IEEE Transactions on Automatic Control* 56, 7 (2011), 1660–1665.
- [15] BRIAT, C. *Linear Parameter-Varying and Time-Delay Systems Analysis, Observation, Filtering & Control*. Springer-Verlag, Heidelberg, 2015.
- [16] BROSILOW, C., AND JOSEPH, B. *Techniques of Model-Based Control*. Prentice Hall, Upper Saddle River, NJ, 2002.
- [17] CAO, G., LUSPAY, T., EBRAHIMI, B., GRIGORIADIS, K., FRANCKEK, M., MARQUES, N., WOLF, J., AND KRAMER, G. Simulator for simulating and monitoring the hypotensive patients blood pressure response of phenylephrine bolus injection and infusion with open-loop and closed-loop treatment. In *International Conference on Computer Modeling and Simulation* (2017), pp. 175–181.
- [18] CHANG, P. H., AND LEE, J. W. A model reference observer for time-delay control and its application to robot trajectory control. *IEEE Transactions on Control Systems Technology* 4, 1 (1996), 2–10.
- [19] CHEN, T., AND FRANCIS, B. A. *Optimal Sampled-Data Control Systems*. Springer Science & Business Media, 2012.

- [20] COLMEGNA, P. H., SANCHEZ-PENA, R. S., GONDHALEKAR, R., DASSAU, E., AND DOYLE, F. J. Switched LPV glucose control in type 1 diabetes. *IEEE Transactions on Biomedical Engineering* 63, 6 (2015), 1192–1200.
- [21] CRAIG, C. R., AND STITZEL, R. E. *Modern Pharmacology with Clinical Applications*. Lippincott Williams & Wilkins, 2004.
- [22] CUI, X., HE, Z., LI, E., CHENG, A., LUO, M., AND GUO, Y. State-of-charge estimation of power lithium-ion batteries based on an embedded micro control unit using a square root cubature Kalman filter at various ambient temperatures. *International Journal of Energy Research* 43, 8 (2019), 3561–3577.
- [23] DA SILVA, S. J., SCARDOVELLI, T. A., DA SILVA BOSCHI, S. R. M., RODRIGUES, S. C. M., AND DA SILVA, A. P. Simple adaptive PI controller development and evaluation for mean arterial pressure regulation. *Research on Biomedical Engineering* 35, 2 (2019), 157–165.
- [24] EBRAHIMI, B., GRIGORIADIS, K., FRANCKEK, M., AND TAFRESHI, R. Output tracking in first-order time-delay systems: A dynamic control approach. *IFAC-PapersOnLine* 48, 12 (2015), 269–274.
- [25] EBRAHIMI, B., TAFRESHI, R., FRANCKEK, M., GRIGORIADIS, K., AND MOHAMMADPOUR, J. A dynamic feedback control strategy for control loops with time-varying delay. *International Journal of Control* 87, 5 (2014), 887–897.
- [26] FLANCAUM, L., DICK, M., DASTA, J. A., SINHA, R., AND CHOBAN, P. A dose-response study of phenylephrine in critically ill, septic surgical patients. *European Journal of Clinical Pharmacology* 51, 6 (1997), 461–465.
- [27] FRIDMAN, E. Stability of systems with uncertain delays: a new "complete" Lyapunov-Krasovskii functional. *IEEE Transactions on Automatic Control* 51, 5 (2006), 885–890.
- [28] FRIDMAN, E. *Introduction to Time-Delay Systems Analysis and Control*. Springer, Basel, 2014.

- [29] FURUTANI, E., ARAKI, M., KAN, S., AUNG, T., ONODERA, H., IMAMURA, M., SHIRAKAMI, G., AND MAETANI, S. An automatic control system of the blood pressure of patients under surgical operation. *International Journal of Control, Automation, and Systems* 2, 1 (2004), 39–54.
- [30] GAO, Y., AND ER, M. J. An intelligent adaptive control scheme for postsurgical blood pressure regulation. *IEEE Transactions on Neural Networks* 16, 2 (2005), 475–483.
- [31] HAHN, J., EDISON, T., AND EDGAR, T. F. Adaptive IMC control for drug infusion for biological systems. *Control Engineering Practice* 10, 1 (2002), 45–56.
- [32] HANLON, P. D., AND MAYBECK, P. S. Multiple-model adaptive estimation using a residual correlation Kalman filter bank. *IEEE Transactions on Aerospace and Electronic Systems* 36, 2 (2000), 393–406.
- [33] HE, W., KAUFMAN, H., AND ROY, R. Multiple model adaptive control procedure for blood pressure control. *IEEE Transactions on Biomedical Engineering* 33, 1 (1986), 10–19.
- [34] HOU, Z.-S., AND WANG, Z. From model-based control to data-driven control: Survey, classification and perspective. *Information Sciences* 235 (2013), 3–35.
- [35] ISAKA, S., AND SEBALD, A. V. Control strategies for arterial blood pressure regulation. *IEEE Transactions on Biomedical Engineering* 40, 4 (1993), 353–363.
- [36] JANKOVIC, M. Control Lyapunov-Razumikhin functions and robust stabilization of time delay systems. *IEEE Transactions on Automatic Control* 46, 7 (2001), 1048–1060.
- [37] JIA, B., XIN, M., AND CHENG, Y. High-degree cubature Kalman filter. *Automatica* 49, 2 (2013), 510–518.
- [38] KASHIHARA, K., KAWADA, T., UEMURA, K., SUGIMACHI, M., AND SUNAGAWA, K. Adaptive predictive control of arterial blood pressure based on a neural network during acute hypotension. *Annals of Biomedical Engineering* 32, 10 (2004), 1365–1383.

- [39] KEE, W. D. N., KHAW, K. S., AND NG, F. F. Prevention of hypotension during spinal anesthesia for cesarean delivery an effective technique using combination phenylephrine infusion and crystalloid cohydration. *The Journal of the American Society of Anesthesiologists* 103, 4 (2005), 744–750.
- [40] KHARITONOV, V. L. Lyapunov–Krasovskii functionals for scalar time delay equations. *Systems & Control Letters* 51, 2 (2004), 133–149.
- [41] KHARITONOV, V. L., AND NICULESCU, S.-I. On the stability of linear systems with uncertain delay. *IEEE Transactions on Automatic Control* 48, 1 (2003), 127–132.
- [42] KNOSPE, C. R., AND ROOZBEHANI, M. Stability of linear systems with interval time delays excluding zero. *IEEE Transactions on Automatic Control* 51, 8 (2006), 1271–1288.
- [43] KOLMANOVSKII, V. B., AND RICHARD, J.-P. Stability of some linear systems with delays. *IEEE Transactions on Automatic Control* 44, 5 (1999), 984–989.
- [44] LÉCHAPPÉ, V., MOULAY, E., AND PLESTAN, F. Prediction-based control for LTI systems with uncertain time-varying delays and partial state knowledge. *International Journal of Control* 91, 6 (2018), 1403–1414.
- [45] LEE, J., TASOUJIAN, S., GRIGORIADIS, K., AND FRANCIOSI, M. Output feedback linear parameter varying control of permanent magnet synchronous motors. In *ASME Dynamic Systems and Control Conference (DSCC)* (2020), pp. 1–11.
- [46] LEHMANN, D., AND LUNZE, J. Event-based control with communication delays and packet losses. *International Journal of Control* 85, 5 (2012), 563–577.
- [47] LIU, K.-Z., AND YAO, Y. *Robust Control: Theory and Applications*. John Wiley & Sons, Singapore, 2016.
- [48] LIU, Y., DONG, K., WANG, H., LIU, J., HE, Y., AND PAN, L. Adaptive Gaussian sum squared-root cubature Kalman filter with split-merge scheme for state estimation. *Chinese Journal of Aeronautics* 27, 5 (2014), 1242–1250.

- [49] LJUNG, L., AND SÖDERSTRÖM, T. *Theory and Practice of Recursive Identification*. MIT Press, 1983.
- [50] LOEHR, N. *Advanced Linear Algebra*. Chapman and Hall/CRC, New York, NY, USA, 2014.
- [51] LOFBERG, J. YALMIP: A toolbox for modeling and optimization in MATLAB. In *IEEE International Conference on Robotics and Automation* (2004), pp. 284–289.
- [52] LU, B., WU, F., AND KIM, S. Switching LPV control of an F-16 aircraft via controller state reset. *IEEE transactions on control systems technology* 14, 2 (2006), 267–277.
- [53] LUSPAY, T., AND GRIGORIADIS, K. Adaptive parameter estimation of blood pressure dynamics subject to vasoactive drug infusion. *IEEE Transactions on Control Systems Technology* 24, 3 (2015), 779–787.
- [54] LUSPAY, T., AND GRIGORIADIS, K. M. Design and validation of an extended Kalman filter for estimating hemodynamic variables. In *American Control Conference* (2014), pp. 4145–4150.
- [55] MAI, H., SONG, G., AND LIAO, X. Time-delayed dynamic neural network-based model for hysteresis behavior of shape-memory alloys. *Neural Computing and Applications* 27, 6 (2016), 1519–1531.
- [56] MALAGUTTI, N. Particle filter-based robust adaptive control for closed-loop administration of sodium nitroprusside. *Journal of Computational Surgery* 1, 1 (2014), 1–19.
- [57] MALAGUTTI, N., DEGHANI, A., AND KENNEDY, R. A. Robust control design for automatic regulation of blood pressure. *IET Control Theory & Applications* 7, 3 (2013), 387–396.
- [58] MICHIELS, W., AND NICULESCU, S.-I. *Stability and Stabilization of Time-Delay Systems: An Eigenvalue-Based Approach*. SIAM, 2007.
- [59] MIRKIN, L. On the extraction of dead-time controllers from delay-free parametrizations. *IFAC Proceedings Volumes* 33, 23 (2000), 169–174.

- [60] MOHAMMADPOUR, J., AND SCHERER, C. W., Eds. *Control of Linear Parameter Varying Systems with Applications*. Springer Science & Business Media, New York, 2012.
- [61] MORARI, M., AND ZAFIRIOU, E. *Robust Process Control*. Prentice Hall, Englewood Cliffs, NJ, 1989.
- [62] NEJEM, I., BOUAZIZI, M. H., AND BOUANI, F.  $\mathcal{H}_\infty$  dynamic output feedback control of LPV time-delay systems via dilated linear matrix inequalities. *Transactions of the Institute of Measurement and Control* 41, 2 (2019), 552–559.
- [63] NEVES, J. F. N. P. D., MONTEIRO, G. A., ALMEIDA, J. R. D., SANT’ANNA, R. S., BONIN, H. B., AND MACEDO, C. F. Phenylephrine for blood pressure control in elective cesarean section: therapeutic versus prophylactic doses. *Revista Brasileira de Anestesiologia* 60, 4 (2010), 395–398.
- [64] NICULESCU, S.-I. A model transformation class for delay-dependent stability analysis. In *American Control Conference (ACC)* (1999), vol. 1, pp. 314–318.
- [65] NICULESCU, S.-I. *Delay Effects on Stability: A Robust Control Approach*, vol. 269. Springer Science & Business Media, 2001.
- [66] PALMOR, Z. *Time-Delay Compensation-Smith Predictor and its Modifications, The Control Handbook*. CRC press, Boca Raton, FL, 1996.
- [67] PARK, P. A delay-dependent stability criterion for systems with uncertain time-invariant delays. *IEEE Transactions on Automatic control* 44, 4 (1999), 876–877.
- [68] RAMEZANIFAR, A., MOHAMMADPOUR, J., AND GRIGORIADIS, K. Output-feedback sampled-data control design for linear parameter-varying systems with delay. *International Journal of Control* 87, 12 (2014), 2431–2445.
- [69] RAMEZANIFAR, A., MOHAMMADPOUR, J., AND GRIGORIADIS, K. M. Sampled-data filtering for linear parameter varying systems. *International Journal of Systems Science* 46, 3 (2015), 474–487.

- [70] RAO, R. R., AUFDERHEIDE, B., AND BEQUETTE, B. W. Experimental studies on multiple-model predictive control for automated regulation of hemodynamic variables. *IEEE Transactions on Biomedical Engineering* 50, 3 (2003), 277–288.
- [71] RIVERA, D. E., MORARI, M., AND SKOGESTAD, S. Internal model control: PID controller design. *Industrial & Engineering Chemistry Process Design and Development* 25, 1 (1986), 252–265.
- [72] ROSA, T. E., FREZZATTO, L., MORAIS, C. F., AND OLIVEIRA, R. C. L. F.  $\mathcal{H}_\infty$  static output-feedback gain-scheduled control for discrete LPV time-delay systems. *IFAC-PapersOnLine* 51, 26 (2018), 137–142.
- [73] SALAVATI, S., GRIGORIADIS, K., AND FRANCKEK, M. Reciprocal convex approach to output-feedback control of uncertain LPV systems with fast-varying input delay. *International Journal of Robust and Nonlinear Control* 29, 16 (2019), 5744–5764.
- [74] SALAVATI DEZFULI, S., EBRAHIMI, B., GRIGORIADIS, K., AND FRANCKEK, M. Internal model control for a class of uncertain time-delay systems. In *American Control Conference* (Boston, MA, USA, 2016), pp. 960–966.
- [75] SANDU, C., AND POPESCU, D. Reinforcement learning for the control of blood pressure in post cardiac surgery patients. *U. P. B. Sci. Bull., Series C* 78, 1 (2016), 139–150.
- [76] SEBORG, D. E., MELLICHAMP, D. A., EDGAR, T. F., AND DOYLE, F. J. *Process Dynamics and Control*, 3rd ed. Wiley, USA, 2011.
- [77] SHAMMA, J. S. *Analysis and Design of Gain Scheduled Control Systems*. PhD thesis, Massachusetts Institute of Technology, 1988.
- [78] SHAMMA, J. S., AND ATHANS, M. Analysis of gain scheduled control for nonlinear plants. *IEEE Transactions on Automatic Control* 35, 8 (1990), 898–907.

- [79] SHAMSUZZOHA, M., SKLIAR, M., AND LEE, M. Design of IMC filter for PID control strategy of open-loop unstable processes with time delay. *Asia-Pacific Journal of Chemical Engineering* 7, 1 (2012), 93–110.
- [80] SHUSTIN, E., AND FRIDMAN, E. On delay-derivative-dependent stability of systems with fast-varying delays. *Automatica* 43, 9 (2007), 1649–1655.
- [81] SIMON, D. Kalman filtering with state constraints: a survey of linear and nonlinear algorithms. *IET Control Theory & Applications* 4, 8 (2010), 1303–1318.
- [82] SKOGESTAD, S., AND POSTLETHWAITE, I. *Multivariable Feedback Control: Analysis and Design*, 2nd ed. New York, 2005.
- [83] SLATE, J., AND SHEPPARD, L. Automatic control of blood pressure by drug infusion. *Physical Science, Measurement and Instrumentation, Management and Education, IET* 129, 9 (1982), 639–645.
- [84] SLATE, J. B., SHEPPARD, L. C., RIDEOUT, V. C., AND BLACKSTONE, E. H. A model for design of a blood pressure controller for hypertensive patients. *IFAC Proceedings* 12, 8 (1979), 867–874.
- [85] SMITH, O. Closer control of loops with dead time. *Journal of Process Control* 53, 5 (1957), 217–219.
- [86] SONDHI, S., AND HOTE, Y. V. Fractional-order PI controller with specific gain-phase margin for MABP control. *IETE Journal of Research* 61, 2 (2015), 142–153.
- [87] SUPLIN, V., FRIDMAN, E., AND SHAKED, U. Sampled-data h control and filtering: Nonuniform uncertain sampling. *Automatica* 43, 6 (2007), 1072–1083.
- [88] TAN, K., GRIGORIADIS, K. M., AND WU, F. Output-feedback control of LPV sampled-data systems. *International Journal of Control* 75, 4 (2002), 252–264.

- [89] TASOUJIAN, S., EBRAHIMI, B., GRIGORIADIS, K., AND FRANCKEK, M. Parameter-varying loop-shaping for delayed air-fuel ratio control in lean-burn SI engines. In *ASME Dynamic Systems and Control Conference (DSCC)* (2016), pp. 1–8.
- [90] TASOUJIAN, S., GRIGORIADIS, K., AND FRANCKEK, M. Delay-dependent output-feedback control for blood pressure regulation using LPV techniques. In *ASME Dynamic Systems and Control Conference (DSCC)* (2019).
- [91] TASOUJIAN, S., SALAVATI, S., FRANCKEK, M., AND GRIGORIADIS, K. Robust IMC-PID and parameter-varying control strategies for automated blood pressure regulation. *International Journal of Control, Automation and Systems* 17, 7 (2019), 1803–1813.
- [92] TASOUJIAN, S., SALAVATI, S., FRANCKEK, M., AND GRIGORIADIS, K. Robust delay-dependent LPV synthesis for blood pressure control with real-time Bayesian parameter estimation. *IET Control Theory & Applications* 14, 10 (2020), 1334–1345.
- [93] TASOUJIAN, S., SALAVATI, S., GRIGORIADIS, K., AND FRANCKEK, M. Real-time cubature Kalman filter parameter estimation of blood pressure response characteristics under vasoactive drugs administration. In *American Control Conference (ACC)* (2020), pp. 3355–3362.
- [94] TOTH, R., HEUBERGER, P. S., AND VAN DEN HOF, P. M. Discretisation of linear parameter-varying state-space representations. *IET control theory & applications* 4, 10 (2010), 2082–2096.
- [95] UROOJ, S., AND SINGH, B. Fractional-order PID control for postoperative mean arterial blood pressure control scheme. *Procedia Computer Science* 152 (2019), 380–389.
- [96] VELÁZQUEZ-VELÁZQUEZ, J. E., AND GALVÁN-GUERRA, R. Robust stability analysis for linear systems with uncertain fast-varying time delay arising from networked control systems. *Research in Computing Science* 118 (2016), 55–64.
- [97] WANG, J., SHI, P., AND GAO, H. Gain-scheduled stabilisation of linear parameter-varying systems with time-varying input delay. *IET Control Theory & Applications* 1, 5 (2007), 1276–1285.

- [98] WASSAR, T., LUSPAY, T., UPENDAR, K. R., MOISI, M., VOIGT, R. B., MARQUES, N. R., KHAN, M. N., GRIGORIADIS, K., FRANCKEK, M., AND KRAMER, G. C. Automatic control of arterial pressure for hypotensive patients using phenylephrine. *International Journal of Modelling and Simulation* 34, 4 (2014), 187–198.
- [99] WITRANT, E., CANUDAS-DE WIT, C., GEORGES, D., AND ALAMIR, M. Remote stabilization via communication networks with a distributed control law. *IEEE Transactions on Automatic control* 52, 8 (2007), 1480–1485.
- [100] XIE, L. Output feedback  $\mathcal{H}_\infty$  control of systems with parameter uncertainty. *International Journal of control* 63, 4 (1996), 741–750.
- [101] ZHANG, H., SHI, Y., AND MEHR, A. S. Robust Static Output Feedback Control and Remote PID Design for Networked Motor Systems. *IEEE Trans. on Industrial Electronics* 58, 12 (2011), 5396–5405.
- [102] ZHANG, X., TSOTRAS, P., AND KNOSPE, C. Stability analysis of LPV time-delayed systems. *International Journal of Control* 75, 7 (2002), 538–558.
- [103] ZHANG, Y., YANG, F., AND HAN, Q.-L.  $\mathcal{H}_\infty$  control of LPV systems with randomly multi-step sensor delays. *International Journal of Control, Automation and Systems* 12, 6 (2014), 1207–1215.
- [104] ZHAO, X., LI, J., YAN, X., AND JI, S. Robust adaptive cubature Kalman filter and its application to ultra-tightly coupled SINS/GPS navigation system. *Sensors* 18, 7 (2018), 1–19.
- [105] ZHONG, Q.-C. *Robust Control of Time-Delay Systems*. Springer-Verlag, London, 2006.
- [106] ZHU, K. Y., ZHENG, H., AND ZHANG, D. G. A computerized drug delivery control system for regulation of blood pressure. *International Journal of Intelligent Computing in Medical Sciences & Image Processing* 2, 1 (2008), 1–13.

- [107] ZOPE, R., MOHAMMADPOUR, J., GRIGORIADIS, K., AND FRANCKEK, M. Delay-dependent  $\mathcal{H}_\infty$  control for LPV systems with fast-varying time delays. In *American Control Conference (ACC)* (2012), pp. 775–780.